Nano-Micro Letters
REVIEW
e-ISSN 2150-5551
CN 31-2103/TB
https://doi.org/10.1007/s40820-023-01162-x

Advances in Mn-Based Electrode Materials for Aqueous Sodium-Ion Batteries

Changsheng Ding[1] ✉, Zhang Chen[1], Chuanxiang Cao[1], Yu Liu[2], Yanfeng Gao[1,3] ✉

Cite as
Nano-Micro Lett.
(2023) 15:192

Received: 28 April 2023
Accepted: 19 June 2023
Published online: 9 August 2023
© The Author(s) 2023

HIGHLIGHTS

- Mn-based electrode materials, including oxides, Prussian blue analogues and polyanion compounds, are introduced systematically for aqueous sodium-ion batteries.
- The composition, crystal structure, morphology and electrochemical performance of Mn-based electrode materials are reviewed.
- The improvement methods of electrochemical performance, such as electrolyte optimization, element doping or substitution, morphology optimization and carbon modification, are discussed.

ABSTRACT Aqueous sodium-ion batteries have attracted extensive attention for large-scale energy storage applications, due to abundant sodium resources, low cost, intrinsic safety of aqueous electrolytes and eco-friendliness. The electrochemical performance of aqueous sodium-ion batteries is affected by the properties of electrode materials and electrolytes. Among various electrode materials, Mn-based electrode materials have attracted tremendous attention because of the abundance of Mn, low cost, nontoxicity, eco-friendliness and interesting electrochemical performance. Aqueous electrolytes having narrow electrochemical window also affect the electrochemical performance of Mn-based electrode materials. In this review, we introduce systematically Mn-based electrode materials for aqueous sodium-ion batteries from cathode and anode materials and offer a comprehensive overview about their recent development. These Mn-based materials include oxides, Prussian blue analogues and polyanion compounds. We summarize and discuss the composition, crystal structure, morphology and electrochemical properties of Mn-based electrode materials. The improvement methods based on electrolyte optimization, element doping or substitution, optimization of morphology and carbon modification are highlighted. The perspectives of Mn-based electrode materials for future studies are also provided. We believe this review is important and helpful to explore and apply Mn-based electrode materials in aqueous sodium-ion batteries.

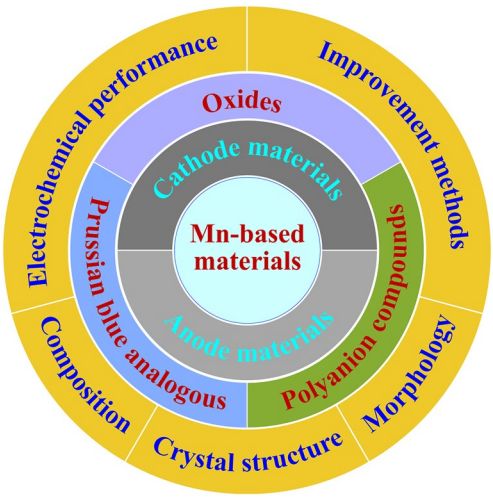

KEYWORDS Sodium-ion batteries; Aqueous electrolytes; Mn-based electrode materials; Electrochemical performance; Improvement methods

✉ Changsheng Ding, dingcs@shu.edu.cn; Yanfeng Gao, yfgao@shu.edu.cn
[1] School of Materials Science and Engineering, Shanghai University, Shanghai 200444, People's Republic of China
[2] Shanghai Institute of Ceramics, Chinese Academy of Sciences, Shanghai 200050, People's Republic of China
[3] Key Laboratory of Comprehensive and Highly Efficient Utilization of Salt Lake Resources, Qinghai Institute of Salt Lakes, Chinese Academy of Sciences, Xining 81000, People's Republic of China

1 Introduction

Solar energy, wind energy and other renewable energy are growing quickly and become progressively more important. Due to the intermittent nature of solar energy and wind energy, energy storage systems are needed to store energy, stable the modern grid and supply round-the-clock power [1, 2]. The development of energy storage systems will drive the growth of renewable energy. Among various energy storage systems, battery energy storage systems based on rechargeable batteries (secondary batteries) have attracted great interest because of their high conversion efficiency, flexibility and simple maintenance [3–6]. Lithium-ion batteries (LIBs) have been developed and are now playing more important role in our lives. Large-scale LIBs have attracted enormous attention and been considered one of the most promising energy storage systems [7–9]. However, the limited resources and growing price of lithium resources hinder LIBs applications in large-scale energy storage.

Sodium-ion batteries (SIBs) are strong candidates for large-scale energy storage because of abundant sodium resources and low cost. Up to now, various materials have been investigated for SIBs including cathode, anode and electrolyte materials [10–16]. Nevertheless, safety issue of organic electrolytes is a much notable realistic factor affecting commercialization. Compared with organic electrolytes, aqueous electrolytes are safer and eco-friendly. Furthermore, the ionic conductivity of aqueous electrolyte is larger by almost two orders of magnitude than that of organic electrolytes [8, 17]. Therefore, aqueous SIBs based on aqueous electrolytes have attracted intensive attention for large-scale energy storage, because of their high safety, low cost, convenient manufacture, environment friendliness and easy recycle [8, 18–21]. However, the electrochemical window of aqueous electrolytes is much narrower than that of organic electrolytes. The stable electrochemical window of water is approximately 1.23 V, beyond which water electrolysis will occur with O_2 or H_2 gas evolution. Hence, the working potential of electrode materials must be located between H_2 and O_2 evolution potentials, which leads to lower energy density of aqueous batteries. To widen the electrochemical window of aqueous electrolytes, many researches have been devoted to optimizing the electrolytes and developing high-voltage electrolytes [22–25]. Hou et al. added surfactant (sodium dodecyl sulfate) to aqueous electrolyte and expanded the electrochemical stability window to about 2.5 V [22]. Tomiyasu et al. reported a saturated sodium perchlorate aqueous solution with a potential window of approximately 3.2 V [23]. In addition, the developed "water-in-salt" electrolytes could expand the electrochemical window to 3 V [24, 25].

The electrochemical performance of aqueous SIBs has also been influenced by electrode materials. The insertion/extraction reactions of Na ions in aqueous electrolytes are more complicated, and thereby affecting the selectivity of electrode materials. The chemical stability of electrode materials is also very important in aqueous electrolyte system. The cycling stability of electrode materials will be affected by side reactions on the electrode surface with H_2O or residual O_2 [20]. For exploring suitable electrode materials, the chemical stability, elemental abundance, charge transfer number, redox potentials and electronic conductivity should be considered. Up to now, various electrode materials have been developed for aqueous SIBs, including manganese-based oxides, vanadium-based oxides, Prussian blue analogues, polyanion compounds and organic materials [8, 20, 21, 26–29]. Among them, Mn-based electrode materials have attracted tremendous interests because of abundant reserves of manganese, low cost, low toxicity, rich valence states of manganese and interesting electrochemical performance [27, 29–33]. Mn has multiple oxidation states, such as Mn^{2+}, Mn^{3+}, Mn^{4+}, Mn^{6+} and Mn^{7+}, and the redox reactions of Mn^{4+}/Mn^{3+} and Mn^{4+}/Mn^{2+} can provide high redox potential and one or two-electron transfer, which will lead to high specific capacity as well as high energy density. For MnO_2 materials, their theoretical capacity is 308 mAh g^{-1} based on one-electron transfer and 617 mAh g^{-1} based on two-electron transfer [34, 35]. Tarascon et al. first reported the electrochemical reaction of sodium with λ-MnO_2 in 1 M $NaClO_4$ in propylene carbonate [36]. They found that Na reaction with λ-MnO_2 induced an irreversible phase transformation to Na_xMnO_2, which could reversibly cycle 0.6 Na atom for each Mn atom. In aqueous electrolyte of 1 M Na_2SO_4, λ-MnO_2 cathode material showed excellent energy storage functionality with a specific capacity of ~ 80 mAh g^{-1} [37]. Using 7 M NaOH solution as electrolyte, γ-MnO_2 cathode material displayed a discharge capacity of 225 mAh g^{-1} [38]. However, the reversible capacity of MnO_2 cathode material was still lower than its theoretical capacity in aqueous electrolyte. Except for MnO_2 materials, $Na_{0.44}MnO_2$, as a promising cathode material, has been

© The authors https://doi.org/10.1007/s40820-023-01162-x

widely investigated for aqueous SIBs because of low cost and high theoretical capacity (120 mAh g^{-1}) [39]. However, $Na_{0.44}MnO_2$ electrode usually showed a reversible capacity lower than 50 mAh g^{-1} in aqueous electrolyte [40, 41]. In addition, Mn-based Prussian blue analogues and polyanion compounds have also been reported. Sun et al. investigated $Na_2MnFe(CN)_6$ electrode in 1 M Na_2SO_4 aqueous solution and obtained a reversible capacity of about 85 mAh g^{-1} [42]. Gao et al. reported $Na_3MnTi(PO_4)_3$ material as cathode and anode, and a symmetric cell based on 1 M Na_2SO_4 electrolyte exhibited a reversible capacity of 57.9 mAh g^{-1} [43]. Different Mn-based electrode materials presented various electrochemical performance.

In order to improve the electrochemical performance of Mn-based electrode materials in aqueous electrolyte, some effective improvement methods, such as electrolyte optimization, element doping, morphology optimization and carbon modification, have been proposed. For example, by adding 2 M $MgSO_4$ to Na_2SO_4 solution, the reversible capacity of δ-MnO_2 electrode in Na_2SO_4 solution increased from 40 to 100 mAh g^{-1} [44]. With calcium doping, rate capability of calcium-doped $Na_{0.4}MnO_2$ electrode in 1 M $NaClO_4$ solution was enhanced (43% capacity increase at 50C rate) [45]. Using reduced graphene oxide to modify $Na_2MnFe(CN)_6$ material, the discharge capacity of $Na_2MnFe(CN)_6$ electrode increased from 71.0 to 115.4 mAh g^{-1}, and its cycling performance was also improved [46]. To date, different Mn-based electrode materials have been investigated for aqueous SIBs and their electrochemical performance has been improved. In this review, we give an overview about Mn-based electrode materials (both cathodes and anodes) for aqueous SIBs, including oxides, Prussian blue analogues and polyanion compounds. Figure 1 shows the contents. We summarize and discuss the composition, crystal structure, morphology, electrochemical properties and improvement methods. We believe this review is helpful to understand and develop Mn-based electrode materials for aqueous SIBs.

2 Mn-Based Cathode Materials

Various Mn-based materials have been reported as cathode materials for aqueous SIBs, including oxides, Prussian blue analogues and polyanion compounds. Different Mn-based cathode materials exhibit diverse electrochemical performance.

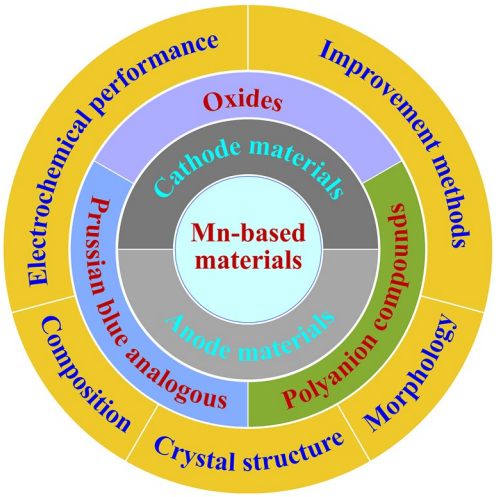

Fig. 1 Outline of the Mn-based electrode materials for aqueous SIBs

2.1 Oxides

Among Mn-based cathode materials for aqueous SIBs, oxides are the most common materials, including MnO_2, Mn_5O_8, Na_xMnO_2, $Na_xMn_yTi_{1-y}O_2$, etc. Different oxides possess various crystal structures and show diverse electrochemical performance. In this section, different Mn-based oxides will be introduced and improvement methods of electrochemical performance are also summarized.

2.1.1 MnO_2

MnO_2 has been widely studied as a cathode material for rechargeable batteries. MnO_2 possesses several crystallographic structures, including α, β, γ, δ and λ crystal structures. The α-, β- and γ-MnO_2 show 1D tunnel structure, the δ-MnO_2 exhibits 2D layered structure, and the λ-MnO_2 possesses 3D spinel structure [47, 48]. MnO_6 octahedra are the basic units for constructing these crystal structures of MnO_2 via sharing corners and/or edges. These crystal structures possess different gaps of tunnels or interlayers, which affect intercalation/deintercalation of alkali cations in MnO_2 lattice [48]. The electrochemical performance of MnO_2 with different crystal structures has also been investigated in aqueous SIBs.

2.1.1.1 Electrochemical Performance MnO_2 with different crystal structures displays various electrochemical per-

formance. Whitacre et al. investigated the electrochemical performance of λ-MnO_2 material in 1 M Na_2SO_4 solution using activated carbon (AC) as anode [37]. Figure 2a shows the discharge curve of λ-MnO_2 electrode, and the discharge capacity is about 80 mAh g^{-1}. The λ-MnO_2 electrode had high specific capacity (twofold increase) and specific energy (threefold increase) compared with the $Na_4Mn_9O_{18}$ electrode. A thin λ-MnO_2/AC full cell (electrode thickness of < 100 μm) exhibited outstanding cycling performance, and there was no loss in initial capacity for 5000 cycles, as shown in Fig. 2b. The stability of λ-MnO_2 cathode material might result from the introduction of proton or hydroxide species into the lattice, the stability of H_2O/MnO_2 interface, and stable AC anode material. Furthermore, using graphite sheet as counter electrode, a high initial discharge capacity of 390.7 mAh g^{-1} at 13.6 mA g^{-1} was obtained for λ-MnO_2 electrode in 1 M Na_2SO_4 solution (Fig. 2c) [49]. The discharge capacity was higher than theoretical capacity (308 mAh g^{-1}), which could result from the surface adsorption–desorption of Na ions resulting in slight capacitive behavior during the initial charge–discharge. However, using AC as anode, a λ-MnO_2|Na_2SO_4|AC capacitor battery showed only a discharge capacity of 115.3 mAh g^{-1} at

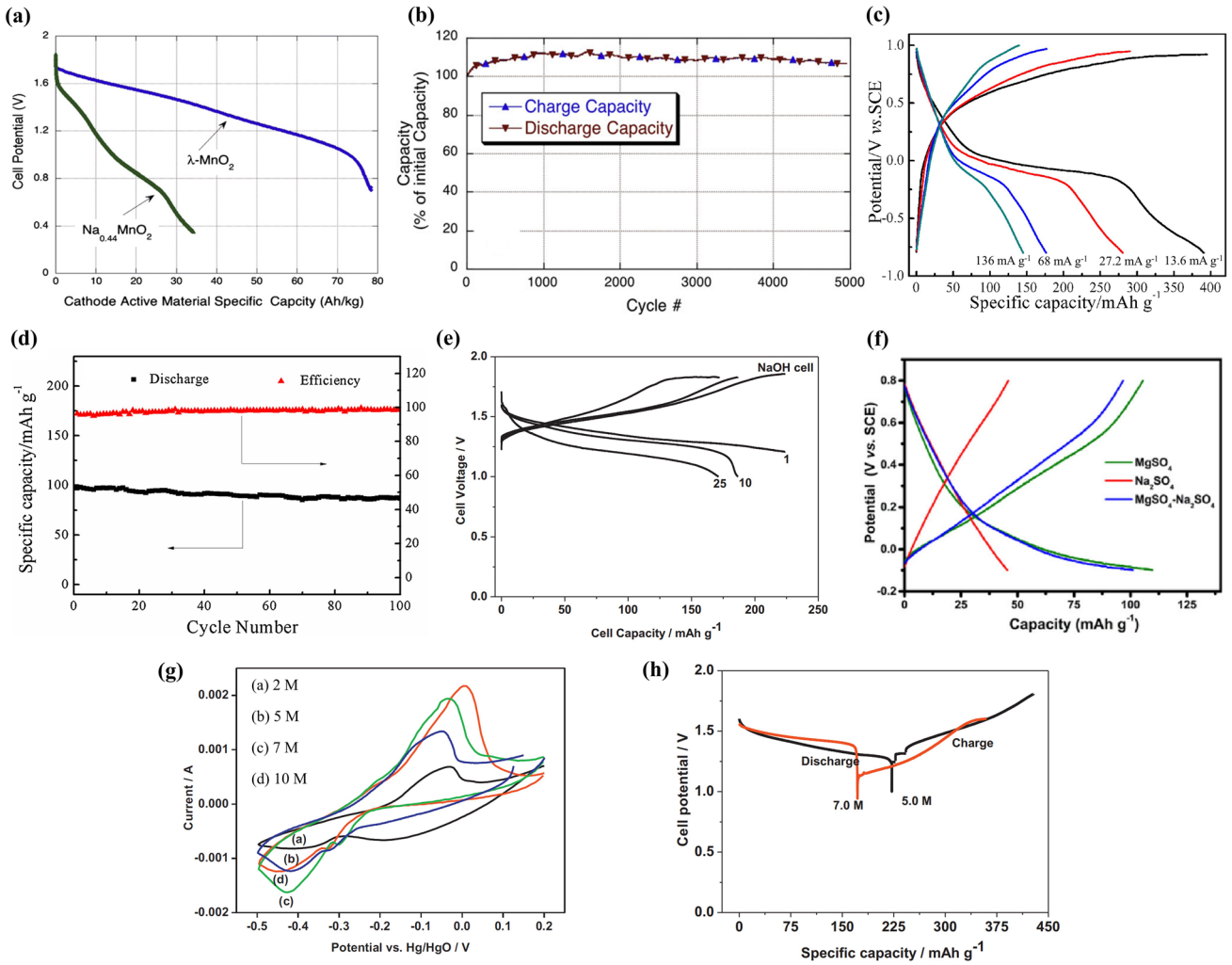

Fig. 2 **a** Discharge curves of λ-MnO_2 and $Na_4Mn_9O_{18}$ in 1 M Na_2SO_4 solution. **b** Charge–discharge cycle testing of a thin λ-MnO_2 electrode cell up to 5000 cycles [37]. Copyright 2012, Elsevier. **c** Charge and discharge curves for λ-MnO_2 electrode in 1 M Na_2SO_4 solution at different current densities. **d** The cycling performance of anλ-MnO_2|Na_2SO_4|AC capacitor battery at 136 mA g^{-1} [49]. Copyright 2014, Elsevier. **e** Cyclability of a γ-MnO_2|NaOH|Zn cell using 7 M NaOH electrolyte [38]. Copyright 2012, Elsevier. **f** Charge and discharge curves of δ-MnO_2 electrode in different electrolytes: 1 M Na_2SO_4, 2 M $MgSO_4$ and 1 M Na_2SO_4-2 M $MgSO_4$ solutions [44]. Copyright 2019, Elsevier. **g** CV curves of γ-MnO_2 electrode in 2, 5, 7 and 10 M NaOH solutions. **h** Discharge–charge profiles of γ-MnO_2|Zn cells using 5 M and 7 M NaOH solutions [50]. Copyright 2013, Elsevier

© The authors https://doi.org/10.1007/s40820-023-01162-x

68 mA g^{-1}, and the capacity retention was more than 90% after 100 cycles (Fig. 2d).

Apart from λ-MnO_2, γ-MnO_2 cathode material was investigated by Minakshi using Zn as anode and 7 M NaOH solution as electrolyte [38]. A γ-MnO_2|NaOH|Zn cell displayed a discharge capacity of 225 mAh g^{-1} at 8 mA g^{-1}, and the discharge capacity decreased to 171 mAh g^{-1} at 25th cycle (Fig. 2e). There was 24% capacity loss after 25 cycles, and the capacity degradation could be attributed to the anodic dissolution of Zn and the MnO_2 electrode incorporating some Zn during discharge processes, which could inhibit the sodium intercalation.

In addition, δ-MnO_2 cathode material was studied in three different electrolyte solutions (1 M Na_2SO_4, 2 M $MgSO_4$ and 1 M Na_2SO_4-2 M $MgSO_4$) using AC as counter electrode [44]. As shown in Fig. 2f, the reversible capacity of δ-MnO_2 in 1 M Na_2SO_4 solution was about 40 mAh g^{-1} at 200 mA g^{-1}, and the reversible capacity increased to 100 mAh g^{-1} for 1 M Na_2SO_4-2 M $MgSO_4$ solution, which suggested that the presence of $MgSO_4$ in the electrolyte changed dramatically the electrochemical performance of δ-MnO_2.

From the above discussion, it is clear that the crystal structure of MnO_2 has a great impact on its reversible capacity and cycling performance. Among various crystal structures, λ-MnO_2 material exhibited better electrochemical performance. In addition, counter electrode and aqueous electrolyte also affected the electrochemical performance of MnO_2 electrode.

2.1.1.2 Improvement Methods MnO_2, especially γ-MnO_2 and δ-MnO_2, presented low electrochemical performance in aqueous electrolyte, which was needed to be further improved. Electrolyte optimization and element doping have been adopted to improve the electrochemical performance of MnO_2 electrode materials.

(1) **Optimization of Electrolyte**

The electrochemical performance of MnO_2 could be improved by optimizing aqueous electrolytes. Minakshi and Meyrick investigated the effect of NaOH concentration on the electrochemical performance of γ-MnO_2 cathode [50]. Cyclic voltammetric (CV) curves of γ-MnO_2 electrode in NaOH solutions with various concentrations (2, 5, 7 and 10 M) are shown in Fig. 2g, and the best electrochemical performance was obtained in 7 M NaOH solution. The discharge capacities of MnO_2|Zn cells were 220 and 170 mAh g^{-1} for 5 and 7 M NaOH solutions (Fig. 2h), respectively. After 40 cycles, the capacity retention for both the MnO_2|Zn cells was more than 90%. As a result, the electrochemical performance of γ-MnO_2 cathode could be optimized by increasing NaOH concentration, and the highest reversible capacity was obtained in 5 M NaOH solution electrolyte.

Except for optimizing electrolyte concentration, electrolyte additive was also adopted to improve electrochemical performance. Liu et al. presented the effect of $MgSO_4$ addition into Na_2SO_4 solution on the electrochemical performance of δ-MnO_2 cathode [44]. With the addition of 2 M $MgSO_4$, the specific capacity of δ-MnO_2 cathode increased from 40 to 100 mAh g^{-1} (Fig. 2f). The improvement could be attributed to the reversible co-intercalation of Na^+ and Mg^{2+}, which is similar to the storage mechanism of Na-Mg hybrid battery. In co-intercalation-type Na-Mg hybrid battery, Na^+ and Mg^{2+} dual-ion electrolyte was adopted, and Na^+ and Mg^{2+} ions could be intercalated/deintercalated into cathode [51]. Therefore, optimizing the aqueous electrolyte can enhance effectively the electrochemical performance of MnO_2 electrodes.

(2) **Element Doping or Incorporating**

Element incorporating was adopted to improve the electrochemical performance of MnO_2. Nanostructured δ-MnO_2 incorporated with K and Na ions was investigated by Liu et al. [52]. The synthesized (K, Na)-incorporated δ-MnO_2 materials were $K_{0.34}MnO_2$ (KMO), $Na_{0.56}MnO_2$ (NMO) and $K_{0.15}Na_{0.26}MnO_2$ (KNMO), which had different morphologies, as shown in Fig. 3a. The reversible discharge capacities were 64, 30 and 66.4 mAh g^{-1} at 200 mA g^{-1} for KMO, NMO and KNMO electrodes in 1 M Na_2SO_4 solution using $NaTi_2(PO_4)_3$ as anodes (Fig. 3b), respectively. The incorporation of K and Na ions into δ-MnO_2 affected greatly the electrochemical properties of layered δ-MnO_2, and the KNMO and KMO electrodes not only had high capacity but also exhibited superior rate capability (Fig. 3c). The KNMO electrode showed superior reversible capacity and outstanding cycling stability with 90% capacity retention (Fig. 3d). The excellent electrochemical performance of the KNMO and KMO nanospheres could be attributed to adequate crystallinity and hierarchical structure.

In addition, hierarchical layered $K_{0.27}MnO_2$ microflowers and hollow $K_{0.27}MnO_2$ nanospheres (Fig. 3e) were also investigated in 1 M Na_2SO_4 solution using $NaTi_2(PO_4)_3$ as

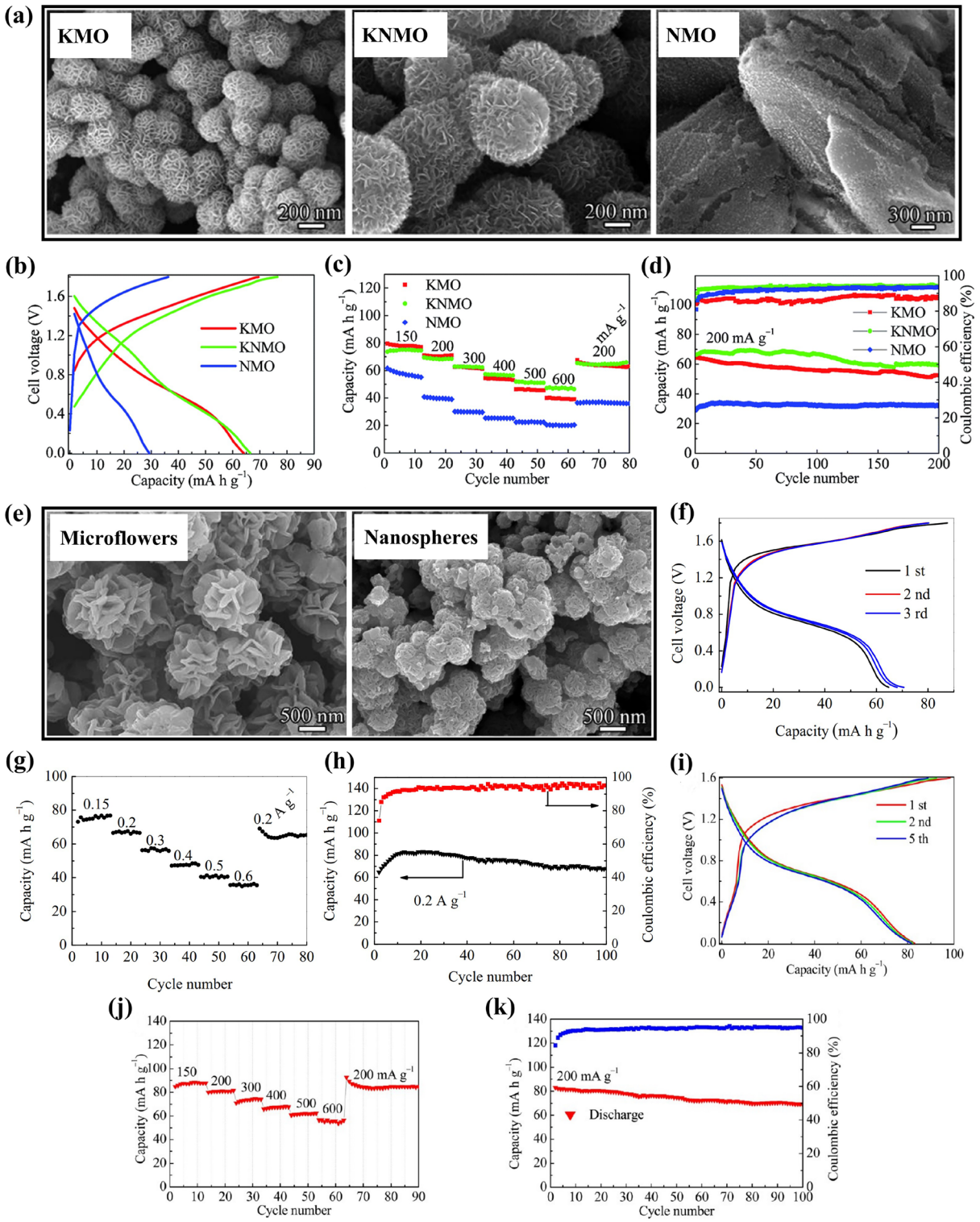

Fig. 3 **a** SEM (scanning electron microscope) images of KMO, KNMO and NMO. **b** Charge/discharge profiles (at 200 mA g^{-1}), **c** Capacity retention at different current densities and **d** Cycling performance (at 200 mA g^{-1}) of $NaTi_2(PO_4)_3$|KMO, $NaTi_2(PO_4)_3$|KNMO and $NaTi_2(PO_4)_3$|NMO full cells [52]. Copyright 2015, Royal Society of Chemistry. **e** SEM images of hierarchical layered $K_{0.27}MnO_2$ microflowers and hollow $K_{0.27}MnO_2$ nanospheres. **f** Charge/discharge profiles (at 200 mA g^{-1}), **g** Capacity retention at different current densities and **h** Cycling performance (at 200 mA g^{-1}) of $NaTi_2(PO_4)_3$|$K_{0.27}MnO_2$ microflowers full cell. [53]. Copyright 2014, Elsevier. **i** Charge/discharge profiles (at 200 mA g^{-1}), **j** Capacity retention at different current densities and **k** Cycling performance (at 200 mA g^{-1}) of $NaTi_2(PO_4)_3$|$K_{0.27}MnO_2$ nanospheres full cell [54]. Copyright 2016, American Chemical Society

© The authors https://doi.org/10.1007/s40820-023-01162-x

anode [53, 54]. A full cell with $K_{0.27}MnO_2$ microflowers attained an initial discharge capacity of 64.7 mAh g^{-1} at 200 mA g^{-1} (Fig. 3f), and exhibited excellent rate capability (Fig. 3g) and long cyclic life without capacity loss after 100 cycles (Fig. 3h). Compared with the full cell with $K_{0.27}MnO_2$ microflowers, a full cell assembled using hollow $K_{0.27}MnO_2$ nanospheres demonstrated a high initial discharge capacity of 83 mAh g^{-1} at 200 mA g^{-1} (Fig. 3i). The full cell with hollow $K_{0.27}MnO_2$ nanospheres also displayed excellent rate performance (Fig. 3j) and high cyclic stability up to 100 cycles with 83% capacity retention (Fig. 3k). By comparing Fig. 3b, f, it could be found that when changing $K_{0.34}MnO_2$ to $K_{0.27}MnO_2$, voltage plateaus in the charge and discharge curves increased, but the reversible capacities were almost the same. From Fig. 3e to Fig. 3k, it could be concluded that the particle size and morphology of $K_{0.27}MnO_2$ particles affected the electrochemical performance of $K_{0.27}MnO_2$ electrode. Thus, the electrochemical performance of (K, Na)-incorporated δ-MnO_2 materials could be significantly enhanced by optimizing incorporation content of K and Na ions and tuning their particle size and morphology.

Apart from element incorporating, doping of Ni, Co and Fe ions into MnO_2 has also been investigated to enhance its electrochemical performance. Shan et al. reported a framework Ni-doped δ-MnO_2 ((Ni)MnO_2) material as cathode material [55]. The (Ni)MnO_2 nanosheets were synthesized by wet chemistry method, and their transmission electron microscopy (TEM) image was shown in Fig. 4a. A symmetric full cell assembled with (Ni)MnO_2 electrodes and 1 M Na_2SO_4 solution as electrolyte delivered a discharge capacity of 63 mAh g^{-1} at 200 mA g^{-1}, and superior cycle stability without capacity loss over 2000 cycles at 200–2000 mA g^{-1} (Fig. 4b-c). The storage of Na ions in (Ni)MnO_2 electrode was a single-phase solid-solution reaction. The pseudocapacitive Na-ion storage, which was promising for high-rate performance [56–58], was enhanced by the framework Ni-doping which formed solid-solution type layered structure with disordered [NiO_6] octahedra in intralayer framework of ordered [MnO_6] octahedra. Similar to Ni doping, Co-doped MnO_2 was also investigated by Shan et al. [59]. However, a framework Co-doped δ-MnO_2 material was unable to be formed by wet chemistry method, and the synthesized material was biphase cobalt-manganese oxide (Co-Mn–O) comprised of $(Co_{0.83}Mn_{0.13}Va_{0.04})_{tetra}(Co_{0.38}Mn_{1.62})_{octa}O_{3.72}$ (Va: vacancy; tetra: tetrahedral sites; octa: octahedral sites) spinel phase and $MnO_2{\cdot}H_2O$ birnessite phase. As shown in Fig. 4d, the synthesized Co-Mn–O nanomaterials had two distinct morphologies: nanoparticle and 2D nanosheet. The biphase Co-Mn–O material displayed also excellent electrochemical performance, and a symmetric full cell based on biphase Co-Mn–O electrodes and 1 M Na_2SO_4 electrolyte demonstrated a reversible discharge capacity of 81 mAh g^{-1} at 2000 mA g^{-1}, high rate performance (57 mAh g^{-1} at 10,000 mA g^{-1}) (Fig. 4e) and long-term cycling stability (no obvious capacity degradation over 5000 cycles) (Fig. 4f). The improved electrochemical performance of the Co-Mn–O material could be attributed to the synergistic interaction between spinel phase and birnessite phase and the vacancy of the tetrahedral sites of spinel phase.

Furthermore, Usui et al. investigated the effect of Fe doping on the electrochemical performance of MnO_2 electrodes in aqueous Na_2SO_4 solution [60]. Compared with MnO_2 electrodes, the Fe-doped MnO_2 electrodes exhibited higher reversible capacity (Fig. 4g). The Fe doping into MnO_2 reduced the IR drop and enhanced the capacity, and in particular, the IR drop reduction and capacity increase for δ-MnO_2 electrode were significant because of the improvement in the conductivity (from 3.7×10^{-7} to 3.0×10^{-6} S cm^{-1} with 11 at% Fe doping). Figure 4h gives the cycling performance of α-MnO_2, δ-MnO_2, Fe-doped α-MnO_2 and Fe-doped δ-MnO_2 electrodes. In the initial 100 cycles, the Fe-doped α-MnO_2 electrode had the highest capacitance. The Fe-doped δ-MnO_2 electrode exhibited the best cycling performance with the capacity retention of 87% after 500 cycles. Accordingly, element doping or incorporating is a very effective approach to improve the electrochemical performance of MnO_2 electrode materials.

In summary, MnO_2 materials are suitable to be used as cathode materials for aqueous SIBs, and their electrochemical performance can be effectively improved by optimizing electrolyte, element doping or incorporating, and tuning particle size and morphology. The electrochemical properties of MnO_2 materials mentioned above are summarized in Table 1.

2.1.2 Na_xMnO_2

Various Na_xMnO_2 materials have been studied as cathode materials for aqueous SIBs, including $Na_{0.27}MnO_2$, $Na_{0.35}MnO_2$, $Na_{0.4}MnO_2$, $Na_{0.44}MnO_2$, $Na_{0.58}MnO_2$,

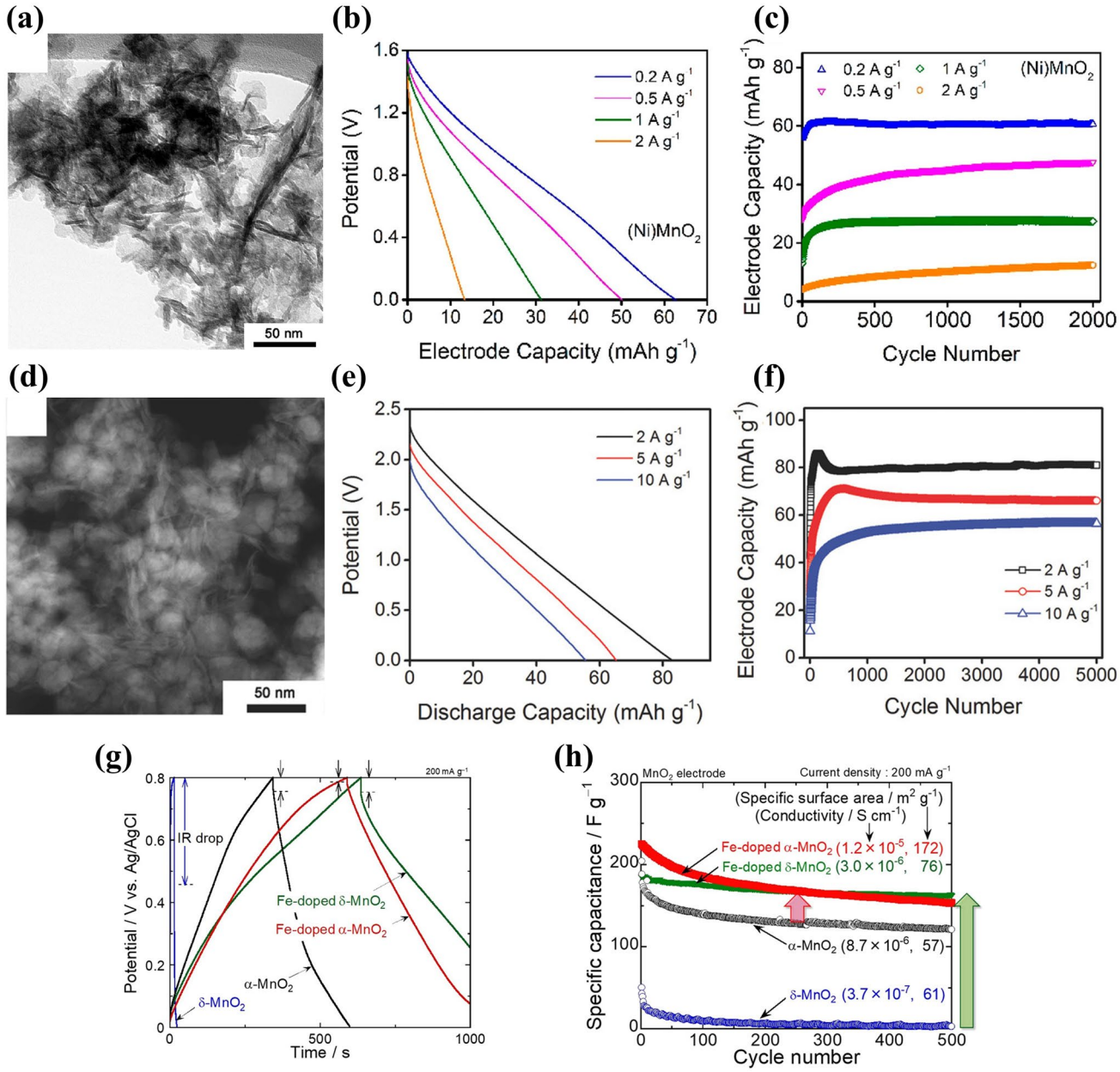

Fig. 4 **a** TEM image of (Ni)MnO_2 nanosheets. **b** Discharge curves of (Ni)MnO_2 electrode at various current densities. **c** Cycling performance of (Ni)MnO_2 electrode at various current densities [55]. Copyright 2019, American Chemical Society. **d** TEM image of Co-Mn–O nanomaterials. **e** Discharge curves of biphase Co-Mn–O electrode at various current densities. **f** Cycling performance of biphase Co-Mn–O electrode at various current densities [59]. Copyright 2017, Wiley–VCH. **g** Charge–discharge curves for MnO_2 and Fe-doped MnO_2 electrodes in 0.5 M Na_2SO_4 solution at the second cycle. **h** Dependence of specific capacitance on cycle number for MnO_2 and Fe-doped MnO_2 electrodes [60]. Copyright 2020, American Chemical Society

$Na_{0.7}MnO_2$, $Na_{0.95}MnO_2$, $NaMnO_2$ and doped/substituted Na_xMnO_2. These Na_xMnO_2 cathode materials have different composition, crystal structures and morphologies, which affect their electrochemical performance.

2.1.2.1 Electrochemical Performance Na_xMnO_2 can be classified into tunnel-type oxides and layered oxides. With Na content $x \geq 0.5$, Na_xMnO_2 presents a two-dimensional layered structure [30, 61, 62]. When $x \leq 0.44$, Na_xMnO_2 exhibits a three-dimensional tunnel structure [61, 63].

© The authors https://doi.org/10.1007/s40820-023-01162-x

Table 1 Electrochemical properties of the Mn-based oxides for aqueous SIBs

Working electrode	Counter electrode	Electrolyte	Voltage range (V)	Capacity (mAh g^{-1}) Rate (mA g^{-1})	Capacity retention (%) (cycles)	Refs.
λ-MnO_2	AC	1 M Na_2SO_4	0.7–1.8	80 (-)	No decay (5000)	[37]
λ-MnO_2	Graphite	1 M Na_2SO_4	−0.8–1.0	390.7 (13.6)	59 (500)	[49]
λ-MnO_2	AC	1 M Na_2SO_4	0.1–2.2	115.3 (68)	90 (100)	[49]
γ-MnO_2	Zn	7 M NaOH	1.0–1.8	225 (8)	76 (25)	[38]
γ-MnO_2	Zn	5 M NaOH	1.0–1.8	220 (8)	90 (40)	[50]
δ-MnO_2	AC	1 M Na_2SO_4	−0.1–0.8	40 (200)	No decay (100)	[44]
δ-MnO_2	AC	1 M Na_2SO_4 − 2 M $MgSO_4$	−0.1–0.8	100 (200)	86 (100)	[44]
$K_{0.15}Na_{0.26}MnO_2$	$NaTi_2(PO_4)_3$	1 M Na_2SO_4	0–1.8	66.4 (200)	90 (200)	[52]
$K_{0.34}MnO_2$	$NaTi_2(PO_4)_3$	1 M Na_2SO_4	0–1.8	64 (200)	81 (200)	[52]
$K_{0.27}MnO_2$	$NaTi_2(PO_4)_3$	1 M Na_2SO_4	0–1.8	64.7 (200)	No decay (100)	[53]
$K_{0.27}MnO_2$	$NaTi_2(PO_4)_3$	1 M Na_2SO_4	0–1.6	83 (200)	83 (100)	[54]
Ni-doped δ-MnO_2	Ni-doped δ-MnO_2	1 M Na_2SO_4	0–1.6	63 (200)	No decay (2000)	[55]
$Co_xMn_{3-x}O_4$-δ-MnO2	$Co_xMn_{3-x}O_4$-δ-MnO_2	1 M Na_2SO_4	0–2.5	81 (2000)	No decay (5000)	[59]
$Na_{0.27}MnO_2$	Pt	0.1 M Na_2SO_4	−0.75–1.25	138 (600)	–	[64]
$Na_{0.27}MnO_2$	$Na_{0.27}MnO_2$	0.5 M Na_2SO_4	0–2.5	83 (1000)	No decay (5000)	[64]
$Na_{0.35}MnO_2$	Ni	0.5 M Na_2SO_4	0–1.0	43.6 (200)	No decay (5000)	[65]
$Na_{0.39}MnO_2$	AC	1 M $NaClO_4$-0.1 M $LiNO_3$	0–0.8	45.1 (60)	90.3 (1000)	[94]
$Na_{0.44}MnO_2$	$Na_{0.44}MnO_2$-coated stainless steel	0.5 M Na_2SO_4	0.25–0.9	40 (12.1)	–	[40]
$Na_{0.44}MnO_2$	Graphite	1.5 M $NaNO_3$	−0.1–0.95	48 (60)	94 (90)	[69]
$Na_{0.44}MnO_2$	Pt	1 M Na_2SO_4	0–0.6	43.7 (122.5)	86.2 (100)	[41]
$Na_{0.44}MnO_2$	$NaTi_2(PO_4)_3$/C	1 M Na_2SO_4	0–1.6	43 (100)	60 (1000)	[72]
$Na_{0.44}MnO_2$	Zn	1 M Na_2SO_4	1.0–1.9	45 (100)	-	[93]
$Na_{0.44}MnO_2$	Zn	1 M Na_2SO_4-0.5 M $ZnSO_4$-0.05 M $MnSO_4$	1.0–1.9	63 (100)	No decay (170)	[93]
$Na_{0.44}MnO_2$	Pt	1 M Na_2SO_4	-0.3–1.0	77.2 (100)	80 (1000)	[98]
$Na_{0.44}MnO_2$-CNT	Pt	1 M Na_2SO_4	0–0.8	65 (50)	63.4 (300)	[104]
$Na_{0.58}MnO_2{\cdot}0.48H_2O$	Ti	1 M Na_2SO_4	-0.1–0.8	80 (80)	No decay (1000)	[83]
$Na_{0.7}MnO_{2.05}$	Ti	1 M Na_2SO_4	0–0.8	52 (50)	90.1(600)	[85]
$Na_{0.95}MnO_2$	Ni	0.5 M Na_2SO_4	0–1.0	25.6 (200)	No decay (5000)	[65]
$Na_{0.95}MnO_2$	Zn	0.5 M CH_3COONa- 0.5 M $Zn(CH_3COO)_2$	1–2	60	92 (1000)	[86]
$NaMnO_2$	Ti	2 M CH_3COONa	0–1.0	55 (60)	No decay (500)	[88]
$Ca_{0.07}Na_{0.26}MnO_2$	AC	1 M $NaClO_4$	-0.1–1.6	40 (-)	98.8 (1000)	[45]
$Na_{0.5}Mn_{0.5}Ti_{0.5}O_2$	Desodiated NiHCF	6 M $NaClO_4$	0–1.0	46 (30)	95 (100)	[100]
$Na_{0.66}Mn_{0.66}Ti_{0.34}O_2$	$NaTi_2(PO_4)_3$/C	1 M Na_2SO_4	0.3–1.7	76 (236)	89 (300)	[99]
Mn_5O_8	Mn_5O_8	1 M Na_2SO_4	0–3.0	116 (5000)	No decay (2000)	[112]
Mn_5O_8	Mn_5O_8	1 M Na_2SO_4	0–3.0	103 (5000)	No decay (5000)	[113]

(1) Na_xMnO_2 ($x < 0.44$)

Only a few Na_xMnO_2 ($x < 0.44$) materials have been reported for aqueous SIBs. A sodium-rich disordered birnessite, $Na_{0.27}MnO_2$, was reported by Shan et al. [64]. The $Na_{0.27}MnO_2$ materials synthesized by solid-state method had planar structure (Fig. 5a). Upon water intercalation, $Na_{0.27}MnO_2$ became $Na_{0.27}MnO_2{\cdot}0.63H_2O$. The $Na_{0.27}MnO_2$ electrode exhibited an initial discharge capacity of 138 at 600 mA g^{-1} in 0.1 M Na_2SO_4 solution using Pt as counter electrode, and the discharge capacity decreased from 115

to 61 mAh g^{-1} at 600–2000 mA g^{-1} with increasing the current density (Fig. 5b). However, a symmetric full cell with $Na_{0.27}MnO_2$ electrodes and 1 M Na_2SO_4 electrolyte showed nearly linear charge–discharge profiles and a discharge capacity of 83 mAh g^{-1} at 1000 mA g^{-1} (Fig. 5c). The full cell exhibited excellent cycle stability without obvious capacity loss up to 5000 cycles at various current densities (Fig. 5d). The improved electrochemical performance could be ascribed to Na-rich disordered structure and structural water, as well as co-deintercalation of sodium-ion and hydrated water at high potential charge.

With increasing Na content, $Na_{0.35}MnO_2$ material was reported. Zhang et al. synthesized nanowire $Na_{0.35}MnO_2$ by hydrothermal method and investigated its electrochemical performance in 0.5 M Na_2SO_4 solution with Ni counter

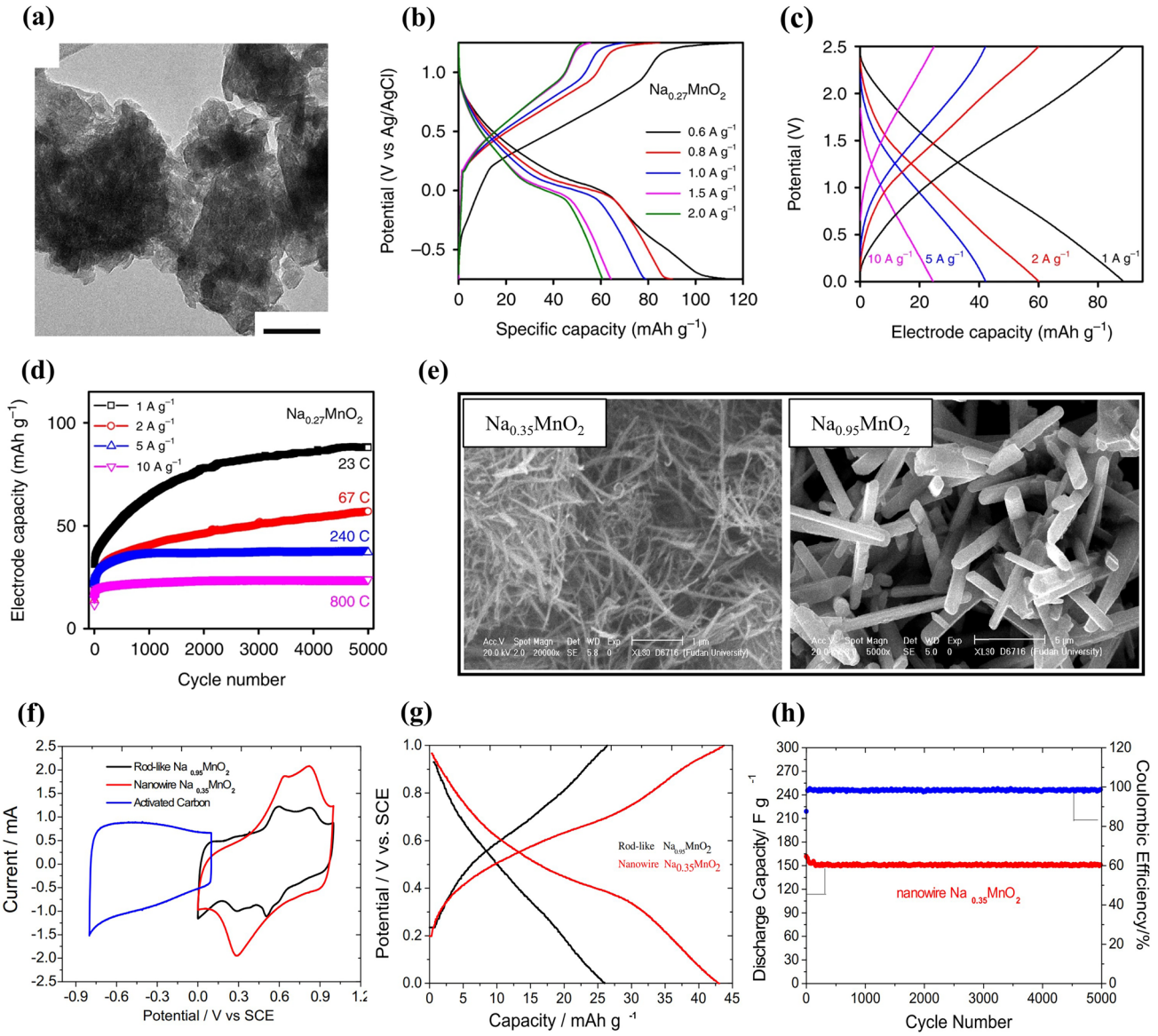

Fig. 5 **a** TEM image of $Na_{0.27}MnO_2$ materials (scale bar, 50 nm). **b** Charge–discharge profiles of $Na_{0.27}MnO_2$ electrode at 600–2000 mA g^{-1} (2^{nd} cycle data). **c** Charge–discharge profiles of a symmetric full cell with $Na_{0.27}MnO_2$ electrodes (after 5000 charge–discharge process). **d** Cycling performance of a symmetric full cell with $Na_{0.27}MnO_2$ electrodes at various current densities [64]. Copyright 2019, The Authors(s). **e** SEM images of nanowire $Na_{0.35}MnO_2$ and rod-like $Na_{0.95}MnO_2$. **f** CV curves of $Na_{0.35}MnO_2$ and $Na_{0.95}MnO_2$ electrodes in 0.5 M Na_2SO_4 solution at 5 mV s^{-1}. **g** Change-discharge curves and **h** Cycling performance of $Na_{0.35}MnO_2$ and $Na_{0.95}MnO_2$ electrodes at 200 mA g^{-1} [65]. Copyright 2013, Elsevier

© The authors
https://doi.org/10.1007/s40820-023-01162-x

electrode [65]. For comparison, rod-like $Na_{0.95}MnO_2$ particles were prepared by solid-state reaction, and their SEM images were shown in Fig. 5e. Two separated sharp redox peaks could be observed in CV curves for $Na_{0.35}MnO_2$ electrode (Fig. 5f), which corresponded to intercalation/deintercalation of sodium ions. In contrast, $Na_{0.95}MnO_2$ electrode showed two small redox couples, indicating capacitive and pseudocapacitive property. The discharge capacity (43.6 mAh g^{-1}) of $Na_{0.35}MnO_2$ electrode was higher than that of $Na_{0.95}MnO_2$ electrode (25.6 mAh g^{-1}) (Fig. 5g), which could be caused by smaller particle size and larger surface area of $Na_{0.35}MnO_2$ nanowires. The $Na_{0.35}MnO_2$ electrode also presented excellent cycling performance without capacity degradation after 5000 cycles (Fig. 5h). In addition, a full cell assembled using $Na_{0.35}MnO_2$ nanowires, polypyrrole (PPy)-coated MoO_3 (PPy@MoO_3) nanobelts and 0.5 M Na_2SO_4 solution delivered an energy density of 20 Wh kg^{-1} at 80 W kg^{-1} and better cycling behavior with only 21% capacity loss after 1000 cycles [66]. Although $Na_{0.35}MnO_2$ electrode exhibited excellent cycle stability without capacity degradation up to 5000 cycles, its reversible capacity was very much low compared to $Na_{0.27}MnO_2$ electrode, which could be related to different structure (disordered structure for $Na_{0.27}MnO_2$) and structural water.

(2) **Na_xMnO_2 (x = 0.44)**

Tunnel-type $Na_{0.44}MnO_2$ materials have been widely studied as cathode materials for SIBs [67, 68]. Many $Na_{0.44}MnO_2$ cathode materials have also been reported for aqueous SIBs. Kim et al. investigated the intercalation/deintercalation behavior of sodium ions in $Na_{0.44}MnO_2$ in both aqueous (0.5 M Na_2SO_4) and non-aqueous (1 M $NaClO_4$) electrolytes [40]. Rod-shaped $Na_{0.44}MnO_2$ particles were synthesized by modified Pechini method, and their morphology was shown in Fig. 6a. Only three plateaus in the discharge curves for $Na_{0.44}MnO_2$ electrode in aqueous electrolyte were observed (Fig. 6b) in comparison with six plateaus for $Na_{0.44}MnO_2$ electrode in non-aqueous electrolyte (Fig. 6c). This indicated that only part of Na ions could be extracted from $Na_{0.44}MnO_2$ electrode in aqueous electrolyte. As a result, the discharge capacity of $Na_{0.44}MnO_2$ electrode in aqueous electrolyte was 40 mAh g^{-1} at 12.1 mA g^{-1}, which was lower than that in non-aqueous electrolyte (65 mAh g^{-1}). However, the $Na_{0.44}MnO_2$ electrode displayed enhanced rate capability in aqueous electrolyte with capacity retention of 82% (from 0.1C to 1C), which was higher than that in non-aqueous electrolyte (49%). The differences could be attributed to different apparent diffusion coefficient of Na ions as well as charge transfer resistance and additional resistance from SEI (solid electrolyte interphase) layer.

Besides, in different aqueous electrolytes, the $Na_{0.44}MnO_2$ electrodes exhibited various electrochemical performance. In 1 M Na_2SO_4 solution, $Na_{0.44}MnO_2$ nanorods demonstrated a reversible discharge capacity of 43.7 mAh g^{-1} with platinum wire as counter electrode [41]. A reversible discharge capacity of about 50 mAh g^{-1} at 60 mA g^{-1} was obtained for $Na_{0.44}MnO_2$ (rod-like morphology) electrode in 1.5 M $NaNO_3$ solution using graphite plate as counter electrode [69]. In 6 M NaOH solution, $Na_{0.44}MnO_2$ electrode displayed a high reversible capacity of 80.2 mAh g^{-1} at 0.5C with Zn as counter electrode [70]. This indicated that aqueous electrolytes had a greatly impact on the electrochemical performance of $Na_{0.44}MnO_2$ electrodes.

Furthermore, some full cells using $Na_{0.44}MnO_2$ cathodes were also investigated. A novel $Na_{0.44}MnO_2$|phenazine full cell based on 10 M NaOH solution showed excellent rate capacity and ultralong cycling life with 80% capacity retention after 13,000 cycles [71]. Based on 1 M Na_2SO_4 solution, $Na_{0.44}MnO_2$|$NaTi_2(PO_4)_3$ full cells also delivered better electrochemical performance [72, 73]. At current rate of 90C, the capacity retention was more than 70% (compared to the capacity at 3C) (Fig. 6d). After 700 cycles at different rates (from 5 to 50C to 5C), the full cell still held about 60% capacity at 5C (compared to the first cycle) (Fig. 6e). The better electrochemical performance could result from good structural stability of anode and cathode in water during high rate electrochemical reaction. Apart from these full cells, similar full cells based on $Na_{0.44}MnO_2$ cathodes with various anodes, including $NaTi_2(PO_4)_3$/C [74], wafer-like $NaTi_2(PO_4)_3$/C [75], frogspawn-like $NaTi_2(PO_4)_3$/C [76], $NaTi_2(PO_4)_3$/MWNTs (multiwalled carbon nanotube) [77], $NaV_3(PO_4)_3$@C nanofiber [78], $Na_2V_6O_{16}{\cdot}nH_2O$ [79], PNP@CNT (polyimide-MWCNT composite) [80], amorphous $FePO_4{\cdot}2H_2O$ [81], TiP_2O_7 [82], have also been reported, and much improved electrochemical performance has been obtained.

In general, among all the Na_xMnO_2 materials, tunnel-type $Na_{0.44}MnO_2$ shows high atmospheric and electrochemical stability [63], leading to high rate capability and better cycling performance, but it usually presents a low specific capacity of less than 80 mAh g^{-1}. Tunnel-type

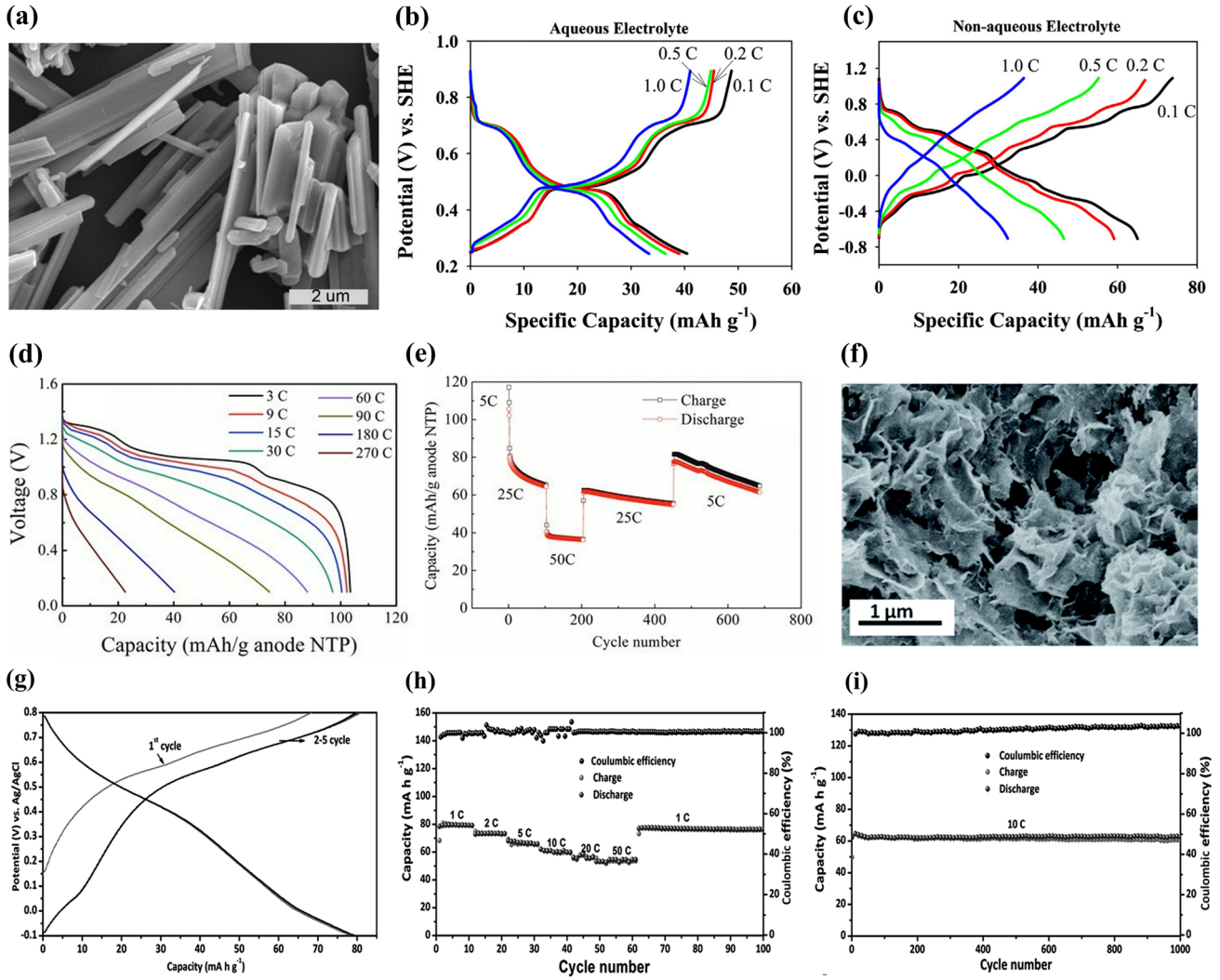

Fig. 6 **a** SEM image of the synthesized $Na_{0.44}MnO_2$ particles. Charge–discharge curves of $Na_{0.44}MnO_2$ electrode in **b** aqueous electrolyte and **c** non-aqueous electrolyte at different current densities [40]. Copyright 2013, Elsevier. **d** Discharge curves and **e** cycling performance of $Na_{0.44}MnO_2$|$NaTi_2(PO_4)_3$ full cell at different rates [73]. Copyright 2013, Wiley-VCH. **f** SEM image of the synthesized $Na_{0.58}MnO_2{\cdot}0.48H_2O$. **g** Charge–discharge profiles of $Na_{0.58}MnO_2{\cdot}0.48H_2O$ electrode at 1C. **h** Rate capability of $Na_{0.58}MnO_2{\cdot}0.48H_2O$ electrode. **i** Cycling performance of $Na_{0.58}MnO_2{\cdot}0.48H_2O$ electrode at 10C [83]. Copyright 2016, Royal Society of Chemistry

$Na_{0.44}MnO_2$ is considered as a promising cathode material for aqueous SIBs due to its unique crystal structure and stability.

(3) Na_xMnO_2 ($x > 0.5$)

Compared with tunnel-type oxides, layered oxides usually exhibited high specific capacity. Zhang et al. synthesized layered structure $Na_{0.58}MnO_2{\cdot}0.48H_2O$ by precipitation method [83]. The $Na_{0.58}MnO_2{\cdot}0.48H_2O$ consisted of wrinkled thin sheets (Fig. 6f). A reversible capacity of 80 mAh g^{-1} was obtained at 1C (80 mA g^{-1}) for $Na_{0.58}MnO_2{\cdot}0.48H_2O$ electrode in 1 M Na_2SO_4 solution using Ti counter electrode (Fig. 6g). The $Na_{0.58}MnO_2{\cdot}0.48H_2O$ electrode exhibited also high rate capability (Fig. 6h) and excellent cycling performance (Fig. 6i). The reversible discharge capacities were 67, 57 and 54 mAh g^{-1} at 5C, 20C and 50C, respectively, and there was no capacity loss after 1000 cycles. The superior electrochemical performance of $Na_{0.58}MnO_2{\cdot}0.48H_2O$ electrode could be attributed to the superior Na-ion storage properties of $Na_{0.58}MnO_2{\cdot}0.48H_2O$ and the crystal water in $Na_{0.58}MnO_2{\cdot}0.48H_2O$ which could decrease charge transfer resistance and improve the conductance of Na ions.

© The authors https://doi.org/10.1007/s40820-023-01162-x

Furthermore, $Na_{0.7}MnO_2$ cathode material was also reported. Rakocevic et al. synthesized 3D tunnel structured $Na_{0.4}MnO_2$ nanorods (800 °C), hexagonal-layered α-$Na_{0.7}MnO_{2.05}$ nanoplates (850 °C), and 3D tunnel structured $Na_{0.44}MnO_2$ powders with rod-like morphology (900 °C) by glycine nitrate method, and investigated their electrochemical behavior in aqueous $NaNO_3$ solution using platinum foil as counter electrode [84]. The $Na_{0.7}MnO_{2.05}$ electrode showed the highest initial discharge capacity, and the initial discharge capacities were 50, 75 and 46 mAh g^{-1} for $Na_{0.4}MnO_2$, $Na_{0.7}MnO_{2.05}$ and $Na_{0.44}MnO_2$, respectively. However, micron-sized $Na_{0.7}MnO_{2.05}$ (about 2 μm, as shown in Fig. 7a) prepared by a sol–gel method delivered a low discharge capacity of 22.1 mAh g^{-1} at 50 mA g^{-1} in 1 M Na_2SO_4 solution (Fig. 7b) [85]. The discharge capacity increased with increasing cycle number and a discharge capacity of 52 mAh g^{-1} was obtained at the 100th cycle, which could be attributed to the battery activation. After 600 cycles, the $Na_{0.7}MnO_{2.05}$ electrode remained 48 mAh g^{-1} capacity with capacity retention of 90.1% (capacity of the 100th cycle) (Fig. 7c). The $Na_{0.7}MnO_{2.05}$ electrode also exhibited good rate performance (Fig. 7d), and the reversible capacities were 42.9, 41.0 and 38.0 mAh g^{-1} at 200, 300 and 400 mA g^{-1}, respectively. However, the electrochemical performance of $Na_{0.7}MnO_{2.05}$ electrode is poor compared to $Na_{0.58}MnO_2{\cdot}0.48H_2O$ electrode.

In addition, Na_xMnO_2 materials with higher sodium content were also investigated for aqueous SIBs. Zhang et al. synthesized rod-like $Na_{0.95}MnO_2$ particles (Fig. 7e) by solid-state reaction [86]. A full cell $Na_{0.95}MnO_2$|Zn with 0.5 M CH_3COONa-0.5 M $Zn(CH_3COO)_2$ electrolyte exhibited a reversible discharge capacity of 60 mAh g^{-1} at 2C and good cycling performance over 1000 cycles at 4C with only 8% capacity loss, as shown in Fig. 7f-g. The full cell was also regarded as Na-Zn hybrid battery, which used two-component electrolyte (Na^+ and Zn^{2+} coexisting) [87]. Compared to single ion batteries, the Na-Zn hybrid battery could exhibit high electrochemical performance due to different ion intercalation mechanisms in different electrolytes. Hou et al. reported that $NaMnO_2$ cathode material (about 1–2 μm, as shown in Fig. 7h) displayed a discharge capacity of 55 mAh g^{-1} at 1C (60 mA g^{-1}) in 2 M CH_3COONa solution using Ti counter electrode (Fig. 7i) [88]. The $NaMnO_2$ electrode also showed high rate performance with discharge capacity of 50 mAh g^{-1} at 10C (Fig. 7j), and good cycling performance without obvious capacity loss after 500 cycles (Fig. 7k). A $NaMnO_2$|$NaTi_2(PO_4)_3$/C full cell gave an energy density of 30 Wh kg^{-1} at 50 W kg^{-1} and showed 75% capacity retention after 500 cycles at 5C.

In brief, the Na_xMnO_2 materials with different sodium content, crystal structure and morphology exhibit various electrochemical performance. Tunnel-type oxides show better cycling performance, and layered oxides display relatively high specific capacity. Among the Na_xMnO_2 materials, $Na_{0.44}MnO_2$ materials have been widely investigated and showed better electrochemical performance.

2.1.2.2 Improvement Methods For practical application, the electrochemical performance of Na_xMnO_2 materials, especially rate capability and cycling performance, should be further enhanced. Some methods have been adopted to improve the electrochemical performance of Na_xMnO_2 cathode materials, including electrolyte optimization, morphology optimization, element doping or substitution, and carbon modification.

(1) **Optimization of Electrolyte**

First, electrolyte salt concentration was optimized to improve the electrochemical performance of Na_xMnO_2 cathode. Wu et al. examined the effect of $NaClO_4$ concentration on electrochemical performance of a $Na_{0.44}MnO_2$|$NaTi_2(PO_4)_3$ full cell [89]. As shown in Fig. 8a, the redox peaks were sharper and closer at higher concentration, which was consistent with ionic conductivity increase of $NaClO_4$ electrolyte (the highest ionic conductivity at 5 M). With increasing concentration, the equilibrium potentials shifted to more positive values. The $NaClO_4$ concentration affected strongly the discharge capacity, in particularly, at higher rate (Fig. 8b), and the capacity retention at 1.5C was 13.3%, 37.8% and 54.8% (capacity at 0.1C) for 0.1, 1 and 5 M $NaClO_4$, respectively. Similarly, high discharge capacity and good capacity retention were obtained for $Na_{0.44}MnO_2$ cathode in saturated $NaClO_4$ solution (not 1 M and 8 M $NaClO_4$) because of low Mn dissolution in high concentration electrolyte [90]. High concentration electrolyte improving the electrochemical performance of $Na_{0.44}MnO_2$ was proved in NaOH aqueous electrolyte [91]. A $Na_{0.44}MnO_2$|Zn dual-ion battery showed the best rate performance in 6–8 M NaOH solution. When the NaOH concentration exceeded 8 M, the rate performance became poor. The capacity retention after 500 cycles was 27.4%,

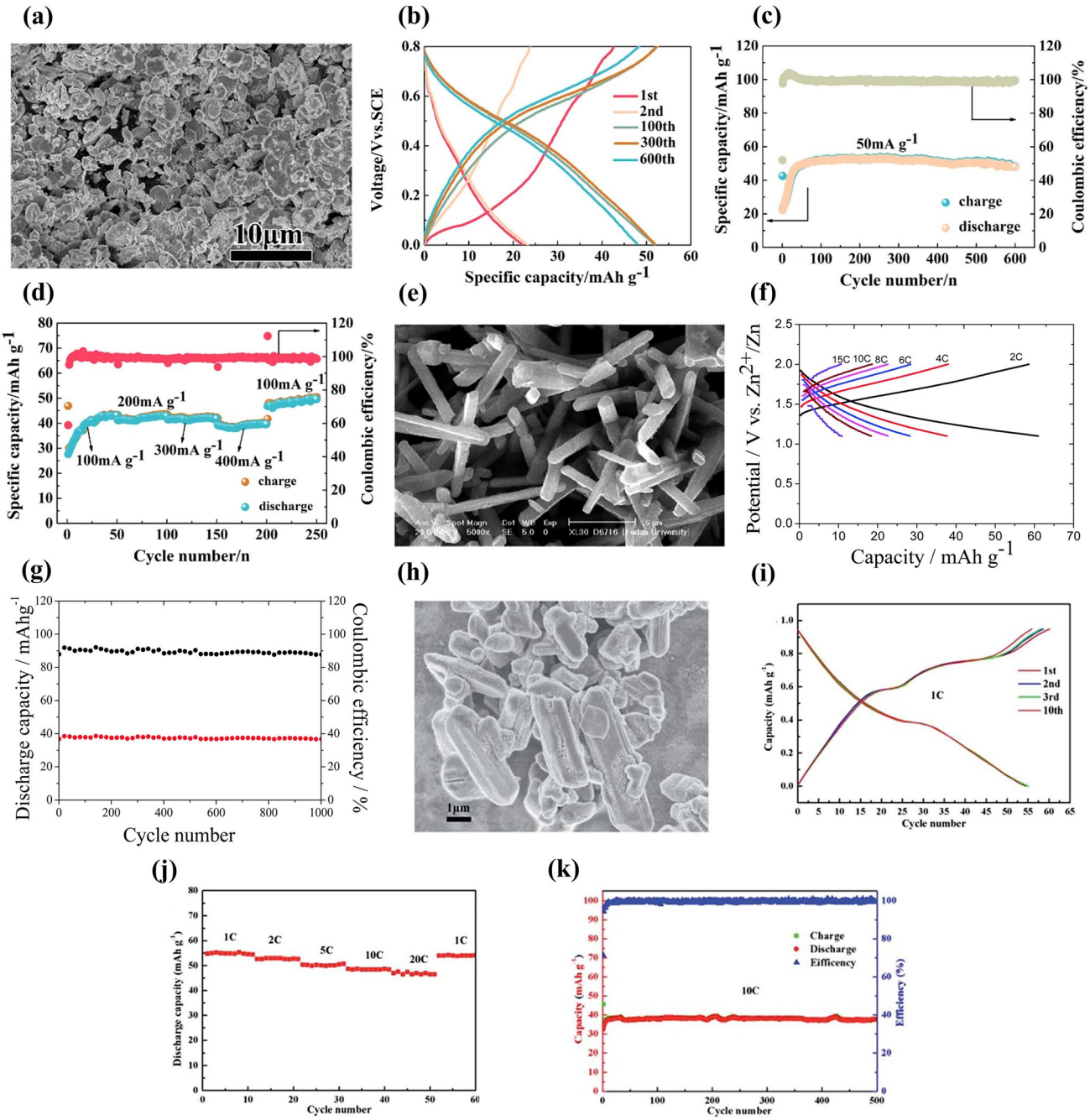

Fig. 7 **a** SEM image of the prepared $Na_{0.7}MnO_{2.05}$ powders. **b** Charge/discharge profiles at 50 mA g^{-1}, **c** Cycling performance at 50 mA g^{-1} and **d** Rate performance of the $Na_{0.7}MnO_{2.05}$ electrodes in 1 M Na_2SO_4 with Ti counter electrode [85]. Copyright 2020, Springer. **e** SEM image of the prepared $Na_{0.95}MnO_2$ particles. **f** Charge–discharge curves of the rod-like $Na_{0.95}MnO_2$ electrode at different rates with Zn counter electrode. **g** Cycling performance of a $Na_{0.95}MnO_2$|Zn full cell at 4C [86]. Copyright 2014, Royal Society of Chemistry. **h** SEM image of the $NaMnO_2$. **i** Discharge/charge curves at 1C, **j** Rate capability and **k** Cycling performance at 10C of the $NaMnO_2$ electrode [88]. Copyright 2015, Royal Society of Chemistry

33.2%, 54.2%, 64.3% and 65.8% in 1, 3, 6, 8 and 10 M NaOH, respectively. Better cycling stability was obtained in higher NaOH concentration, which could be caused by the reduction of water redox activity and side reactions in high concentration. In addition, $Na_{0.66}Mn_{0.66}Ti_{0.34}O_2$ electrode also presented better electrochemical performance in

© The authors https://doi.org/10.1007/s40820-023-01162-x

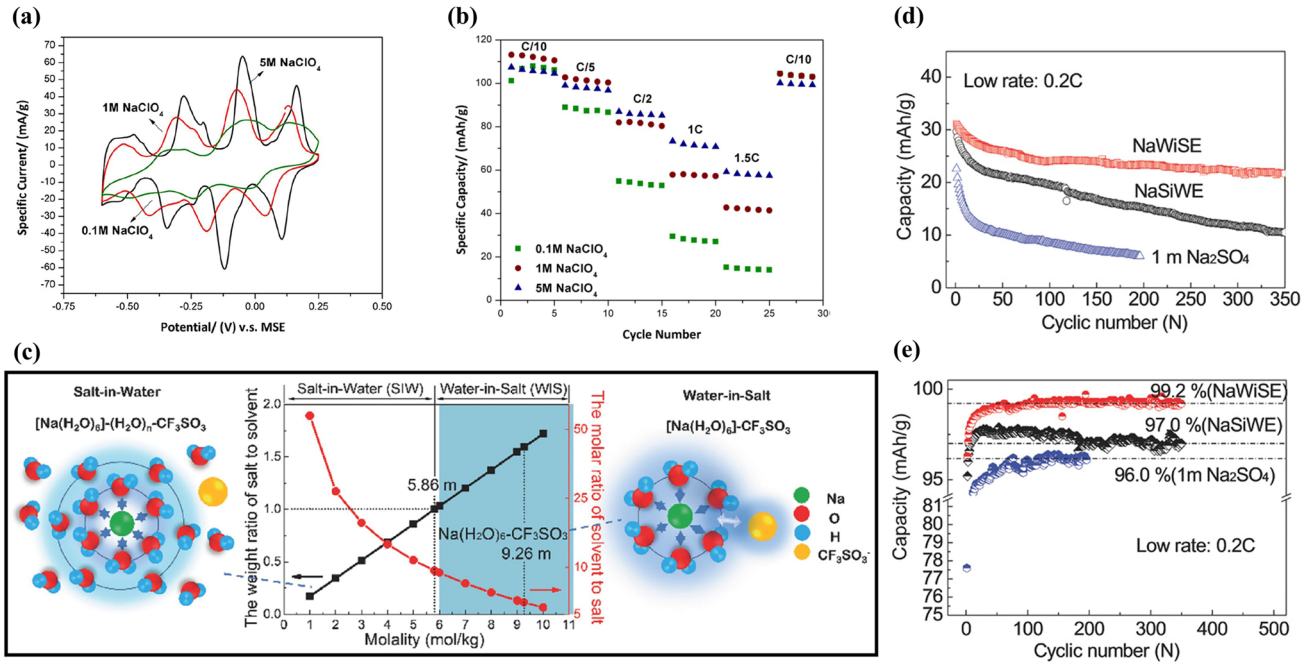

Fig. 8 **a** CV curves of $Na_{0.44}MnO_2$ electrode in 0.1–5 M $NaClO_4$ solution at scan rate of 0.1 mV s^{-1}. **b** Rate performance of $Na_{0.44}MnO_2$|$NaTi_2(PO_4)_3$ full cell ($Na_{0.44}MnO_2$ electrode: 100 mg cm^{-2} with thickness of 950 μm; carbon-coated $NaTi_2(PO_4)_3$ electrode: 113 mg cm^{-2} with thickness of 530 μm) with different $NaClO_4$ concentrations: 0.1 M, 1 M and 5 M [89]. Copyright 2015, The Author(s). **c** The molar and weight salt/solvent ratios in $NaCF_3SO_3$-H_2O binary system. **d** Cycle life and **e** Coulombic efficiency of $Na_{0.66}Mn_{0.66}Ti_{0.34}O_2$|$NaTi_2(PO_4)_3$ full cells in 1 M Na_2SO_4, 2 M $NaCF_3SO_3$ (NaSiWE) and 9.26 M $NaCF_3SO_3$ (NaWiSE) electrolytes at 0.2C [92]. Copyright 2017, Wiley-VCH

"water-in-salt" electrolyte compared to in "salt-in-water" electrolyte [92]. As shown in Fig. 8c, for Na^+ in dilute aqueous solutions with salt concentration below 5 M (salt-in-water), its solvation sheath was composed of at least two layers. However, when salt concentration was above 9 M (water-in-salt), the resultant solution could be visualized as a liquefied salt, which could lead to some new properties including transport and interphasial chemistry. As a result, among the full cells $Na_{0.66}Mn_{0.66}Ti_{0.34}O_2$|$NaTi_2(PO_4)_3$ with 1 M Na_2SO_4, 2 M $NaCF_3SO_3$ (NaSiWE) and 9.26 M $NaCF_3SO_3$ (NaWiSE) electrolytes, the full cell with NaWiSE displayed the highest capacity, the best cycling stability and the highest coulombic efficiency (Fig. 8d–e). The superior electrochemical performance could be attributed to the formation of Na^+-conducting SEI, which suppressed the water decomposition. Therefore, optimizing the electrolyte salt concentration can effectively improve the electrochemical performance.

Second, electrolyte additives were adopted to improve the electrochemical performance of Na_xMnO_2 cathode. Bai et al. investigated the effect of addition of $ZnSO_4$ and $MnSO_4$ into Na_2SO_4 solution on electrochemical performance of $Na_{0.44}MnO_2$ cathode [93]. The $Na_{0.44}MnO_2$ electrode in various electrolytes exhibited different CV curves (Fig. 9a–d). With the addition of $ZnSO_4$ and $MnSO_4$, there were new redox couples observed, which could be related to the intercalation/deintercalation of Zn ions and oxidation/reduction of Mn^{2+}. Therefore, the $Na_{0.44}MnO_2$ electrode in various electrolytes also displayed different charge–discharge behavior (Fig. 9e–h). With $ZnSO_4$ addition, the discharge capacity decreased from 45 to 17 mAh g^{-1}, and became very small in the subsequent cycles (Fig. 9f). The rapid fading of capacity implied crystal structure change of $Na_{0.44}MnO_2$. It might be inferred that some Zn ions were inserted into $Na_{0.44}MnO_2$ resulting in collapse of crystal structure. In contrast, with $MnSO_4$ addition, the discharge capacity was enhanced significantly (Fig. 9g), which might be caused by overcharge process. However, with the addition of $ZnSO_4$ and $MnSO_4$, the voltage plateaus became more significant and the discharge capacity increased (Fig. 9h), which could be attributed to synergistic effect between Mn and Zn ions in addition to quasi-reversible

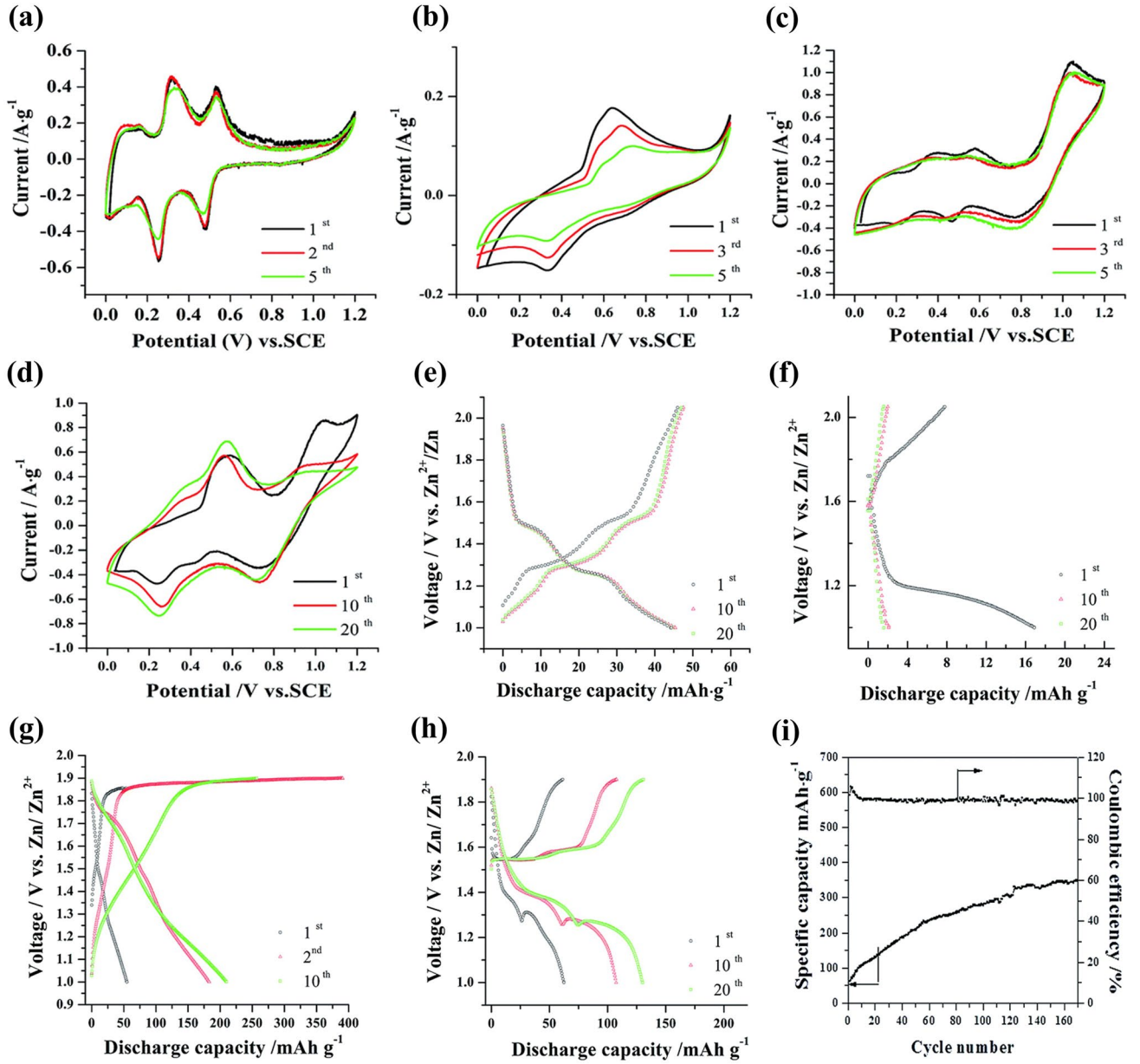

Fig. 9 CV curves at a scan rate of 1 mV s^{-1} of $Na_{0.44}MnO_2$ in different electrolytes: **a** 1 M Na_2SO_4; **b** 1 M Na_2SO_4 + 0.5 M $ZnSO_4$; **c** 1 M Na_2SO_4 + 0.05 M $MnSO_4$; **d** 1 M Na_2SO_4 + 0.5 M $ZnSO_4$ + 0.05 M $MnSO_4$. Charge–discharge profiles of $Na_{0.44}MnO_2$ at 100 mA g^{-1} in different electrolytes: **e** 1 M Na_2SO_4; **f** 1 M Na_2SO_4 + 0.5 M $ZnSO_4$; **g** 1 M Na_2SO_4 + 0.05 M $MnSO_4$; **h** 1 M Na_2SO_4 + 0.5 M $ZnSO_4$ + 0.05 M $MnSO_4$. **i** Cycling performance of $Na_{0.44}MnO_2$ in 1 M Na_2SO_4 + 0.5 M $ZnSO_4$ + 0.05 M $MnSO_4$ at 100 mA g^{-1}. Zinc sheets as counter electrodes [93]. Copyright 2016, Royal Society of Chemistry

deposition/dissolution process of Mn ions. The discharge capacity of $Na_{0.44}MnO_2$ electrode in 1 M Na_2SO_4 + 0.5 M $ZnSO_4$ + 0.05 M $MnSO_4$ electrolyte increased dramatically and then remained steady with increasing cycling number (Fig. 9i). Thus, the addition of Zn and Mn ions in aqueous electrolytes has significantly influence on electrochemical performance of $Na_{0.44}MnO_2$ electrode. Except for $ZnSO_4$ and $MnSO_4$, $LiNO_3$ was also used to improve the electrochemical performance of tunnel-type $Na_{0.39}MnO_2$ cathode [94]. A full cell $Na_{0.39}MnO_2$|AC with 1 M $NaClO_4$ + 0.1 M $LiNO_3$ solution delivered an increased discharge capacity of 45.1 mAh g^{-1} at 1C (60 mA g^{-1}) (Fig. 10a), ultrafast rate

© The authors https://doi.org/10.1007/s40820-023-01162-x

capability with a capacity increase of 43% at 16C (Fig. 10b), and superior cycling stability with capacity retention increased from 84.1 to 90.3% after 1000 cycles (Fig. 10c), compared with a full cell without $LiNO_3$ addition in electrolyte. The improved electrochemical performance with $LiNO_3$ addition could be ascribed to increased ionic conductivity of electrolyte solution, co-intercalation of Na ions and Li ions, and lower surface resistance of cathode. Li ions established additional diffusion paths, which activated Na sites. In addition, Guo et al. reported an electrolyte additive of sodium dodecyl sulfate (SDS) for aqueous sodium/zinc battery [95]. The addition of SDS could form an artificial passivation film on $Na_{0.44}MnO_2$ electrode. The passivation film could reduce the formation of the insulating by-product $Zn_4SO_4(OH)_6{\cdot}xH_2O$ on $Na_{0.44}MnO_2$ surface and inhibit the dissolution of $Na_{0.44}MnO_2$. Therefore, a $Na_{0.44}MnO_2$|Zn battery using SDS-modified aqueous electrolyte displayed excellent cycling stability with capacity retention of 93% after 1500 cycles compared with the battery without SDS addition (only 45% capacity retention).

Third, solvent was optimized to improve the electrochemical performance of Na_xMnO_2 cathode. Chua et al. adopted hybrid electrolytes with an ethanol-rich media to attain highly stable Na-ion electrochemistry [96]. An ethanol–water solvent with ethanol–water (Et-Di) volume ratio of 5:1 was used due to the lowest contact angle, and hydrogen bonds were readily formed between ethanol and water molecules. In 1 M NaAc (sodium acetate)-Et/Di electrolyte, a wider electrochemical window of ~ 2.5 V was obtained (Fig. 10d), and the $Na_{0.44}MnO_2$ electrode displayed overlapping CV curves (Fig. 10e), indicating highly reversible insertion/extraction process of Na ions. The discharge capacities were 71.6 and 76.8 mAh g^{-1} at 100 mA g^{-1} in 1 M NaAc-Di and 1 M NaAc-Et/Di electrolytes (Fig. 10f-g), respectively. Notably, the $Na_{0.44}MnO_2$ electrode in 1 M NaAc-Et/Di electrolyte demonstrated much better rate capability (Fig. 10h) and excellent cycling stability (Fig. 10i). The improved electrochemical performance might be attributed to the intrinsic hydrogen-bonding interaction suppressing the water proton's activity. Figure 10j exhibits schematics of the structural evolution and ions storage of $Na_{0.44}MnO_2$ electrode in NaAc-Di and NaAc-Et/Di systems. In water system, Na ions and protons could co-insert into $Na_{0.44}MnO_2$ electrode, and $Na_{0.44}MnO_2$ suffered Mn^{2+} dissolution and irreversible phase transformation to MnOOH during cycling process. In contrast, water proton activity was effectively suppressed by hydrogen bonds with ethanol oxygens in the ethanol–water system. Therefore, the ethanol–water system could result in much higher electrochemical performance. In addition, a deep eutectic electrolyte was developed to improve the electrochemical performance of $Na_{0.44}MnO_2$ cathode by Hou et al. [97]. The deep eutectic electrolyte consisted of 1 mol $NaClO_4{\cdot}H_2O$, 3 mol water and 2 mol urea (named 1-4-2 electrolyte), which had low eutectic point of − 19 °C. The $Na_{0.44}MnO_2$ electrode in the 1-4-2 electrolyte with Pt as counter electrode exhibited a discharge capacity of 75.16 mAh g^{-1} at 0.2C (Fig. 11a) and outstanding rate capacity with discharge capacity of 53.29 mAh g^{-1} at 20C (Fig. 11b). More importantly, the $Na_{0.44}MnO_2$ electrode in the 1-4-2 electrolyte demonstrated a longer cycle life with capacity retention of 95% compared with the $Na_{0.44}MnO_2$ electrode in 1 M Na_2SO_4 electrolyte (65% capacity retention) (Fig. 11c). The water activity and Mn dissolution were suppressed in the 1-4-2 eutectic electrolyte, which were helpful for maintaining the structural integrity of $Na_{0.44}MnO_2$ and improving the cycling stability. Thus, optimizing the solvent can effectively enhance the electrochemical performance.

In a word, the electrochemical performance of Na_xMnO_2 electrodes could be effectively improved by optimizing electrolyte salt concentration, choosing suitable electrolyte additive and optimizing solvent. Therefore, optimizing electrolyte is a very effective method for improving electrochemical performance of aqueous batteries.

(2) Optimization of Morphology

Morphology of electrode materials affects their electrochemical performance. Chua et al. synthesized $Na_{0.44}MnO_2$ rods and $Na_{0.44}MnO_2$ plates by sol–gel method and $Na_{0.44}MnO_2$ particulates by solid-state method, and investigated their electrochemical performance in 1 M Na_2SO_4 solution using Pt foil as counter electrode [98]. The SEM images of the synthesized $Na_{0.44}MnO_2$ samples were shown in Fig. 11d. Among the three samples, $Na_{0.44}MnO_2$ plates delivered the highest discharge capacity of 77.2 mAh g^{-1} at 100 mA g^{-1}, as shown in Fig. 11e. Compared with $Na_{0.44}MnO_2$ particulates and rods, $Na_{0.44}MnO_2$ plates exhibited superior rate capability, and delivered discharge capacities of 83.5, 59.1 and 51.3 mAh g^{-1} at 25, 100 and 500 mA g^{-1} (Fig. 11f). In addition, the $Na_{0.44}MnO_2$ plates also showed excellent cycling performance with a capacity of about 60 mAh

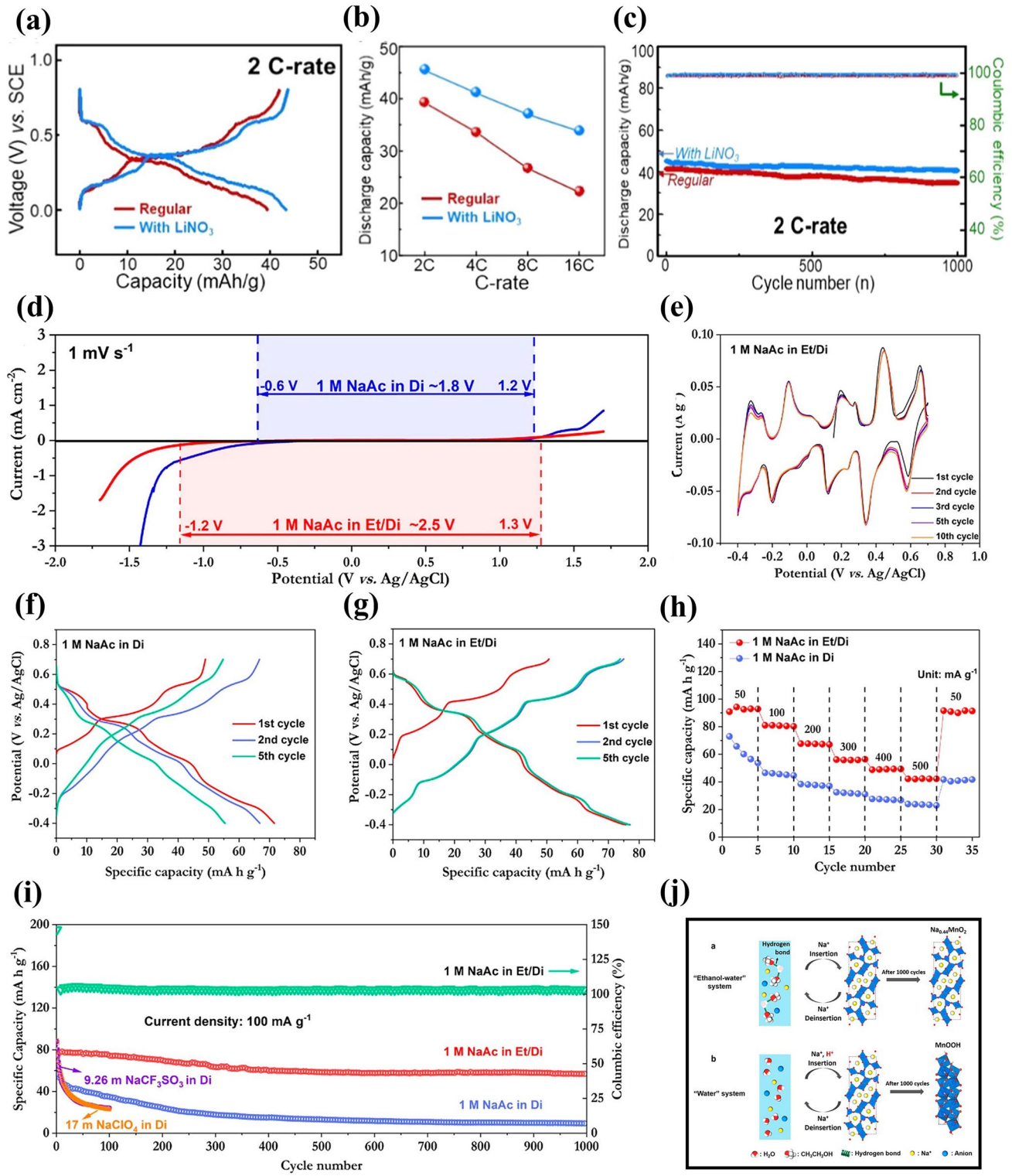

Fig. 10 **a** Charge–discharge profiles, **b** Rate capabilities, **c** Cycling performance of $Na_{0.39}MnO_2$|AC full cells using 1 M $NaClO_4$ electrolytes without and with $LiNO_3$ (0.1 M) addition [94]. Copyright 2020, American Chemical Society. **d** Electrochemical stability of $Na_{0.44}MnO_2$ electrode in 1 M NaAc-Di and 1 M NaAc-Et/Di electrolytes. **e** CV profiles of $Na_{0.44}MnO_2$ electrode in 1 M NaAc–Et/Di electrolyte. Charge–discharge profiles of $Na_{0.44}MnO_2$ electrode in **f** 1 M NaAc-Di and **g** 1 M NaAc-Et/Di electrolytes. **h** Rate capability comparison and **i** Cycling performance of $Na_{0.44}MnO_2$ electrode in 1 M NaAc-Di and 1 M NaAc-Et/Di electrolytes. Using platinum foil and Ag/AgCl as counter and reference electrodes. **j** Schematics of ions storage in water and ethanol–water systems [96]. Copyright 2020, American Chemical Society

© The authors https://doi.org/10.1007/s40820-023-01162-x

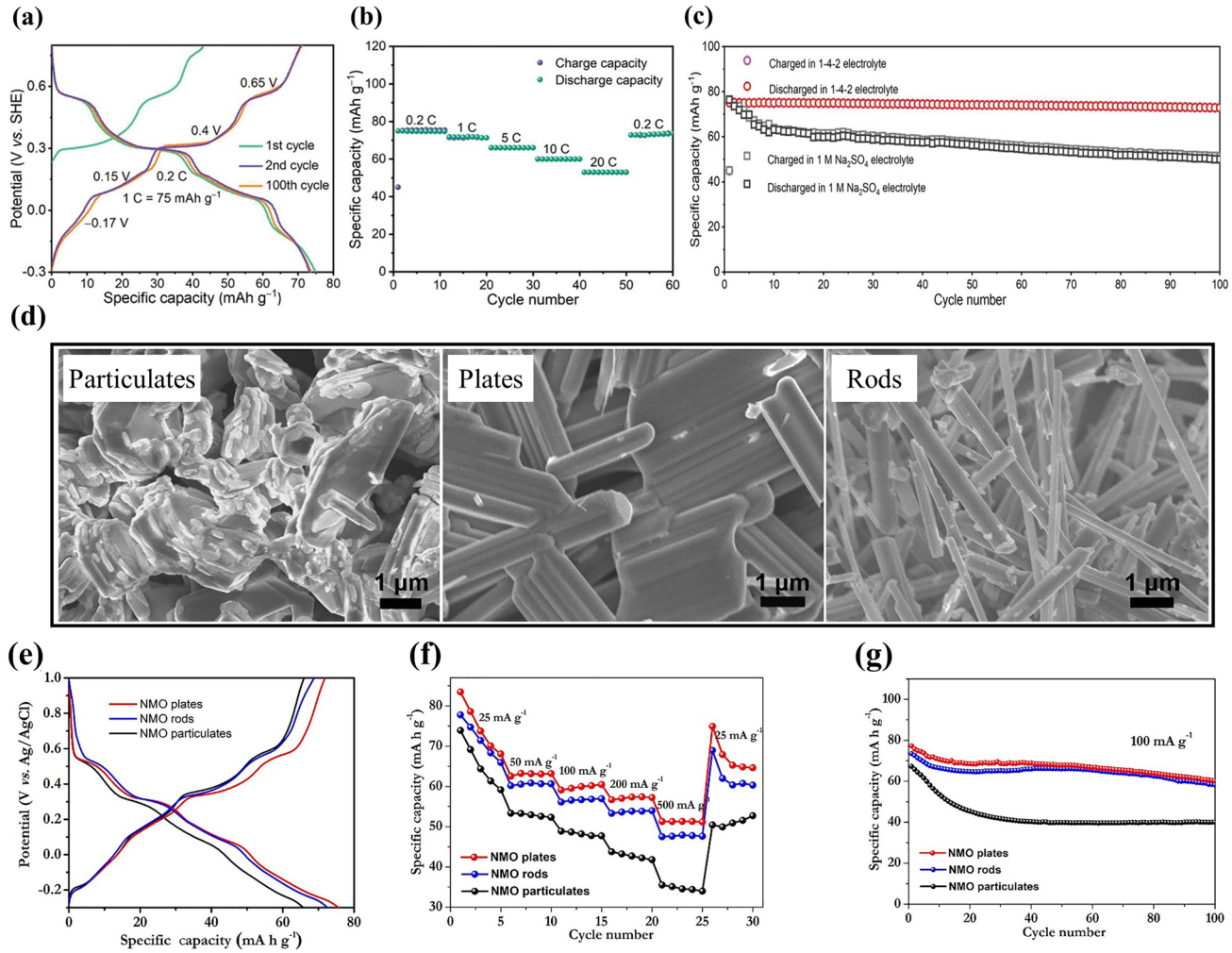

Fig. 11 **a** Charge–discharge curves and **b** Rate performance of $Na_{0.44}MnO_2$ electrode in 1-4-2 electrolyte. **c** Cycling performance of $Na_{0.44}MnO_2$ electrode in 1-4-2 electrolyte and in 1 M Na_2SO4 electrolyte [97]. Copyright 2022, Wiley-VCH. **d** SEM images of the synthesized $Na_{0.44}MnO_2$ samples. **e** Charge and discharge curves from the second cycle of the $Na_{0.44}MnO_2$ samples with different shapes at 100 mA g^{-1}. **f** Rate capability of the $Na_{0.44}MnO_2$ samples with different shapes. **g** Cycling performance of the $Na_{0.44}MnO_2$ samples with different shapes at 100 mA g^{-1} [98]. Copyright 2019, Elsevier

g^{-1} after 100 cycles (Fig. 11g). The excellent electrochemical performance of $Na_{0.44}MnO_2$ plates could be ascribed to the chemical bonded plate structure and the formation of sheet-like Na-birnessite layer on the surface of $Na_{0.44}MnO_2$ plates during charge–discharge cycling. Therefore, the electrochemical performance of Na_xMnO_2 cathode materials can be improved by optimizing their morphology.

(3) Element Doping or Substitution

Element doping is an effective way to improve the electrochemical properties of electrode materials. Calcium-doped $Na_{0.4}MnO_2$, $Ca_{0.07}Na_{0.26}MnO_2$, as cathode material was investigated in 1 M $NaClO_4$ solution by Chae et al. [45]. Figure 12a-c shows the crystal structure of tunnel-type $Na_{0.4}MnO_2$ and its local diffusion pathways of Na(1), Na(2) and Na(3) sites. The doped calcium was placed at the Na(1) site, reduced the neighboring manganese, and formed sodium defects (Na(2) and Na(3) sites) inside the manganese oxide framework. Compared with $Na_{0.4}MnO_2$, $Ca_{0.07}Na_{0.26}MnO_2$ exhibited a broad CV curve with three redox peaks (Fig. 12d). The charge–discharge curve of $Ca_{0.07}Na_{0.26}MnO_2$ electrode also showed three voltage regions divided clearly and a discharge capacity of 40 mAh g^{-1} at 1C (Fig. 12e). The $Ca_{0.07}Na_{0.26}MnO_2$ electrode

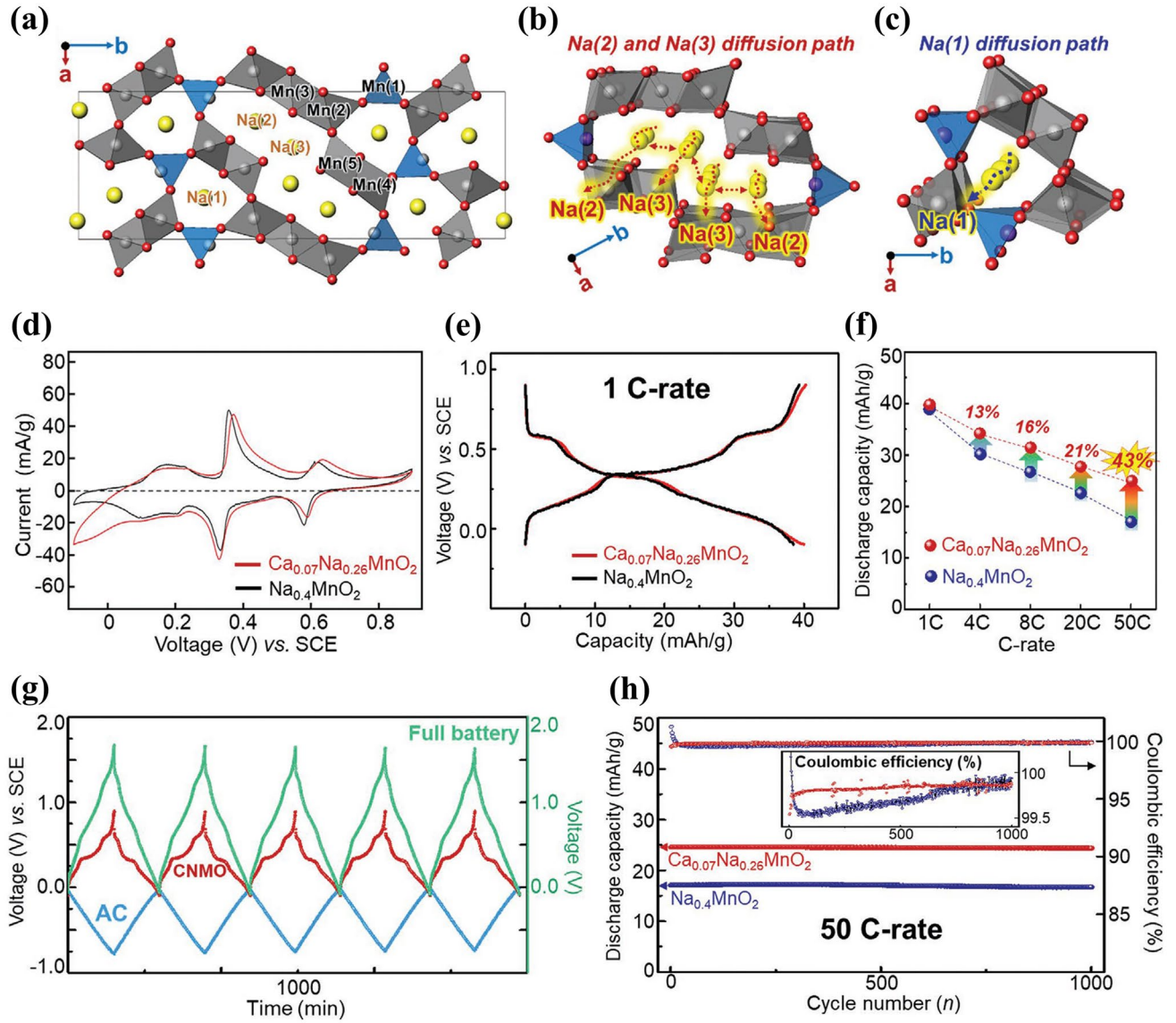

Fig. 12 **a** Unit cell crystal structure, **b** Na(2) and Na(3) diffusion pathways and **c** Na(1) diffusion pathway of tunnel-type $Na_{0.4}MnO_2$. **d** CV curves at a scan rate of 0.1 mV s^{-1} and **e** Charge/discharge curves at 1C of $Na_{0.4}MnO_2$ and $Ca_{0.07}Na_{0.26}MnO_2$ electrodes in 1 M $NaClO_4$ aqueous solution. **f** Rate capability, **g** Charge–discharge profiles, and **h** Cycling performance at 50C of a $Ca_{0.07}Na_{0.26}MnO_2$|AC full cell with 1 M $NaClO_4$ aqueous solution electrolyte [45]. Copyright 2020, Wiley-VCH

demonstrated much enhanced rate capability compared with the $Na_{0.4}MnO_2$ electrode with an increase of 43% at 50C (Fig. 12f). A $Ca_{0.07}Na_{0.26}MnO_2$|AC full cell displayed stable operation of both anode and cathode sides (Fig. 12g) and exhibited superior cycling stability with capacity retention of 98.8% after 1000 cycles (Fig. 12h). The cycling stability could be attributed to the presence of calcium cations (Ca^{2+}) in the structure. Therefore, the calcium doping improved the rate capability and cycling stability of $Na_{0.4}MnO_2$ electrode.

Partial substitution for Mn in Na_xMnO_2 is another effective approach to improve its electrochemical performance. Ti-substituted $Na_xMn_xTi_{1-x}O_2$ cathode materials were investigated for aqueous SIBs. Wang et al. reported a Na-rich tunnel-type $Na_{0.66}Mn_{0.66}Ti_{0.34}O_2$ cathode material [99]. A full cell $Na_{0.66}Mn_{0.66}Ti_{0.34}O_2$|$NaTi_2(PO_4)_3$/C with 1 M Na_2SO_4 electrolyte showed a higher reversible capacity of 76 mAh g^{-1} at 236 mA g^{-1} (2C), which was much higher than that of $Na_{0.44}Mn_{0.44}Ti_{0.56}O_2$|$NaTi_2(PO_4)_3$/C full cell (45 mAh g^{-1}).

© The authors https://doi.org/10.1007/s40820-023-01162-x

In addition, the $Na_{0.66}Mn_{0.66}Ti_{0.34}O_2$|$NaTi_2(PO_4)_3$/C full cell also displayed excellent rate performance with a discharge capacity of 54 mAh g^{-1} at 10C and long-term cycling stability with capacity retention of 89% after 300 cycles at 2C. With increasing Ti content, a $Na_{0.5}Mn_{0.5}Ti_{0.5}O_2$ electrode in 6 M $NaClO_4$ aqueous electrolyte exhibited a discharge capacity of 46 mAh g^{-1} at 30 mA g^{-1} [100], and a $Na_4Mn_4Ti_5O_{18}$ (or $Na_{0.44}Mn_{0.44}Ti_{0.56}O_2$) electrode in 1 M Na_2SO_4 solution delivered an initial discharge capacity of 36 mAh g^{-1} [101]. It can be found that the Ti substitution for Mn can improve the electrochemical performance, but increasing Ti content decreases the reversible discharge capacity. Apart from Ti substitution, partial substitutions of Cu, Fe, Ni and Co have also been reported. Boyd et al. investigated some P2 oxides in 1 M Na_2SO_4 aqueous solution, including $Na_{0.64}Mn_{0.62}Cu_{0.31}O_2$ (NaMCu), $Na_{0.64}Ni_{0.22}Mn_{0.66}Cu_{0.11}O_2$ (NaNMCu), $Na_{0.62}Ni_{0.22}Mn_{0.66}Fe_{0.10}O_2$ (NaNMFe) and $Na_{0.61}Ni_{0.22}Mn_{0.66}Co_{0.10}O_2$ (NaNMCo) [102]. These oxides were synthesized by coprecipitation method and had similar structures and morphologies. The anodic capacities in the first cycle were 30.4, 32.0, 47.7 and 60.9 mAh g^{-1} for NaMCu, NaNMCu, NaNMFe and NaNMCo, respectively. Although NaNMCo displayed higher initial anodic capacity, the water intercalation and phase transformation resulted in microscopic exfoliation and severe damage occurred in NaNMCo. In addition, a $Na_{0.8}Ni_{0.33}Co_{0.33}Mn_{0.33}O_2$ cathode material was reported by Nwanya et al. [103]. The synthesized powders consisted of sheath-like nanoparticles and quasi-spherical nanoparticles. The $Na_{0.8}Ni_{0.33}Co_{0.33}Mn_{0.33}O_2$ electrode showed a discharge capacity of 86 mAh g^{-1} at 50 mA g^{-1} using Pt as counter electrode in 0.5 M Na_2SO_4 solution. Therefore, element doping and partial substitution for Mn in Na_xMnO_2 can greatly enhance its electrochemical performance.

(4) **Carbon Modification**

Carbon nanotubes (CNT) and reduced graphene oxide (RGO) has been used to improve the electrochemical performance of electrode materials. Gu et al. investigated the effect of CNT wrapping on the electrochemical performance of $Na_{0.44}MnO_2$ [104]. CNT wrapping rod-like $Na_{0.44}MnO_2$ ($Na_{0.44}MnO_2$-CNT) was synthesized by solid-state method, and its morphology is shown in Fig. 13a. The CNT wrapping around $Na_{0.44}MnO_2$ particles enhanced the electronic conductivity of $Na_{0.44}MnO_2$. The $Na_{0.44}MnO_2$-CNT electrode in 1 M Na_2SO_4 solution demonstrated a charge capacity of 70.4 mAh g^{-1} at 1C (50 mA g^{-1}), which was higher than that of $Na_{0.44}MnO_2$ electrode (Fig. 13b). After 300 cycles, the reversible capacity retention was about 63.4% for $Na_{0.44}MnO_2$-CNT electrode. The $Na_{0.44}MnO_2$-CNT electrode also showed better rate performance compared with $Na_{0.44}MnO_2$ electrode (Fig. 13c). Therefore, CNT wrapping could improve reversible capacity, rate capability and cycling performance of $Na_{0.44}MnO_2$-CNT electrode.

In addition, $Na_4Mn_9O_{18}$ (more commonly $Na_{0.44}MnO_2$) materials were modified by RGO or CNT for enhancing their electrochemical performance. Yin et al. prepared spherical $Na_4Mn_9O_{18}$-RGO composites by spray-drying method [105]. The $Na_4Mn_9O_{18}$-RGO electrode in 1 M Na_2SO_4 + 0.5 M $ZnSO_4$ solution showed a discharge capacity of 61.7 mAh g^{-1} at 4C in the first cycle (Fig. 13d), which was higher than that of reported $Na_4Mn_9O_{18}$ electrodes [106–108]. The $Na_4Mn_9O_{18}$-RGO electrode also displayed higher rate capability and good cycle stability compared with $Na_4Mn_9O_{18}$ electrode (Fig. 13e-f). The addition of RGO could form interlaced network, which provided fast electron conduction pathways and held the mechanical stresses induced by insertion/extraction of Na ions. Thus, a free-standing $Na_4Mn_9O_{18}$-RGO composite film also delivered a high discharge capacity of 83 mAh g^{-1} at 100 mA g^{-1} in 0.5 M $NaCH_3COO$ + 0.5 M $Zn(CH_3COO)_2$ solution using Zn counter electrode [109]. Apart from $Na_4Mn_9O_{18}$-RGO composites, Yin et al. also prepared $Na_4Mn_9O_{18}$/CNT composites with microspherical structure by spray-drying method [110]. The $Na_4Mn_9O_{18}$/CNT electrode in 1 M Na_2SO_4 + 0.5 M $ZnSO_4$ solution showed an initial discharge capacity of 85.6 mAh g^{-1} at 4 C (Fig. 13g), which was higher than that of $Na_4Mn_9O_{18}$-RGO electrode [105]. Compared with the $Na_4Mn_9O_{18}$ electrode, the $Na_4Mn_9O_{18}$/CNT electrode also exhibited good rate capability (Fig. 13h) and cycling stability. The superior electrochemical performance of the $Na_4Mn_9O_{18}$/CNT electrode could be ascribed to spherical structure and CNT addition, which improved the conductivity of the composites. Based on the advantages of CNT and RGO, Shan et al. prepared $Na_4Mn_9O_{18}$/CNT/RGO composites with microsphere structure [111]. Compared with $Na_4Mn_9O_{18}$, $Na_4Mn_9O_{18}$/CNT and $Na_4Mn_9O_{18}$/RGO electrodes, the $Na_4Mn_9O_{18}$/CNT/RGO electrode in 0.5 M Na_2SO_4 + 1 M $ZnSO_4$ solution displayed a higher initial discharge capacity of 96.2 mAh g^{-1} at 4C. Therefore, the modification of CNT and RGO

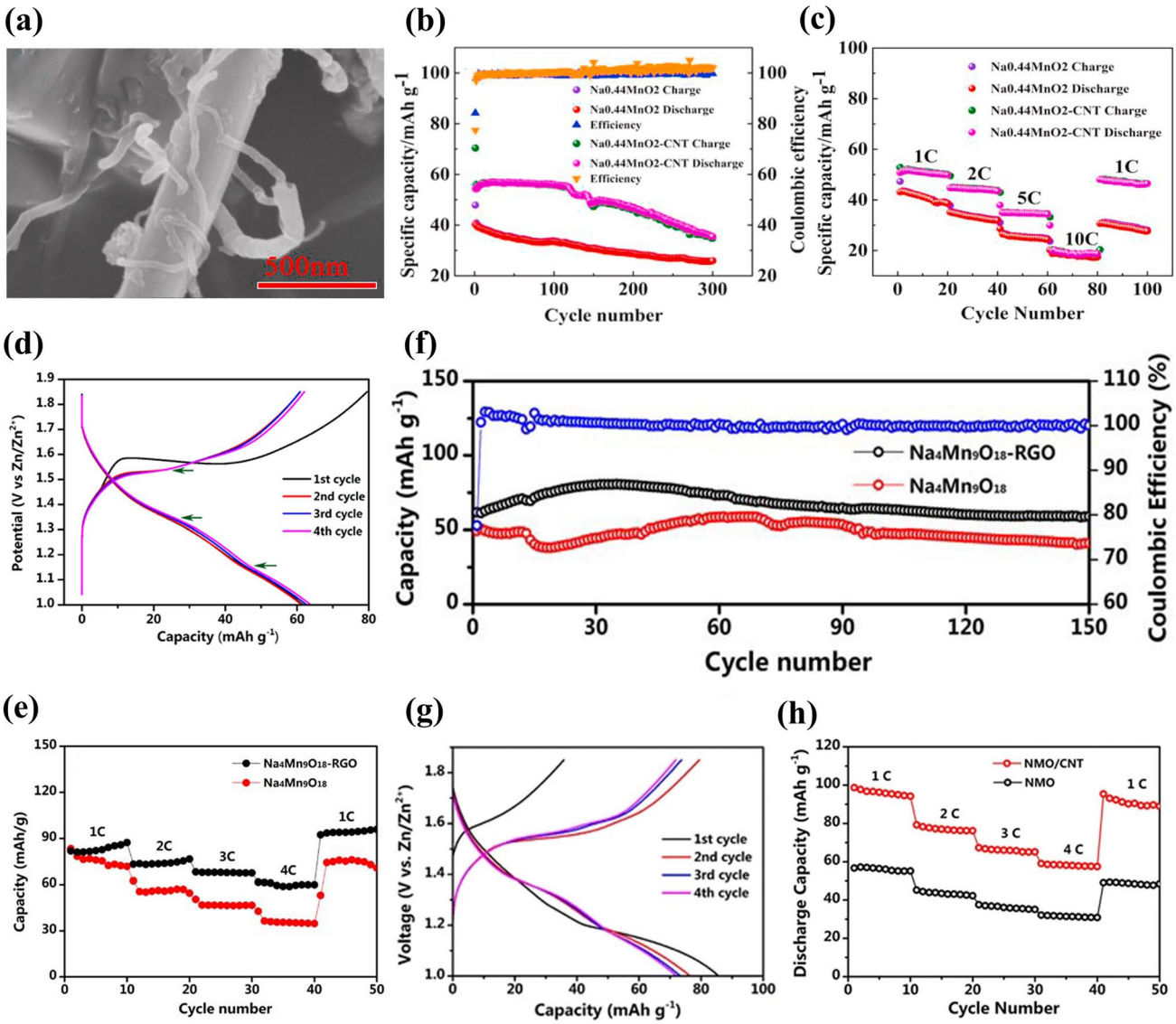

Fig. 13 **a** SEM image of the synthesized $Na_{0.44}MnO_2$-CNT. **b** Cycling performance at 1C and **c** Rate performance of $Na_{0.44}MnO_2$-CNT and $Na_{0.44}MnO_2$ electrodes in 1 M Na_2SO_4 solution with Pt counter electrode [104]. Copyright 2020, Elsevier. **d** Charge/discharge curves at 4C of $Na_4Mn_9O_{18}$-RGO electrode in 1 M Na_2SO_4 + 0.5 M $ZnSO_4$ solution using Zn as counter electrode. **e** Cycling performance of $Na_4Mn_9O_{18}$ and $Na_4Mn_9O_{18}$-RGO electrodes at 4C. **f** Rate capability of $Na_4Mn_9O_{18}$ and $Na_4Mn_9O_{18}$-RGO electrodes. [105]. Copyright 2017, The authors. **g** Discharge/charge profiles at 4C of $Na_4Mn_9O_{18}$/CNT electrode in 1 M Na_2SO_4 + 0.5 M $ZnSO_4$ solution using Zn as counter electrode. **h** Rate performance of $Na_4Mn_9O_{18}$/CNT (NMO/CNT) and $Na_4Mn_9O_{18}$ (NMO) electrodes [110]. Copyright 2017, The Author(s)

can enhance the electronic conductivity of Na_xMnO_2 cathode materials, and improve effectively their reversible capacity, rate capability and cycling performance.

2.1.3 Others

Some other Mn-based oxides as cathode materials have also been reported for aqueous SIBs. Shan et al. synthesized a layered Mn_5O_8 material which had a well-ordered hydroxylated interphase, and investigated its electrochemical performance [112]. A symmetric full cell with Mn_5O_8 electrodes (1 M Na_2SO_4 electrolyte) showed nearly linear potential-capacity curves at various current densities and characteristic of pseudocapacitive response, and delivered a discharge capacity of 116 mAh g^{-1} at 5000 mA g^{-1} and good cycling stability. This system suppressed the oxygen and hydrogen

© The authors https://doi.org/10.1007/s40820-023-01162-x

evolution reactions, exhibited a high-stable potential window of 3.0 V, and demonstrated a two-electron charge transfer reaction involving Mn^{2+}/Mn^{4+} redox couple by means of the interplay between the unique bivalence structure and hydroxylated interphase of Mn_5O_8. Subsequently, Shan et al. also synthesized high purity Mn_5O_8 nanoparticles by oxidation of Mn_3O_4 spinel, and the synthesized nanoparticles were binary Mn_5O_8 expressed as $[Mn^{2+}{}_2][Mn^{4+}{}_3O^{2-}{}_8]$ [113]. A symmetric full cell constructed using Mn_5O_8 electrodes and 1 M Na_2SO_4 solution displayed a stable discharge capacity of about 103 mAh g^{-1} at 5000 mA g^{-1}, and excellent cycling performance without capacity fade upon 5000 cycles.

In conclusion, Mn-based oxides, such as MnO_2, Mn_5O_8 and Na_xMnO_2, have been extensively investigated as cathode materials for aqueous SIBs. Different Mn-based oxides showed various electrochemical performance, and their electrochemical performance can be improved by electrolyte optimization, morphology optimization, element doping or substitution, and carbon modification. A comprehensive summary of the electrochemical performance of some Mn-based oxides discussed previously is presented in Table 1.

2.2 Prussian Blue Analogues

Prussian blue analogues have been widely investigated as cathode materials [14, 114, 115]. Open-framework structures of Prussian blue analogues possess wide channels, which allow rapid insertion/extraction of Na ions in aqueous solution. In this part, some Mn-based Prussian blue analogues will be introduced, including their electrochemical performance and improvement methods.

2.2.1 Electrochemical Performance

Sodium manganese hexacyanoferrate, $Na_xMnFe(CN)_6$, is a promising cathode material for aqueous SIBs. $Na_2MnFe(CN)_6$ material was prepared by precipitation method and its electrochemical performance was studied using $NaTi_2(PO_4)_3$ as anode in 1 M Na_2SO_4 aqueous solution [42]. The $Na_2MnFe(CN)_6$ electrode delivered a reversible discharge capacity of about 85 mAh g^{-1} at 1C, but the discharge capacity decreased to 66.8 mAh g^{-1} after 30 cycles, indicating poor cycling stability. In a "water-in-salt" electrolyte (WiSE) with sodium acetate (8 M) + potassium acetate (32 M), the $Na_2MnFe(CN)_6$ electrode displayed a discharge capacity of 75 mAh g^{-1} at 100 mA g^{-1} using AC as counter electrode (Fig. 14a) [116]. However, a $Na_2MnFe(CN)_6$|WiSE|$NaTi_2(PO_4)_3$/C full cell showed a discharge capacity of only 57 mAh g^{-1} at 100 mA g^{-1} (Fig. 14b) and poor rate performance (Fig. 14c), due to irreversible deintercalation of Na ions from $NaTi_2(PO_4)_3$/C and the instability of $Na_2MnFe(CN)_6$ in the alkaline environment. The WiSE consisting of sodium acetate and potassium acetate was a hybrid electrolyte, and the battery based on the WiSE could be called Na–K hybrid battery, where Na^+/K^+ hybrid-ion electrolyte could enhance electrochemical performances of battery [117]. Moreover, in 17 M $NaClO_4$ aqueous electrolyte, a $Na_2MnFe(CN)_6$|$Na_3Fe_2(PO_4)_3$ full cell presented a discharge capacity of 31 mAh g mAh g^{-1} (based on the mass of cathode and anode) and energy density of 27 Wh kg^{-1} [118]. The full cell exhibited promising rate performance and good cycling performance with 75% capacity retention after 700 cycles. In contrast, when using $K_{0.01}Cr_3[Cr(CN)_6]_2{\cdot}3.8H_2O$ as anode, a $Na_2MnFe(CN)_6$|$K_{0.01}Cr_3[Cr(CN)_6]_2{\cdot}3.8H_2O$ full cell displayed a high discharge capacity of 52.8 mAh g^{-1} at 1C (based on the mass of cathode and anode), corresponding to a high energy density of 81.6 Wh kg^{-1} [119]. The full cell also displayed excellent rate performance with a discharge capacity of 23 mAh g^{-1} at 150C and excellent cycling stability with capacity retention of 93% after 500 cycles at 30C. These researches suggest that aqueous electrolyte and counter electrode have a great influence on the electrochemical performance of $Na_2MnFe(CN)_6$ electrodes. Accordingly, by using graphite/amorphous carbon film as the current collector, a prototype pouch cell stacking using six $Na_2MnFe(CN)_6$|$NaTi_2(PO_4)_3$ bipolar electrodes and "water-in polymer" gel electrolyte delivered a discharge capacity of 114 mAh g^{-1} at 1C and had an energy density of 86 Wh kg^{-1} at 23 W kg^{-1} (based on the mass of cathode and anode) [120]. The prototype pouch cell also demonstrated excellent rate capability with a discharge capacity of 86 mAh g^{-1} at 30C and pre-long cycling performance with 80% capacity maintained after 4000 cycles at 10C.

Apart from $Na_2MnFe(CN)_6$, $Na_{1.33}Mn[Fe(CN)_6]_{0.79}{\cdot}\gamma_{0.21}{\cdot}1.88H_2O$ (γ = $Fe(CN)_6$ vacancy) (NaMnHCFe) was also investigated as cathode material [121]. Figure 14d shows the CV curve of NaMnHCFe electrode in a saturated (10 M) $NaClO_4$ solution using AC anode. Three electrochemical processes could be observed at 0.8, 0.9 and 1.4 V, which

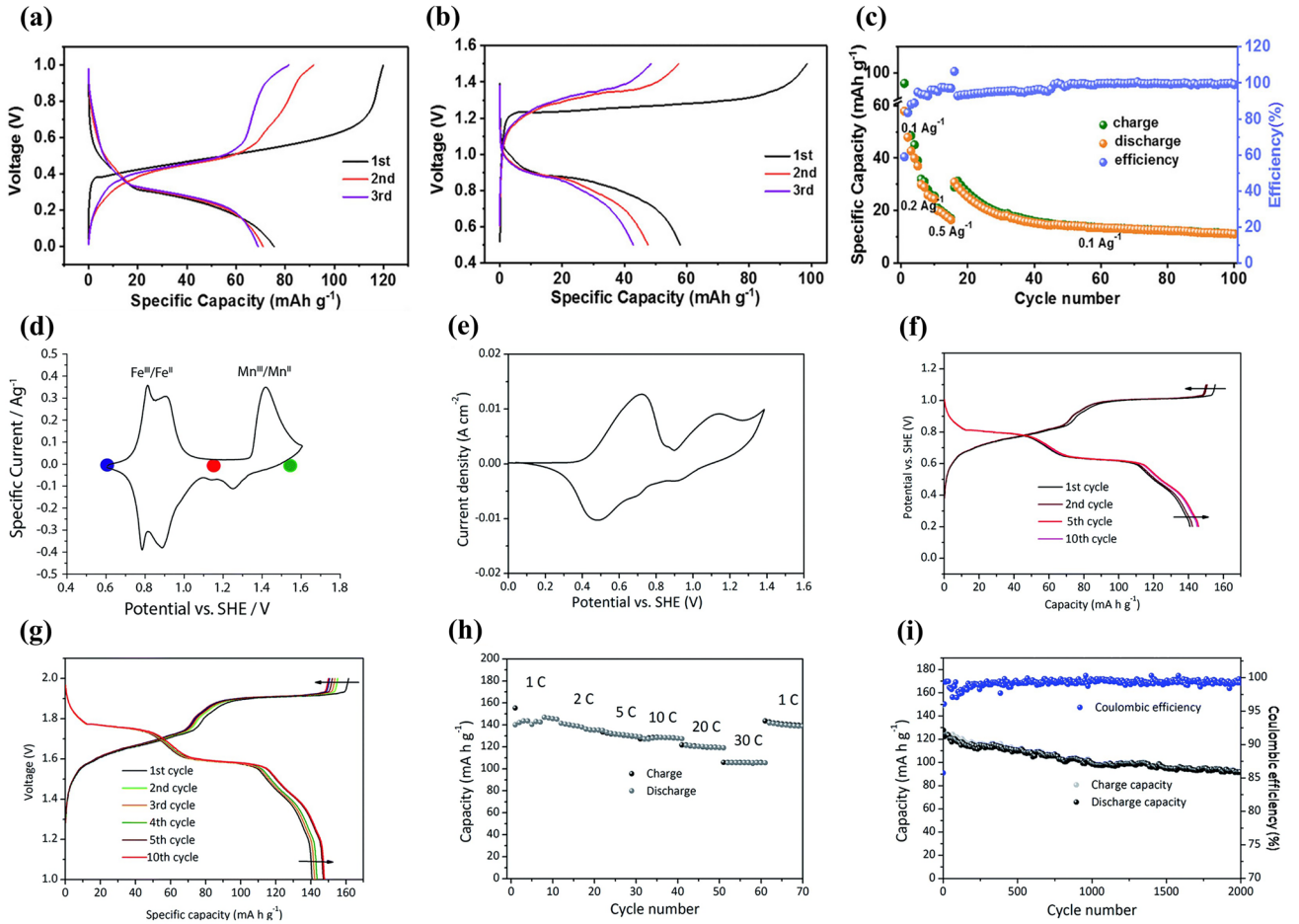

Fig. 14 **a** Charge–discharge curves of $Na_2MnFe(CN)_6$ electrode at 100 mA g^{-1} in WiSE electrolyte using AC as counter electrode. **b** Charge–discharge curves at 100 mA g^{-1} and **c** Rate performance of $Na_2MnFe(CN)_6$|WiSE|$NaTi_2(PO_4)_3$/C full cell [116]. Copyright 2018, Wiley-VCH. **d** CV curve of MnHCFe in a saturated $NaClO_4$ solution (pH = 2) using AC anode [121]. Copyright 2016, Royal Society of Chemistry **e** CV curve of $Na_2MnFe(CN)_6$ electrode in aqueous electrolyte (1 M Na_2SO_4 + 1 M $ZnSO_4$) with SDS addition at 5 mV s^{-1} (standing for one day before testing). **f** Charge/discharge profiles of $Na_2MnFe(CN)_6$ electrode in aqueous electrolyte (1 M Na_2SO_4 + 1 M $ZnSO_4$) with SDS addition at 0.5C. **g** Charge/discharge profiles at 0.5C, **h** Rate capability and **i** Cycling performance at 5C of $Na_2MnFe(CN)_6$|Zn full cell using the electrolyte with SDS addition [22]. Copyright 2017, Royal Society of Chemistry

were ascribed to the electrochemical activity of C-coordinated Fe and N-coordinated Mn. The NaMnHCFe electrode showed a high discharge capacity of 125 mAh g^{-1} at 1C (120 mA g^{-1}) with a low coulombic efficiency of 83%. The reversible capacity of NaMnHCFe was very high; however, there was no report on its rate and cycling performance.

2.2.2 Improvement Methods

Although Mn-based Prussian blue analogues displayed high reversible capacity, they usually showed low rate capability and poor cycle stability due to poor conductivity and easy collapse of structure. Some improvement methods have been developed to improve the electrochemical performance of Mn-based Prussian blue analogues, including electrolyte optimization, carbon modification, and optimization of vacancies in Mn-based Prussian blue analogues.

(1) **Optimization of Electrolyte**

First, electrolyte additives were adopted to enhance the electrochemical performance of batteries. Hou et al. investigated the effect of SDS addition to aqueous electrolyte (1 M

© The authors https://doi.org/10.1007/s40820-023-01162-x

Na_2SO_4 + 1 M $ZnSO_4$) on electrochemical performance of a hybrid battery using $Na_2MnFe(CN)_6$ nanocubes as cathode and Zn as anode [22]. The addition of SDS expanded the electrochemical stability window to about 2.5 V, and there were two cathodic peaks (0.7 and 1.1 V) and three reduction peaks (0.4, 0.7 and 0.9 V) in the CV curve (Fig. 14e). The $Na_2MnFe(CN)_6$ electrode delivered a discharge capacity of 140 mAh g^{-1} at 0.5C (80 mA g^{-1}) (Fig. 14f), which was higher than that of reported $Na_2MnFe(CN)_6$ [42]. Based on the electrolyte with SDS addition, a $Na_2MnFe(CN)_6$|Zn full cell displayed a discharge capacity of 137 mAh g^{-1} at 0.5C (Fig. 14g) and a high energy density of about 170 Wh kg^{-1} at 64 W kg^{-1}. The full cell also showed a high rate performance with a discharge capacity of 100 mAh g^{-1} at 30C (Fig. 14h), which could be attributed to fast intercalation kinetics of $Na_2MnFe(CN)_6$ electrode. In particular, the full cell exhibited excellent cycling stability and the capacity retention after 2000 cycles was about 75% at 5C with coulombic efficiency of nearly 100% (Fig. 14i). The addition of SDS could effectively inhibit the water decomposition (evolution of oxygen or hydrogen), suppress the Mn dissolution and Zn corrosion, and improve the rate capability and cycle life.

Second, optimizing electrolyte salt concentration was used to improve the electrochemical performance of batteries. Nakamoto et al. reported the effect of $NaClO_4$ concentration on electrochemical performance of $Na_2MnFe(CN)_6$ cathode [122]. The electrochemical window for 17 M $NaClO_4$ aqueous electrolyte was 2.8 V, which was wider than that for 1 M $NaClO_4$ (only 1.9 V). The discharge capacities of $Na_2MnFe(CN)_6$ electrodes in 1, 7, 14 and 17 M $NaClO_4$ aqueous electrolytes were about 64, 119, 120 and 123 mAh g^{-1} at 2.0 mA cm^{-2}, respectively. Higher discharge capacity could be obtained in the electrolyte with higher salt concentration. With increasing the $NaClO_4$ concentration, the cycle performance was also improved and the best cycling performance was achieved in highly concentrated (17 M) electrolyte. A $Na_2MnFe(CN)_6$|$NaTi_2(PO_4)_3$ full cell with 17 M $NaClO_4$ aqueous electrolyte exhibited a first discharge capacity of 117 mAh g^{-1} at 2.0 mA cm^{-2} and capacity retention of 81% after 50 cycles. The high salt concentration could suppress water activity, decrease the amount of free water, and improve the electrochemical performance of aqueous batteries.

Third, optimizing the composition of electrolyte salts also was very effective in enhancing the electrochemical performance of batteries. Jiang et al. used an inert-cation-assisted water-in-salt (IC-WiS) electrolyte to improve the electrochemical performance of $Na_{1.88}Mn[Fe(CN)_6]_{0.97}\cdot 1.35H_2O$ (NaMnHCF) cathode [123]. The IC-WiS electrolyte consisted of 9 M sodium triflate (NaOTF) and 22 M tetraethylammonium triflate (TEAOTF), which expanded the electrochemical window to 3.3 V. The IC-WiS electrolyte could suppress the dissolution of transition metal from NaMnHCF electrode and avoid the mixed-cation co-intercalation because of the larger radius of the TEA^+ cation, which could improve cycling performance of battery. The NaMnHCF electrode showed a first discharge capacity of 140 mAh g^{-1} at 1C in both 9 M NaOTF electrolyte and 9 M NaOTF + 22 M TEAOTF electrolyte, as shown in Fig. 15a. However, after 50 cycles, the discharge capacities decreased to 84 and 137 mAh g^{-1} for 9 M NaOTF electrolyte and 9 M NaOTF + 22 M TEAOTF electrolyte, respectively. In the 9 M NaOTF + 22 M TEAOTF electrolyte, the NaMnHCF electrode exhibited superior cycling stability with negligible capacity loss. A NaMnHCF|IC-WiS|$NaTiOPO_4$ full battery displayed a discharge capacity of 41 mAh g^{-1} (based on cathode and anode) at 0.25C (Fig. 15b), corresponding to 71 Wh kg^{-1} energy density. The full battery also delivered excellent cycling stability with capacity retention of 90% after 200 cycles at 0.25C and limited self-discharge behavior (Fig. 15c). In addition, the anion in water-in-salt electrolytes affects tremendously solution structure and electrochemical stability in aqueous high-voltage batteries. Reber et al. compared systematically water-in-salt electrolytes based on 11 sodium salts [124]. Multi-solvent systems and ternary electrolytes could improve the cycling stability. A $Na_2Mn[Fe(CN)_6]$|$NaTi_2(PO_4)_3$ full cell based on a highly concentrated electrolyte with a mixed water/ionic liquid solvent system presented excellent cycling performance. The full cell showed high coulombic efficiency of 99.8% and capacity retention of 79% after 300 cycles at 1C in 80 M NaTFSI/EMImTFSI (TFSI: bis(trifluoromethanesulfonyl)imide; EMIm: 1-ethyl-3-methylimidazolium) electrolyte, as shown in Fig. 15d.

All in all, optimizing aqueous electrolyte by choosing suitable electrolyte additive, adjusting electrolyte salt concentration and adopting suitable sodium salts (one or a combination of multiple sodium salts) could effectively improve the reversible capacity and cycling performance of Mn-based Prussian blue analogues.

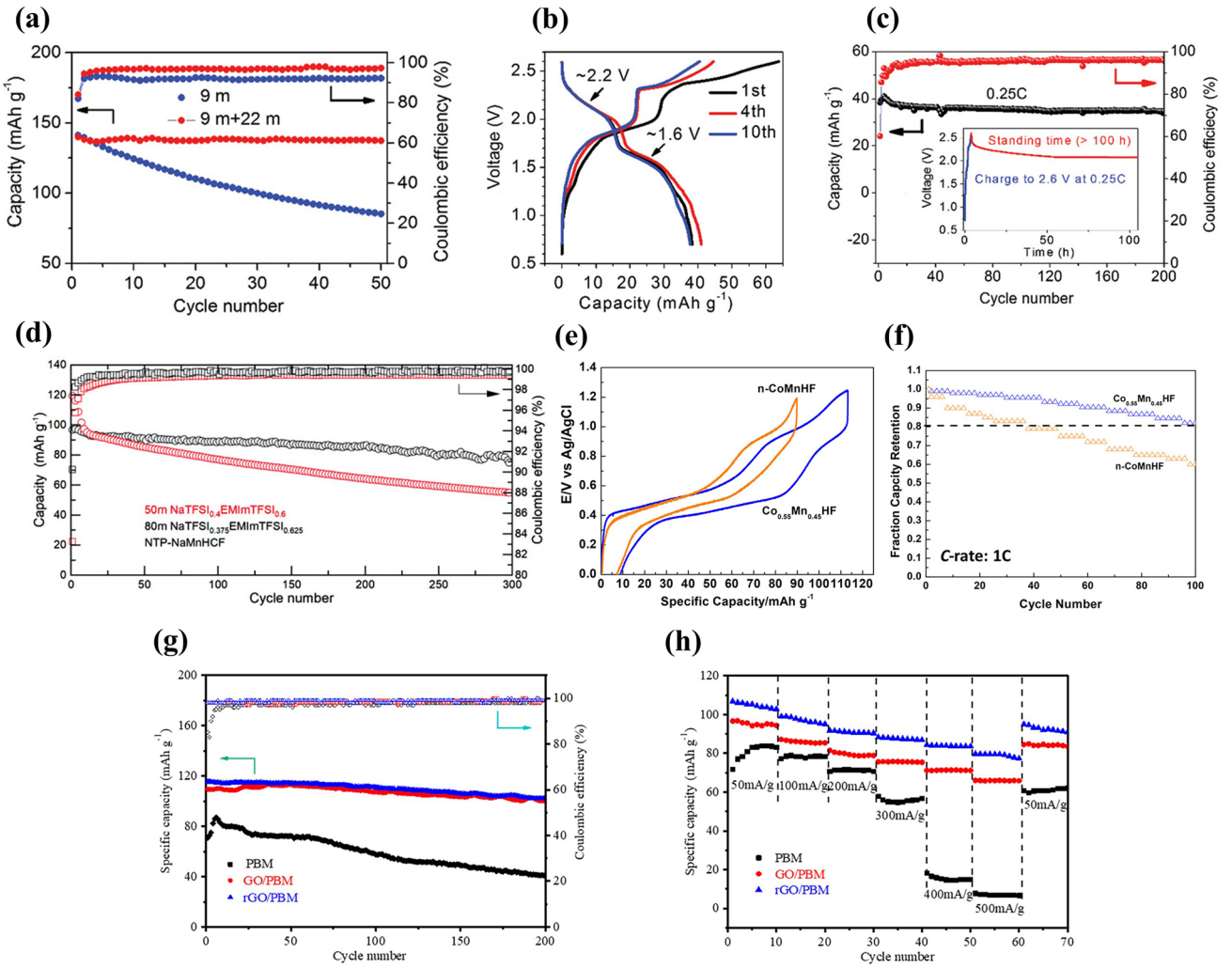

Fig. 15 **a** Cycling performance of NaMnHCF electrode at 1C in 9 M NaOTF electrolyte and 9 M NaOTF + 22 M TEAOTF electrolyte. **b** Charge/discharge curves and **c** cycling performance of NaMnHCF|IC-WiS|$NaTiOPO_4$ full battery at 0.25C (1C = 140 mA g^{-1}) [123]. Copyright 2019, Wiley-VCH. **d** Cycling performance of $Na_2Mn[Fe(CN)_6]$|$NaTi_2(PO_4)_3$ full cells with 80 M $NaTFSI_{0.375}EMImTFSI_{0.625}$ and 50 M $NaTFSI_{0.4}EMImTFSI_{0.6}$ electrolyte at 1C [124]. Copyright 2020, Wiley-VCH. **e** Charge/discharge profiles and **f** Fraction capacity retention of $Co_{0.55}Mn_{0.45}HF$ and *n*-CoMnHF electrodes at 1C in 1 M $NaNO_3$ solution [125]. Copyright 2020, American Chemical Society. **g** Cycling performance at 85 mA g^{-1} and **h** rate capabilities of PBM, GO/PBM, and RGO/PBM electrodes in 1 M Na_2SO_4 + 1 M $ZnSO_4$ aqueous solution using Zn as anode [46]. Copyright 2021, American Chemical Society

(2) Optimization of Vacancies in Prussian Blue Analogues

The presence of vacancies in Prussian blue analogues affects their stability. Reguera et al. investigated the effect of vacancies on electrochemical performance of $Na_xCo_{1-y}Mn_y[Fe(CN)_6]$ [125]. $Na_{1.88}Co_{0.55}Mn_{0.45}[Fe(CN)_6]_{0.97}$ (labeled as $Co_{0.55}Mn_{0.45}HF$) material without vacancies was synthesized by precipitation method using citrate as chelating agent. For comparison, a similar compound $Na_{1.65}Mn_{0.50}Co_{0.50}[Fe(CN)_6]_{0.87}$ (labeled as *n*-CoMnHF) with $[Fe(CN)_6]^{4-}$ vacancies was also prepared. As shown in Fig. 15e, the *n*-CoMnHF electrode in 1 M $NaNO_3$ solution exhibited a lower discharge capacity of 87 mAh g^{-1} than the $Co_{0.55}Mn_{0.45}HF$ electrode (112.82 mAh g^{-1}), due to the presence of $[Fe(CN)_6]^{4-}$ vacancies. The $Co_{0.55}Mn_{0.45}HF$ electrode showed high electrochemical stability with capacity retention of 80% after 100 cycles,

© The authors https://doi.org/10.1007/s40820-023-01162-x

while the *n*-CoMnHF electrode only displayed 60% capacity retention (Fig. 15f). The improvement in electrochemical stability of $Co_{0.55}Mn_{0.45}HF$ without vacancies could be related to electronic interaction between external metals. In a vacancy-free framework, the charge transfer between Fe and Mn was disrupted due to the interaction between Mn and Co, which improved the electrochemical properties. Therefore, reducing the content of vacancies in Mn-based Prussian blue analogues could greatly enhance their electrochemical performance.

(3) **Carbon Modification**

Graphene oxide (GO) and RGO were adopted to improve the electrochemical performance of Mn-based Prussian blue analogues. Zhang et al. investigated the electrochemical performance of GO or RGO-modified $Na_2MnFe(CN)_6$ (PBM) cathode materials in 1 M Na_2SO_4 + 1 M $ZnSO_4$ aqueous solution using Zn anode [46]. The initial discharge capacities were 71.0, 109.5 and 115.4 mAh g^{-1} at 85 mA g^{-1} for PBM, GO/PBM and RGO/PBM electrodes (Fig. 15g), respectively. The capacity retention was 57.5% after 200 cycles for PBM electrode. In contrast, after 200 cycles, the GO/PBM and RGO/PBM electrodes delivered high capacity retention with discharge capacities of 100.5 and 102.2 mAh g^{-1}, respectively. In addition, the PBM electrode showed poor rate capability with a discharge capacity of 7 mAh g^{-1} at 500 mA g^{-1}. On the contrary, the GO/PBM and RGO/PBM electrodes displayed excellent rate capability (Fig. 15h), and the discharge capacities were 66 and 79 mAh g^{-1} at 500 mA g^{-1} for GO/PBM and RGO/PBM electrodes, respectively. An energy density of 165 Wh kg^{-1} was achieved for RGO/PBM|Zn battery. The improvement of electrochemical performance could be attributed to the coating of GO or RGO film on PBM, which could increase electronic conductivity, prevent structure collapse and make the PBM material more stable.

In short, Mn-based Prussian blue analogues, as suitable cathode materials for aqueous SIBs, could show good electrochemical performance and high energy density by optimizing electrolyte, using carbon modification, and reducing vacancies. The electrochemical performance of the Mn-based Prussian blue analogues introduced previously is summarized in Table 2.

2.3 Polyanion Compounds

Polyanion compounds are among the most promising cathode materials for SIBs, because of their safety, stability and suitable operating voltages [126, 127]. Many polyanion compounds have been investigated for aqueous SIBs [128, 129]. However, there are only a few Mn-based polyanion compounds reported as cathodes for aqueous SIBs, including $NaMn_{1/3}Co_{1/3}Ni_{1/3}PO_4$, $Na_3MnTi(PO_4)_3$, $Na_4MnV(PO_4)_3$, $Na_3MnPO_4CO_3$ and $Mn_2(PO_4)F$.

(1) **Mn-based Phosphates**

Minakshi et al. synthesized $NaMn_{1/3}Co_{1/3}Ni_{1/3}PO_4$ cathode materials by sol–gel and combustion routes, and investigated their electrochemical properties in 7 M NaOH solution using Zn as counter electrode [130]. For $NaMn_{1/3}Co_{1/3}Ni_{1/3}PO_4$ electrode electrodes, the electrochemical redox process was fully reversible. The $NaMn_{1/3}Co_{1/3}Ni_{1/3}PO_4$ electrode prepared by sol–gel route showed only 55% cyclic efficiency after 20 cycles (Fig. 16a). In contrast, the $NaMn_{1/3}Co_{1/3}Ni_{1/3}PO_4$ electrode prepared by combustion route delivered excellent cyclic efficiency and cycling stability, with 87% efficiency after 100 cycles (Fig. 16b). As a result, Na ions diffusion into the $NaMn_{1/3}Co_{1/3}Ni_{1/3}PO_4$ might be affected by the synthesis technique and associated physical properties.

Besides, NASICON-structured $Na_3MnTi(PO_4)_3$ materials have also been explored. Gao et al. reported a symmetric battery using NASICON-structured $Na_3MnTi(PO_4)_3$ as cathode and anode (Fig. 16c) [43]. A three-dimensional framework was formed in $Na_3MnTi(PO_4)_3$, where MnO_6 or TiO_6 octahedra was sharing its corners with PO_4 tetrahedra. The insertion/extraction of Na ions in $Na_3MnTi(PO_4)_3$ could occur by the redox couples of Mn^{3+}/Mn^{2+} and Ti^{4+}/Ti^{3+} in 1 M Na_2SO_4 aqueous solution. The symmetric cell with 1 M Na_2SO_4 electrolyte delivered a reversible discharge capacity of 57.9 mAh g^{-1} at 0.5C (1C = 58.7 mA g^{-1}) (Fig. 16d), and had an energy density of about 40 Wh kg^{-1} (based on anode and cathode). The symmetric cell also demonstrated excellent rate capability with a discharge capacity of 46.7 mAh g^{-1} at 10C (Fig. 16e) and excellent cycling performance with coulombic efficiency exceeding 99% and capacity retention of 98% after 100 cycles at 1C (Fig. 16f). After

Table 2 Electrochemical properties of the Mn-based Prussian Blue analogues and Mn-based polyanion compounds for aqueous SIBs

Working electrode	Counter electrode	Electrolyte	Voltage range (V)	Capacity (mAh g^{-1}) / Rate (mA g^{-1})	Capacity retention (%) (cycles)	Refs.
$Na_2MnFe(CN)_6$	$NaTi_2(PO_4)_3$	1 M Na_2SO_4	–	85 (-)	78.6 (30)	[42]
$Na_2MnFe(CN)_6$	AC	8 M CH_3COONa-32 M CH_3COOK	0–1.0	75 (100)	–	[116]
$Na_2MnFe(CN)_6$	AC	17 M $NaClO_4$	0–1.5	119 (500)	92.5 (100)	[119]
$Na_2MnFe(CN)_6$	Pt	1 M Na_2SO_4-1 M $ZnSO_4$ + SDS	0.2–1.2	140 (80)	–	[22]
$Na_2MnFe(CN)_6$	Zn	1 M Na_2SO_4-1 M $ZnSO_4$ + SDS	1.0–2.0	137 (80)	75 (2000)	[22]
$Na_2MnFe(CN)_6$	$NaTi_2(PO_4)_3$	17 M $NaClO_4$	0.5–2.0	117 (-)	81 (50)	[122]
$Na_{1.88}Mn[Fe(CN)_6]_{0.97}{\cdot}1.35H_2O$	AC	9 M NaOTF-22 M TEAOTF	0–1.3	140 (140)	No decay (50)	[123]
$Na_{1.88}Co_{0.55}Mn_{0.45}[Fe(CN)_6]_{0.97}$	C	1 M $NaNO_3$	0–1.25	113 (60)	80 (100)	[125]
$Na_{1.65}Mn_{0.50}Co_{0.50}[Fe(CN)_6]_{0.87}$	C	1 M $NaNO_3$	0–1.2	87 (60)	60 (100)	[125]
$Na_{1.33}Mn[Fe(CN)_6]_{0.79}{\cdot}1.88H_2O$	AC	10 M $NaClO_4$	0.5–1.5	125 (120)	–	[121]
$Na_2MnFe(CN)_6$	Zn	1 M Na_2SO_4-1 M $ZnSO_4$	0.9–2.0	71 (85)	57.5 (200)	[46]
GO/$Na_2MnFe(CN)_6$	Zn	1 M Na_2SO_4-1 M $ZnSO_4$	0.9–2.0	109.5 (85)	91.8 (200)	[46]
RGO/$Na_2MnFe(CN)_6$	Zn	1 M Na_2SO_4-1 M $ZnSO_4$	0.9–2.0	115.4 (85)	88.6 (200)	[46]
$Na_3MnTi(PO_4)_3$	$Na_3MnTi(PO_4)_3$	1 M Na_2SO_4	0.4–1.8	57.9 (29.3)	98 (100)	[43]
$Na_4MnV(PO_4)_3$-RGO	C	10 M $NaClO_4$	0–0.82	92 (110)	–	[133]
$Na_4MnV(PO_4)_3$-RGO	$NaTi_2(PO_4)_3$-MWCNT	10 M $NaClO_4$	0.8–1.65	97 (1100)	51.5 (100)	[133]
$Na_3MnPO_4CO_3$	Zn	17 M $NaClO_4$	-1.2–1.3	134 (-)	55 (30)	[134]
$Na_3MnPO_4CO_3$	$NaTi_2(PO_4)_3$	5 M $NaNO_3$	0–1.5	77.09 (-)	78 (100)	[136]
$Mn_2(PO_4)F$-CeO_2	Zn	4 M $NaClO_4$	0–2.0	104 (12)	99 (300)	[137]
$Mn_2(PO_4)F$–C-CeO_2	Zn	4 M $NaClO_4$	0–2.0	195 (12)	78 (300)	[137]

that, Zhou et al. investigated a hybrid sodium/zinc battery based on $Na_3MnTi(PO_4)_3$ cathode and Zn anode with 0.5 M CH_3COONa and $Zn(CH_3COO)_2$ mixed aqueous electrolyte [131]. The first charge profile delivered a charge capacity of 40.6 mAh g^{-1} at 1.5C (175.5 mA g^{-1}) with only one charge plateau (Fig. 16g), and the subsequent discharge–charge profiles showed two reversible voltage plateaus corresponding to insertion/extraction reaction of Na ions, with an initial discharge capacity of 112.3 mAh g^{-1}. The $Na_3MnTi(PO_4)_3$|Zn battery also demonstrated outstanding rate capability and the discharge capacities were 86.5, 70.9, 65.3 and 59.8 mAh g^{-1} at 3C, 10C, 20C and 30C (Fig. 16h), respectively. More importantly, the $Na_3MnTi(PO_4)_3$|Zn battery displayed superior cycling performance with capacity retention of 93.6% after 2000 cycles (Fig. 16i), indicating good structural stability of $Na_3MnTi(PO_4)_3$ electrode. Very recently, wu et al. reported that the reversible discharge capacity of $Na_3MnTi(PO_4)_3$ could be improved by increasing Mn content [132]. The discharge capacity of $Na_{3.4}Mn_{1.2}Ti_{0.8}(PO_4)_3$ was 68.2 mAh g^{-1} at 100 mA g^{-1} in 1 M Na_2SO_4, which was higher than that (52.6 mAh g^{-1}) of $Na_3MnTi(PO_4)_3$. However, a capacity reduction occurred when Mn content increased to form $Na_{3.8}Mn_{1.4}Ti_{0.6}(PO_4)_3$, which showed a discharge capacity of 60.8 mAh g^{-1}. It might be caused by the impurity phase in the sample and some side reactions.

Furthermore, $Na_4MnV(PO_4)_3$-RGO composites were developed as cathode by Kumar et al. [133]. The $Na_4MnV(PO_4)_3$-RGO electrode in 10 M $NaClO_4$ (with 2 vol% vinylene carbonate) using carbon paper as counter electrode delivered a discharge capacity of 92 mAh g^{-1} at 1C (110 mA g^{-1}) with 82% capacity retained after 10 cycles, and a stable discharge capacity of

© The authors https://doi.org/10.1007/s40820-023-01162-x

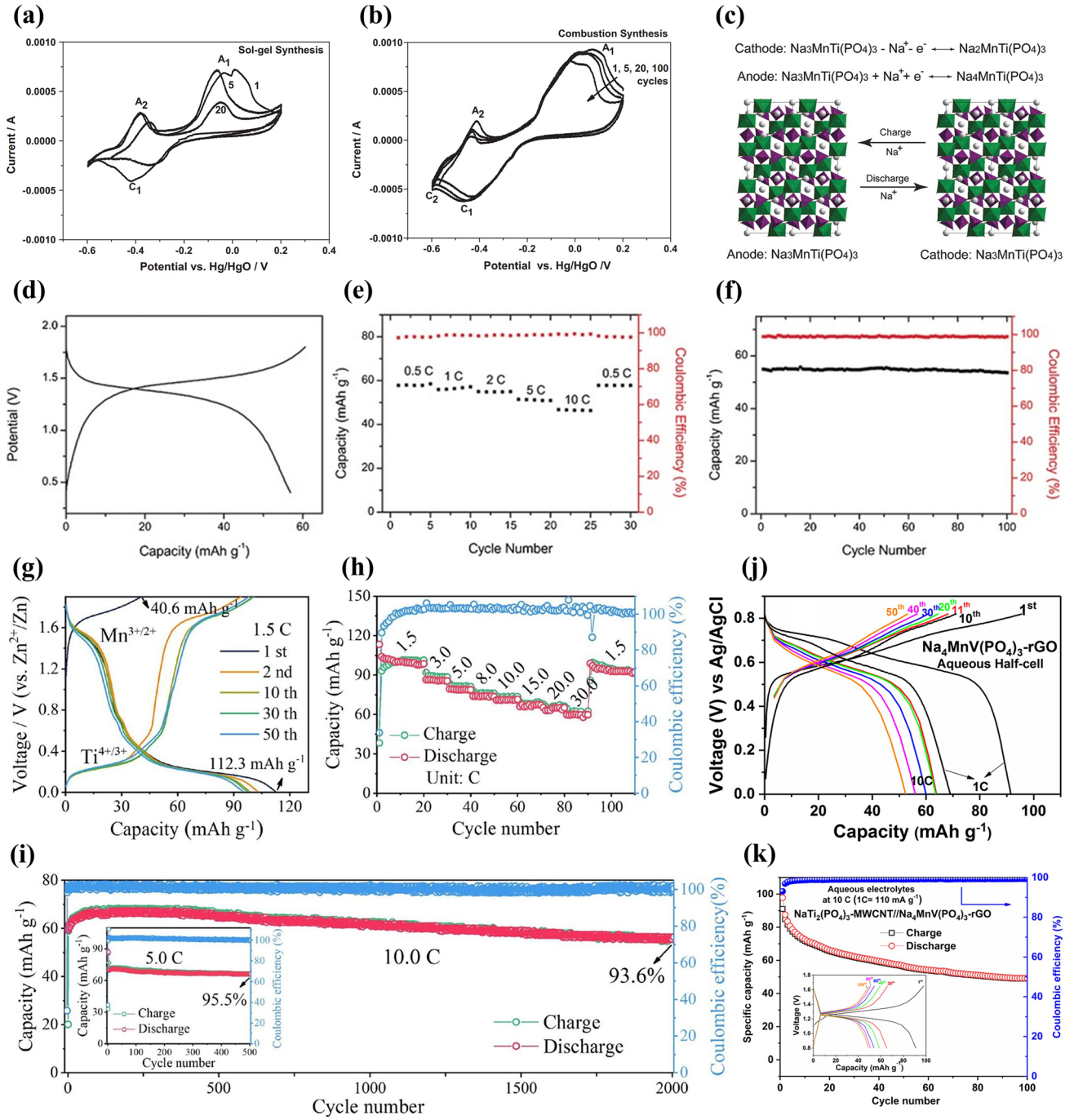

Fig. 16 CV curves of $NaMn_{1/3}Co_{1/3}Ni_{1/3}PO_4$ electrodes synthesized by **a** sol–gel and **b** combustion method [130]. Copyright 2012, Elsevier. **c** Schematic illustration of aqueous symmetric sodium-ion battery with $Na_3MnTi(PO_4)_3$ as anode and cathode. **d** Charge/discharge curve at 0.5C, **e** rate performance and **f** cycling performance at 1C of the symmetric battery with $Na_3MnTi(PO_4)_3$ as anode and cathode in 1 M Na_2SO_4 aqueous solution [43]. Copyright 2016, Wiley-VCH. **g** Charge/discharge profiles at 1.5C, **h** rate capability and **i** cycling performance at 10C of $Na_3MnTi(PO_4)_3$|Zn battery with 0.5 M CH_3COONa and $Zn(CH_3COO)_2$ mixed aqueous electrolyte at 0.01–1.9 V [131]. Copyright 2021, Elsevier. **j** Charge–discharge profiles for $Na_4MnV(PO_4)_3$-RGO electrode in 10 M $NaClO_4$ (with 2 vol% VC). **k** Cycling performance at 10C for $Na_4MnV(PO_4)_3$-RGO|$NaTi_2(PO_4)_3$-MWCNT full cell in 10 M $NaClO_4$ (with 2 vol% VC) electrolyte [133]. Copyright 2019, Elsevier

60 mAh g^{-1} at 10C for 40 cycles (Fig. 16j). A full cell $Na_4MnV(PO_4)_3$-RGO|$NaTi_2(PO_4)_3$-MWCNT showed an initial discharge capacity of 97 mAh g^{-1} at 10C and 51.5% capacity retention after 100 cycles, as shown in Fig. 16k. The enhanced electrochemical performance could be ascribed to the improved electronic conductivity in the RGO network, which was homogenously integrated with $Na_4MnV(PO_4)_3$ particles.

In brief, the Mn-based phosphates, especially NASICON-structured $Na_3MnTi(PO_4)_3$ materials, show better electrochemical performance. More efforts should be made to explore new Mn-based phosphates for aqueous SIBs. Some improvement methods should be adopted to further enhance their electrochemical performance.

(2) **Mn-based Mixed-Polyanions**

Mixed-polyanions $Na_3MnPO_4CO_3$ materials were developed as cathode materials for aqueous SIBs [134–136]. Xie et al. synthesized $Na_3MnPO_4CO_3$ by mechanical ball milling method and investigated its electrochemical performance in 17 M $NaClO_4$ aqueous solution using Zn as anode [134]. The $Na_3MnPO_4CO_3$ synthesized from Na_3PO_4 and $MnCO_3$ was denoted as MM_NMPC ($MnCO_3$), and the average particle size (d_{50}) was 5.6 μm. The $Na_3MnPO_4CO_3$ synthesized from $Mn(NO_3)_2{\cdot}4H_2O$, $Na_2HPO_4{\cdot}2H_2O$ and $Na_2CO_3{\cdot}H_2O$ was denoted as MM_NMPC ($Mn(NO_3)_2$), and the d_{50} was 12.7 μm. The MM_NMPC ($MnCO_3$) electrode delivered a discharge capacity of 134 mAh g^{-1} at 2 mA cm^{-2}, and had a retention capacity of near 74 mAh g^{-1} after 30 cycles (Fig. 17a). However, the MM_NMPC ($Mn(NO_3)_2$) electrode displayed only a first discharge capacity of 113 mAh g^{-1} and had a retention capacity of near 16 mAh g^{-1} after 30 cycles, which could be caused by its larger overvoltage resulting from larger particle size. Compared with MM_NMPC ($Mn(NO_3)_2$) electrode, the MM_NMPC ($MnCO_3$) electrode also exhibited better rate capability with a specific capacity of 68 mAh g^{-1} at 20 mA cm^{-2} (Fig. 17b). Furthermore, Shiprath et al. synthesized $Na_3MnPO_4CO_3$ nanoparticles with average particle size of 20–30 nm by low temperature ionothermal method [136]. A $Na_3MnPO_4CO_3$|$NaTi_2(PO_4)_3$ full cell constructed using 5 M $NaNO_3$ aqueous electrolyte delivered a low discharge capacity of 77.09 mAh g^{-1} at C/5 (1C = 191 mA g^{-1}) in the first cycle (Fig. 17c), and the lower capacity could be caused by poor electronic conductivity of $Na_3MnPO_4CO_3$. The full cell had poor rate capability with a discharge capacity of about 31 mAh g^{-1} at C/2 (Fig. 17d) and exhibited good cycling performance with about 78% capacity retention after 100 cycles (Fig. 17e). In short, the mixed-polyanions $Na_3MnPO_4CO_3$ materials exhibit high reversible capacity but have poor rate capability and cycling performance, and some optimization strategies should be developed to improve their electrochemical performance.

(3) **Mn-based Fluorophosphates**

Fluorophosphates, $Mn_2(PO_4)F$ (MFP), as cathode material was reported by Nzimande et al. [137]. MFP, ceria-coated MFP (MFP-CeO_2) and ceria- and carbon-coated MFP (MFP-C-CeO_2) were synthesized by microwave-assisted hydrothermal process. As shown in Fig. 17f, the redox behavior of MPF in 4 M $NaClO_4$ aqueous electrolyte was improved by ceria coating and ceria-carbon coating. The MFP electrode displayed extremely poor charge–discharge response with a reversible discharge capacity of 2 mAh g^{-1} at 12 mA g^{-1} (Fig. 17g). With ceria coating, the MFP-CeO_2 electrode exhibited a discharge capacity of 104 mAh g^{-1} at 12 mA g^{-1} and excellent rate capability with a discharge capacity of 58 mAh g^{-1} at 1198 mA g^{-1} (Fig. 17h). With ceria-carbon coating, the MFP-C-CeO_2 electrode showed a discharge capacity of 195 mAh g^{-1} at 12 mA g^{-1} and good rate capability with a discharge capacity of 60 mAh g^{-1} at 1198 mA g^{-1} (Fig. 17i). However, the MFP-CeO_2 electrode demonstrated excellent cycling stability with capacity retention of 99% after 300 cycles (Fig. 17j) compared to the MFP-C-CeO_2 electrode (78% capacity retention) (Fig. 17k). The ceria coating could stable the electrode structure, improve ionic conductivity of electrode, protect electrode from the etching effect of electrolyte, and induce catalytic activity, which enhanced the redox behavior of electrode. Therefore, ceria coating and carbon coating can be used to further enhance the electrochemical performance of electrode by optimizing the carbon/ceria content.

Based on the above discussion, it can be found that different Mn-based polyanion compounds show various electrochemical performance, which were affected by compound composition, particle size, carbon modification and electrolyte solution. The electrochemical performance of the Mn-based polyanion compounds mentioned above is summarized in Table 2.

© The authors
https://doi.org/10.1007/s40820-023-01162-x

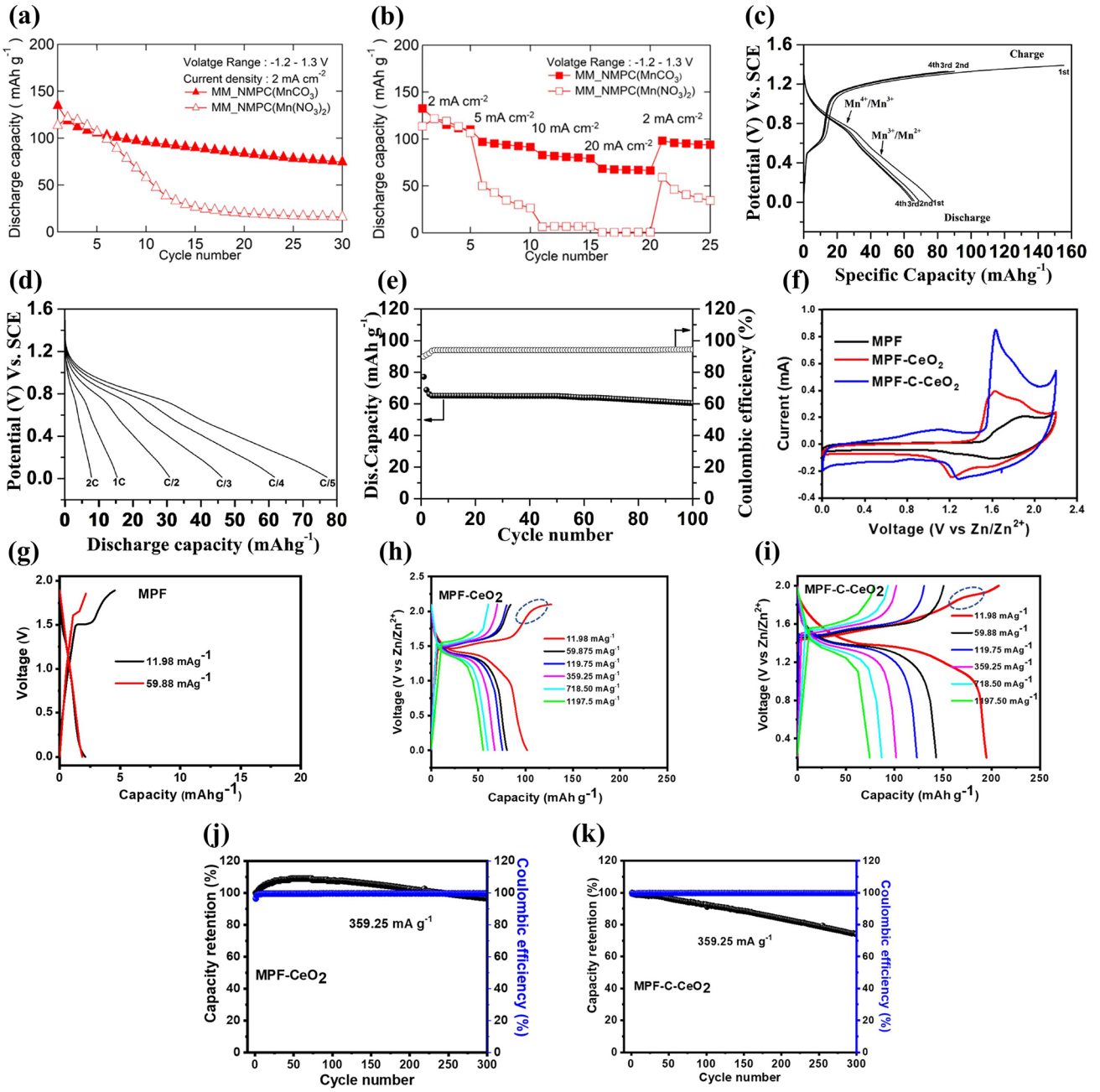

Fig. 17 **a** Cycling performance and **b** Rate capability of $Na_3MnPO_4CO_3$ electrodes with various starting materials (MM_NMPC ($MnCO_3$) and MM_NMPC ($Mn(NO_3)_2$)) [134]. Copyright 2019, The authors. **c** Charge–discharge curves at C/5, **d** discharge curves at various C rates and **e** cycling performance at C/5 of $Na_3MnPO_4CO_3$|$NaTi_2(PO_4)_3$ full cell in 5 M $NaNO_3$ aqueous electrolyte [136]. Copyright 2020, Elsevier. **f** CV curves of MFP, MFP-CeO_2 and MFP-C-CeO_2 electrodes in 4 M $NaClO_4$ aqueous electrolyte using Zn as anode at 2.5 mV s^{-1} (after 5 charge–discharge cycles at 12 mA g^{-1}). Charge–discharge curves at different current density of **g** MPF electrode, **h** MPF-CeO_2 electrode and **i** MPF-C-CeO_2 electrode. Cycling performance at 359.25 mA g^{-1} of **j** MPF-CeO_2 electrode and **k** MPF-C-CeO_2 electrode [137]. Copyright 2021, American Chemical Society

3 Mn-based Anode Materials

There are only a few Mn-based materials investigated as anode materials for aqueous SIBs, including oxides, Prussian blue analogues and polyanion compounds.

3.1 Oxides

As cathode materials, δ-MnO_2, $Na_{0.27}MnO_2$ and Mn_5O_8 have been introduced. At the same time, these materials were also used as anode materials to assemble symmetric full cells. A (Ni)MnO_2|Na_2SO_4(1 M)|(Ni)MnO_2 full cell delivered a discharge capacity of 63 mAh g^{-1} at 200 mA g^{-1} and superior cycle stability without capacity loss over 2000 cycles [55]. Similarly, a $Na_{0.27}MnO_2$|Na_2SO_4(1 M)|$Na_{0.27}MnO_2$ full cell demonstrated a discharge capacity of 83 mAh g^{-1} at 1000 mA g^{-1} and excellent cycling performance without obvious capacity loss over 5000 cycles [64]. Moreover, a higher discharge capacity of 103 mAh g^{-1} at 5000 mA g^{-1} was obtained for Mn_5O_8|Na_2SO_4(1 M)|Mn_5O_8 full cell, which also showed excellent cycling performance without capacity fade upon 5000 cycles [113]. Based on these oxides, the symmetric full cells exhibited high reversible and excellent cycling performance.

Apart from these oxides, Wang et al. investigated Ti-substituted $Na_{0.44}MnO_2$ ($Na_{0.44}[Mn_{1-x}Ti_x]O_2$) as anode material [138]. The initial discharge capacities were about 37 and 39 mAh g^{-1} at 2C (100 mA g^{-1}) for $Na_{0.44}MnO_2$ and $Na_{0.44}[Mn_{0.44}Ti_{0.56}]O_2$ electrodes in Na_2SO_4 aqueous electrolytes (Fig. 18a-b), respectively. The $Na_{0.44}MnO_2$ electrode displayed a stable capacity of 32 mAh g^{-1} after 50 cycles and capacity retention of 86.5% after 400 cycles (Fig. 18c). Compared to the $Na_{0.44}MnO_2$ electrode, the $Na_{0.44}[Mn_{0.44}Ti_{0.56}]O_2$ electrode demonstrated excellent cycling performance with capacity retention of 95% after 400 cycles (Fig. 18d). However, compared to δ-MnO_2, $Na_{0.27}MnO_2$ and Mn_5O_8, the Ti-substituted $Na_{0.44}MnO_2$ had lower reversible capacity and poor cycling stability. More recently, $Na_2[Mn_3Vac_{0.1}Ti_{0.4}]O_7$ (Vac represents vacancy) was studied as anode material for aqueous SIBs [139]. A full cell $Na_{0.44}MnO_2$|$Na_2[Mn_3Vac_{0.1}Ti_{0.4}]O_7$ using 9 M NAOTF + 22 M TEAOTF aqueous electrolyte delivered a reversible capacity of 57.4 mAh g^{-1} at 2C (based on the mass of anode active material). The reversible capacity of $Na_2[Mn_3Vac_{0.1}Ti_{0.4}]O_7$ was still lower. Therefore, among all the Mn-based oxides as anode materials, Mn_5O_8 material exhibits the best electrochemical performance.

3.2 Prussian Blue Analogues

Prussian blue analogues have exhibited excellent electrochemical performance as cathode materials for aqueous SIBs. Due to their large channels and interstices, Prussian blue analogues were also investigated as anode materials for aqueous SIBs.

(1) Manganese Hexacyanomanganate

Pasta et al. reported a manganese hexacyanomanganate open-framework anode, $K_{0.11}Mn[Mn(CN)_6]_{0.83}\cdot\square_{0.17}\cdot 3.64H_2O$ ($\square = Mn(CN)_6$ vacancy) [140]. A full cell assembled with copper hexacyanoferrate cathode, manganese hexacyanomanganate anode and 10 M $NaClO_4$ saturated with $Mn(ClO_4)_2$ as electrolyte had an average discharge voltage of 0.95 V and delivered a specific capacity of about 26 mAh g^{-1} at 10C. In particular, the full cell showed high rate capability with 73.3% capacity retention at 50C and excellent cycling performance with no capacity loss after 1000 cycles. Moreover, Firouzi et al. investigated $Na_{1.24}Mn[Mn(CN)_6]_{0.81}\cdot 2.1H_2O$ as anode for aqueous SIBs [141]. The $Na_{1.24}Mn[Mn(CN)_6]_{0.81}\cdot 2.1H_2O$ electrode delivered a specific capacity of 67 mAh g^{-1} at 60 mA g^{-1} in cosolvent electrolyte (1 M $NaClO_4$, 90% acetonitrile, 10% water) (Fig. 18e). The $Na_{1.24}Mn[Mn(CN)_6]_{0.81}\cdot 2.1H_2O$ electrode also displayed excellent cycling stability with a specific capacity of 66 mAh g^{-1} at 60 mA g^{-1} after 700 cycles corresponding to 98.5% capacity retention. In addition, Yun et al. developed $Na_xMn[Mn(CN)_6]$ thin films as anode materials [142]. The $Na_xMn[Mn(CN)_6]$ thin film showed

© The authors
https://doi.org/10.1007/s40820-023-01162-x

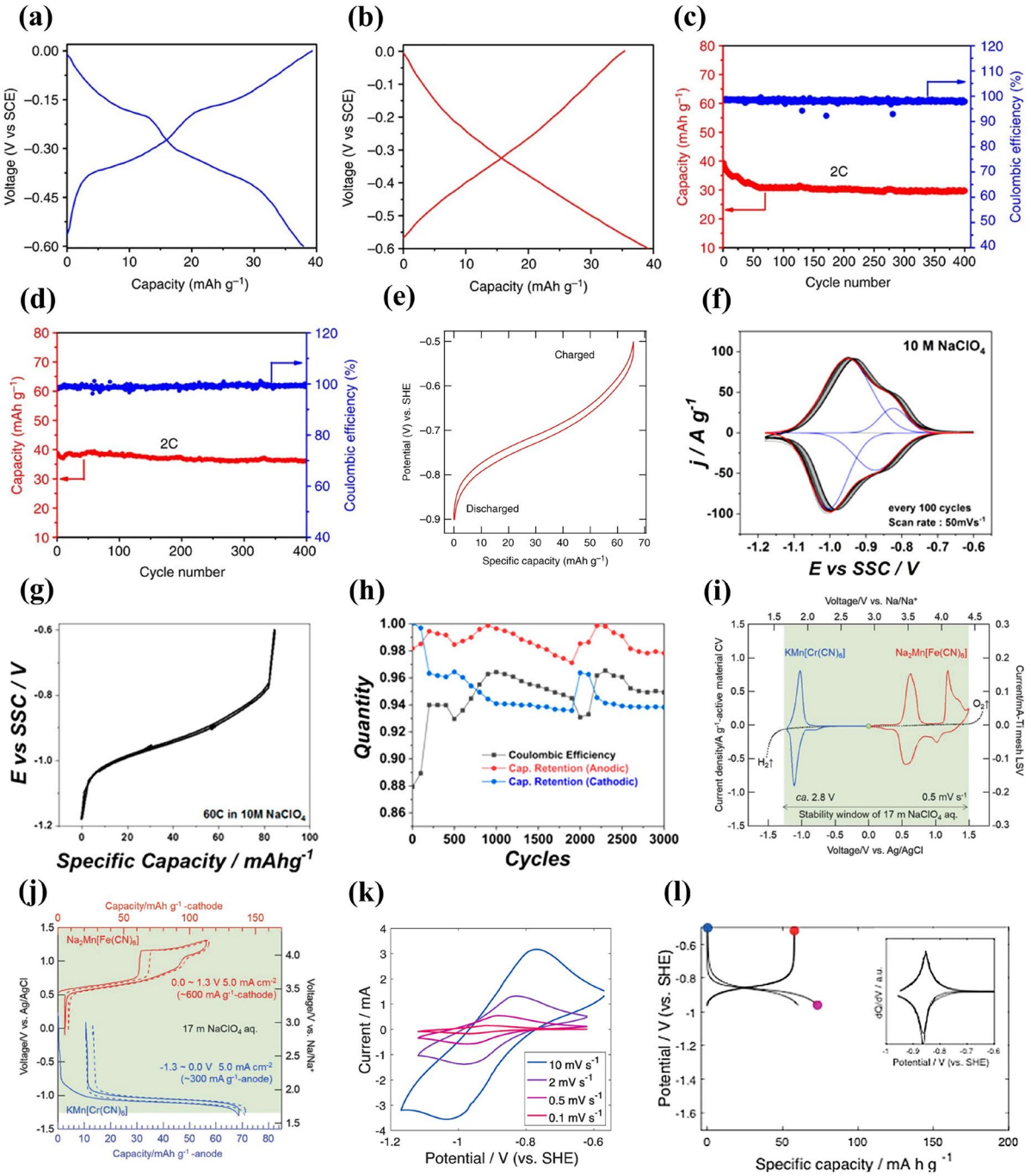

Fig. 18 Charge/discharge curves in the first cycle at 2C for **a** $Na_{0.44}MnO_2$ electrode and **b** $Na_{0.44}[Mn_{0.44}Ti_{0.56}]O_2$ electrode in Na_2SO_4 aqueous electrolytes (pH = 13.5) using platinum electrode as counter electrode. Cycling performance at 2C for **c** $Na_{0.44}MnO_2$ electrode and **d** $Na_{0.44}[Mn_{0.44}Ti_{0.56}]O_2$ electrode in Na_2SO_4 aqueous electrolytes [138]. Copyright 2015, Springer Nature. **e** Charge–discharge profile of $Na_{1.24}Mn[Mn(CN)_6]_{0.81}{\cdot}2.1H_2O$ electrode vs. SHE at 60 mA g^{-1} in cosolvent electrolyte (1 M $NaClO_4$, 90% acetonitrile, 10% water) [141]. Copyright 2018, The Author(s). **f** CV curves at 50 mV s^{-1} of $Na_xMn[Mn(CN)_6]$ thin film in 10 M $NaClO_4$ solution using Pt as counter electrode for over 3000 cycles (every 100th cycle shown). **g** Charge–discharge profile of $Na_xMn[Mn(CN)_6]$ thin film in 10 M $NaClO_4$ solution at 60C. **h** Cathodic and anodic capacity retention of $Na_xMn[Mn(CN)_6]$ thin film [142]. Copyright 2018, American Chemical Society. **i** CV curves of $Na_2Mn[Fe(CN)_6]$ and KMHCC ($KMn[Cr(CN)_6]$) electrodes in 17 M $NaClO_4$ aqueous electrolyte. **j** Charge/discharge curves of $Na_2Mn[Fe(CN)_6]$ and KMHCC ($KMn[Cr(CN)_6]$) electrodes [143]. Copyright 2018, Wiley-VCH. **k** CV curves of NMHCC electrode in 37 M NaFSI aqueous solution with manganese Hexacyanoferrate as counter electrode. **m** Charge–discharge profiles of NMHCC electrode at 15 mA g^{-1} [144]. Copyright 2019, American Chemical Society

very low half-charge potential of about − 0.73 V vs SHE (− 0.93 V vs SSC), which could inhibit hydrogen evolution reaction. Figure 18f displays the CV curves at 50 mV s^{-1} of $Na_xMn[Mn(CN)_6]$ thin film in 10 M $NaClO_4$ solution using Pt as counter electrode for over 3000 cycles (every 100th cycle shown). There was no hydrogen evolution reaction observed. After 100 cycles, the anodic and cathodic half-charged potentials were as low as − 0.930 and − 0.958 V, respectively, showing superior cycling stability. A specific discharge capacity of about 85 mAh g^{-1} was obtained at 60C (5 A g^{-1}) (Fig. 18g). The $Na_xMn[Mn(CN)_6]$ thin film also exhibited superior cycling stability with capacity retention of 97% over 3000 cycles (Fig. 18h).

(2) **Manganese Hexacyanochromate**

Nakamoto et al. investigated manganese hexacyanochromate, $K_{0.01}Mn[Cr(CN)_6]_{0.72}{\cdot}2.01H_2O$ (KMHCC), as anode material [143]. Figure 18i shows the CV curve at 0.5 mV s^{-1} of KMHCC anode in 17 M $NaClO_4$ aqueous electrolyte, and a pair of symmetrical redox peaks and few irreversible reduction peaks could be observed. The KMHCC anode exhibited one voltage plateau at − 1.1 V and a discharge capacity of about 58 mAh g^{-1} at 5.0 mA cm^{-2} (Fig. 18j). A full cell with KMHCC anode, $Na_2MnFe(CN)_6$ cathode and 17 M $NaClO_4$ aqueous electrolyte demonstrated a discharge capacity of about 37 mAh g^{-1} at 5C (200 mA g^{-1}). At high rate of 60C, a capacity of 16 mAh g^{-1} was maintained, indicating high rate capability. However, the full cell showed poor cycling performance at low rate of 5C and good cyclability at high rate of 30C. In addition, manganese hexacyanochromate, $Na_{0.04}Mn[Cr(CN)_6]_{0.70}{\cdot}2.80H_2O$ (NMHCC), with the lowest redox potential was studied by Wheeler et al. [144]. Figure 18k shows the CV curves of NMHCC electrode in 37 M sodium bis(fluorosulfonyl)imide (NaFSI) aqueous solution with manganese hexacyanoferrate as counter electrode. The increase of peak separation and peak current with an increase in scan rate indicated a one-electron one-step quasi-reversible reaction. There was a voltage plateau centered at − 0.86 V in the charge–discharge profiles, and a reversible capacity of 62 mAh g^{-1} at 15 mA $g^{-1}$was obtained for NMHCC electrode (Fig. 18m).

In a word, manganese hexacyanomanganate presents high reversible capacity and superior cycling stability compared with manganese hexacyanochromate. Among all the Mn-based Prussian blue analogues anodes, $Na_xMn[Mn(CN)_6]$ exhibits the best electrochemical performance. The electrochemical performance is affected by aqueous electrolyte and composition and vacancies of Prussian blue analogues, and some improvement approaches should be adopted to enhance the electrochemical performance.

3.3 Polyanion Compounds

NASICON-type $NaTi_2(PO_4)_3$ with an open framework is a typical anode material for aqueous SIBs [20, 145]. Some Mn-based polyanion compounds were also investigated as anode materials. NASICON-type $Na_3MnTi(PO_4)_3$ was reported by Gao et al. as anode and cathode materials, and a $Na_3MnTi(PO_4)_3|Na_3MnTi(PO_4)_3$ symmetric cell with 1 M Na_2SO_4 electrolyte showed a reversible discharge capacity of 57.9 mAh g^{-1} at 29.35 mA g^{-1} [43]. The symmetric cell also demonstrated excellent rate capability and cycling performance with capacity retention of 98% after 100 cycles. Furthermore, $Na_2Ti_{3/2}Mn_{1/2}(PO_4)_3$ nanodots planted in carbon matrix was also reported as low-cost anode by Lei et al. [146]. The $Na_2Ti_{3/2}Mn_{1/2}(PO_4)_3$ material displayed an initial discharge capacity of 88.6 mAh g^{-1} at 0.5C in 6 M $NaClO_4$ aqueous electrolyte using nickel hexacyanoferrate as counter electrode. Owing to ultrafast Na-intercalation chemistry, the $Na_2Ti_{3/2}Mn_{1/2}(PO_4)_3$ material had excellent high rate performance with stable capacity of 65.1 mAh g^{-1} at 10C and stable cycling performance (90% capacity retention after 1000 cycles at 10C). Therefore, as anode materials, Mn-based polyanion compounds demonstrated excellent electrochemical performance, although there were only a few materials reported.

From the above discussion, it can be found that different types of Mn-based anode materials showed diverse electrochemical performance, and oxides exhibited better electrochemical performance. A comprehensive summary of the electrochemical performance of the Mn-based anode materials introduced previously is presented in Table 3.

4 Summary and Perspectives

Aqueous sodium-ion batteries are promising candidates for large-scale energy storage systems because of abundant sodium resources, low cost, high safety, convenient manufacture and eco-friendliness. The electrode materials and

© The authors https://doi.org/10.1007/s40820-023-01162-x

Table 3 Electrochemical properties of the Mn-based anode materials for aqueous SIBs

Working electrode	Counter electrode	Electrolyte	Voltage range (V)	Capacity (mAh g^{-1}) / Rate (mA g^{-1})	Capacity retention (%) (cycles)	Refs.
Ni-doped δ-MnO_2	Ni-doped δ-MnO_2	1 M Na_2SO_4	0–1.6	63 (200)	No decay (2000)	[55]
$Na_{0.27}MnO_2$	$Na_{0.27}MnO_2$	0.5 M Na_2SO_4	0–2.5	83 (1000)	No decay (5000)	[64]
Mn_5O_8	Mn_5O_8	1 M Na_2SO_4	0–3.0	103 (5000)	No decay (5000)	[113]
$Na_{0.44}MnO_2$	Pt	Na_2SO_4 (pH = 13.5)	-0.6–0	37 (100)	86.5 (400)	[138]
$Na_{0.44}[Mn_{1-x}Ti_x]O_2$	Pt	Na_2SO_4 (pH = 13.5)	− 0.6–0	39 (100)	95 (400)	[138]
$K_{0.11}Mn[Mn(CN)_6]_{0.83}$	$K_{0.05}Cu[Fe(CN)_6]_{0.67}$	10 M $NaClO_4$	0.65–1.35	26 (10C)	No decay (1000)	[140]
$K_{0.01}Mn[Cr(CN)_6]_{0.72}$	$Na_2MnFe(CN)_6$	17 M $NaClO_4$	0.5–2.6	37 (200)	84 (100)	[143]
$Na_{0.04}Mn[Cr(CN)_6]_{0.70}$	MnHCFe	17 M NaFSI	− 0.97– − 0.5	62 (15)	–	[144]
$Na_{1.24}Mn[Mn(CN)_6]_{0.81}$	CuHCF	1 M $NaClO_4$	− 0.9– − 0.5	67 (60)	98.5 (700)	[141]
$NaxMn[Mn(CN)_6]$	Pt	10 M $NaClO_4$	− 1.2– − 0.6	85 (5000)	97 (3000)	[142]
$Na_3MnTi(PO_4)_3$	$Na_3MnTi(PO_4)_3$	1 M Na_2SO_4	0.4–1.8	57.9 (29.3)	98 (100)	[43]
$Na_2Ti_{3/2}Mn_{1/2}(PO_4)_3$	NiHCF	6 M $NaClO_4$	− 1.0–0	88.6 (0.5C)	90 (1000)	[146]

aqueous electrolytes affect the electrochemical performance of aqueous batteries. In this review, the recent development of Mn-based electrode materials for aqueous SIBs, including oxides, Prussian blue analogues and polyanion compounds, are overviewed. The electrochemical performance and improvement methods of Mn-based electrode materials are highlighted. The reported progress of Mn-based electrode materials is focused on cathode materials, oxides cathode materials in particular. However, the Mn-based Prussian blue analogues and Mn-based polyanion compounds also show high specific capacities and good cycling performance. It is believed that the Mn-based electrode materials are promising materials for aqueous SIBs. Therefore, the Mn-based electrode materials are worthy of further investigation. The following is some perspectives of Mn-based electrode materials in aqueous SIBs.

4.1 Mn-Based Electrode Materials

Mn-based electrode materials include oxides, Prussian blue analogues and polyanion compounds, and each type of material has its distinctive advantages and disadvantages. Mn-based oxides materials have high theoretical capacity, however, most of them also suffer from phase transitions, leading to structural degradation and capacity decay during Na ions intercalation/deintercalation. Also, Mn dissolution and water protons co-insertion are some issues in aqueous electrolytes. Therefore, some improvement methods have been developed to alleviate these problems, including electrolyte optimization, morphology optimization, element doping or substitution, and carbon modification. For electrode materials, the synthesis of materials is very important, which determines the morphology and carbon coating quality of materials. Continued efforts should be devoted to optimizing material morphology (nanostructured materials in particular) combining with carbon modification in order to improve electrochemical performance of Mn-based oxides. In addition, element doping or substitution is also a powerful approach for improving the electrochemical performance. The effect of different dopants or element substitutions should be systematically investigated, which will provide a guide for designing advanced Mn-based materials with excellent electrochemical performance. For Mn-based Prussian Blue analogues, they have wide channels allowing rapid insertion/extraction of Na ions; however, they also suffer from poor cycling stability. Prussian blue analogues usually contain $[Fe(CN)_6]^{4-}$ vacancies, which affect the electrochemical performance. Reducing the number of $[Fe(CN)_6]^{4-}$ vacancies can improve its cycling stability [125]. However, the existence of unconventional Mn vacancies on the surface of Mn-based Prussian blue analogues is helpful to improve its long-term cycling stability [147]. Furthermore, carbon modification is also an attractive strategy to improve electrochemical performance of Mn-based Prussian blue analogues. For Mn-based polyanion compounds, their inferior electronic conductivity leads to low electrochemical performance. Surface-coating should be an

effective way to enhance the electrochemical performance of Mn-based polyanion compounds [137]. Much attention should be devoted to these improvement strategies, which are related to material synthesis. The composition, crystal structure, morphology, element doping or substitution, and carbon modification are able to be controlled and optimized during synthesis process of materials. Therefore, the material synthesis is very important, where some improvement strategies could be combined together to enhance greatly the electrochemical performance.

4.2 Aqueous Electrolytes

Aqueous electrolytes affect the electrochemical performance of Mn-based electrode materials. Optimizing the aqueous electrolytes is conducive to increase specific capacity and improve cycling stability of Mn-based electrode materials. Some optimization methods, such as optimizing electrolyte salt concentration, choosing suitable electrolyte additive and optimizing solvent, have been developed. The high concentration electrolytes or "water-in-salt" electrolytes can widen the stable electrochemical window, suppress Mn dissolution and some side reactions between electrode and water, and significantly improve the cycling stability of Mn-based electrodes. Therefore, developing innovative high concentration electrolytes or "water-in-salt" electrolytes is a promising way to obtain high electrochemical performance of aqueous batteries. In addition, the use of electrolyte additives, for example SDS [22, 95], in low concentration electrolytes could expand the electrochemical window, inhibit the water decomposition, suppressed the Mn dissolution, and improve the rate capability and cycling stability of Mn-based electrodes. Moreover, the addition of Zn, Mn and Li cations in low concentration electrolytes can also improve effectively the electrochemical performance of Mn-based electrode materials [93, 94]. Thus, the use of electrolyte additives is a very attractive improvement strategy. The effect of different electrolyte additives should be systematically studied, and the joint use of multiple additives, for example SDS and metal cations, should also be considered, which may have immense effect on enhancing electrochemical performance. Furthermore, hybrid electrolyte and eutectic electrolyte have been also proven effective to improve the electrochemical performance of Mn-based electrode materials, and they are worthy of further investigation.

For practical application in aqueous SIBs, it is expected that Mn-based electrode materials can exhibit high special capacity, superior rate capability and excellent cycling performance. Thus, high-performance Mn-based electrode materials need to be designed and developed. However, for aqueous SIBs, aqueous electrolytes have an important impact on the electrochemical performance of batteries. Optimizing aqueous electrolytes is a very effective approach for improving the electrochemical performance of Mn-based electrode materials. In especial, the expanded electrochemical stability window of aqueous electrolytes can allow the full and reversible use of sodium storage sites in Mn-based electrode materials, which will greatly enhance the electrochemical performance. Therefore, more efforts should be made to optimize aqueous electrolytes in addition to developing high-performance Mn-based electrode materials.

Acknowledgements This work was partly supported by the National Natural Science Foundation of China (Grant No. 52272225), and Independent deployment project of Qinghai Institute of Salt Lakes, Chinese Academy of Sciences (E260GC0401).

Funding Open access funding provided by Shanghai Jiao Tong University.

Declarations

Conflict of interest The authors declare no interest conflict. They have no known competing financial interests or personal relationships that could have appeared to influence the work reported in this paper.

Open Access This article is licensed under a Creative Commons Attribution 4.0 International License, which permits use, sharing, adaptation, distribution and reproduction in any medium or format, as long as you give appropriate credit to the original author(s) and the source, provide a link to the Creative Commons licence, and indicate if changes were made. The images or other third party material in this article are included in the article's Creative Commons licence, unless indicated otherwise in a credit line to the material. If material is not included in the article's Creative Commons licence and your intended use is not permitted by statutory regulation or exceeds the permitted use, you will need to obtain permission directly from the copyright holder. To view a copy of this licence, visit http://creativecommons.org/licenses/by/4.0/.

References

1. W.A. Braff, J.M. Mueller, J.E. Trancik, Value of storage technologies for wind and solar energy. Nat. Clim. Change **6**(10), 964–969 (2016). https://doi.org/10.1038/Nclimate3045
2. O.J. Guerra, J.Z. Zhang, J. Eichman, P. Denholm, J. Kurtz et al., The value of seasonal energy storage technologies for

the integration of wind and solar power. Energy Environ. Sci. **13**(7), 1909–1922 (2020). https://doi.org/10.1039/d0ee00771d

3. K.C. Divya, J. Ostergaard, Battery energy storage technology for power systems-an overview. Electr. Power Syst. Res. **79**(4), 511–520 (2009). https://doi.org/10.1016/j.epsr.2008.09.017
4. B. Dunn, H. Kamath, J.M. Tarascon, Electrical energy storage for the grid: a battery of choices. Science **334**(6058), 928–935 (2011). https://doi.org/10.1126/science.1212741
5. H. Kim, H. Kim, Z. Ding, M.H. Lee, K. Lim et al., Recent progress in electrode materials for sodium-ion batteries. Adv. Energy Mater. **6**(19), 1600943 (2016). https://doi.org/10.1002/aenm.201600943
6. Y.Q. Yang, S. Bremner, C. Menictas, M. Kay, Battery energy storage system size determination in renewable energy systems: a review. Renew. Sust. Energy Rev. **91**, 109–125 (2018). https://doi.org/10.1016/j.rser.2018.03.047
7. Y.G. Wang, J. Yi, Y.Y. Xia, Recent progress in aqueous lithium-ion batteries. Adv. Energy Mater. **2**(7), 830–840 (2012). https://doi.org/10.1002/aenm.201200065
8. H. Kim, J. Hong, K.Y. Park, H. Kim, S.W. Kim et al., Aqueous rechargeable Li and Na ion batteries. Chem. Rev. **114**(23), 11788–11827 (2014). https://doi.org/10.1021/cr500232y
9. J. Lamb, J.A. Jeevarajan, New developments in battery safety for large-scale systems. MRS Bull. **46**(5), 395–401 (2021). https://doi.org/10.1557/s43577-021-00098-0
10. J.Y. Hwang, S.T. Myung, Y.K. Sun, Sodium-ion batteries: present and future. Chem. Soc. Rev. **46**(12), 3529–3614 (2017). https://doi.org/10.1039/c6cs00776g
11. K. Chayambuka, G. Mulder, D.L. Danilov, P.H.L. Notten, Sodium-ion battery materials and electrochemical properties reviewed. Adv. Energy Mater. **8**(16), 1800079 (2018). https://doi.org/10.1002/aenm.201800079
12. T. Perveen, M. Siddiq, N. Shahzad, R. Ihsan, A. Ahmad et al., Prospects in anode materials for sodium ion batteries—a review. Renew. Sustain. Energy Rev. **119**, 109549 (2020). https://doi.org/10.1016/j.rser.2019.109549
13. P. Barpanda, L. Lander, S. Nishimura, A. Yamada, Polyanionic insertion materials for sodium-ion batteries. Adv. Energy Mater. **8**(17), 1703055 (2018). https://doi.org/10.1002/aenm.201703055
14. J. Peng, W. Zhang, Q.N. Liu, J.Z. Wang, S.L. Chou et al., Prussian blue analogues for sodium-ion batteries: past, present, and future. Adv. Mater. **34**(15), 2108384 (2022). https://doi.org/10.1002/adma.202108384
15. A. Ponrouch, D. Monti, A. Boschin, B. Steen, P. Johansson et al., Non-aqueous electrolytes for sodium-ion batteries. J. Mater. Chem. A **3**(1), 22–42 (2015). https://doi.org/10.1039/c4ta04428b
16. H. Hijazi, P. Desai, S. Mariyappan, Non-aqueous electrolytes for sodium-ion batteries: challenges and prospects towards commercialization. Batter. Supercaps. **4**(6), 881–896 (2021). https://doi.org/10.1002/batt.202000277
17. W. Tang, Y.S. Zhu, Y.Y. Hou, L.L. Liu, Y.P. Wu et al., Aqueous rechargeable lithium batteries as an energy storage system of superfast charging. Energy Environ. Sci. **6**(7), 2093–2104 (2013). https://doi.org/10.1039/c3ee24249h
18. M. Liu, H. Ao, Y. Jin, Z. Hou, X. Zhang et al., Aqueous rechargeable sodium ion batteries: developments and prospects. Mater. Today Energy **17**, 100432 (2020). https://doi.org/10.1016/j.mtener.2020.100432
19. H.X. Yang, J.F. Qian, Recent development of aqueous sodium ion batteries and their key materials. J. Inorg. Mater. **28**(11), 1165–1171 (2013). https://doi.org/10.3724/SP.J.1077.2013.13388
20. D. Bin, F. Wang, A.G. Tamirat, L.M. Suo, Y.G. Wang et al., Progress in aqueous rechargeable sodium-ion batteries. Adv. Energy Mater. **8**(17), 1703008 (2018). https://doi.org/10.1002/aenm.201703008
21. H. Ma, H.R. Zhang, M.Q. Xue, Research progress and practical challenges of aqueous sodium-ion batteries. Acta. Chim. Sin. **79**(4), 388–405 (2021). https://doi.org/10.6023/A20100492
22. Z.G. Hou, X.Q. Zhang, X.N. Li, Y.C. Zhu, J.W. Liang et al., Surfactant widens the electrochemical window of an aqueous electrolyte for better rechargeable aqueous sodium/zinc battery. J. Mater. Chem. A **5**(2), 730–738 (2017). https://doi.org/10.1039/c6ta08736a
23. H. Tomiyasu, H. Shikata, K. Takao, N. Asanuma, S. Taruta et al., An aqueous electrolyte of the widest potential window and its superior capability for capacitors. Sci. Rep. **7**, 45048 (2017). https://doi.org/10.1038/srep45048
24. H. Gao, K.K. Tang, J. Xiao, X. Guo, W.H. Chen et al., Recent advances in "water in salt" electrolytes for aqueous rechargeable monovalent-ion (Li^+, Na^+, K^+) batteries. J. Energy Chem. **69**, 84–99 (2022). https://doi.org/10.1016/j.jechem.2021.12.025
25. Y.H. Shen, B. Liu, X.R. Liu, J. Liu, J. Ding et al., Water-in-salt electrolyte for safe and high-energy aqueous battery. Energy Storage Mater. **34**, 461–474 (2021). https://doi.org/10.1016/j.ensm.2020.10.011
26. J.H. Huang, X.L. Dong, Z.W. Guo, Y.G. Wang, Progress of organic electrodes in aqueous electrolyte for energy storage and conversion. Angew. Chem. Int. Ed. **59**(42), 18322–18333 (2020). https://doi.org/10.1002/anie.202003198
27. Y.N. Gao, H.Y. Yang, Y. Bai, C. Wu, Mn-based oxides for aqueous rechargeable metal ion batteries. J. Mater. Chem. A **9**(19), 11472–11500 (2021). https://doi.org/10.1039/d1ta01951a
28. Y.Y. Wang, D. Liu, M.L. Sun, J.P. Liu, Recent progress in electrode materials for aqueous sodium and potassium ion batteries. Mater. Chem. Front. **5**(20), 7384–7402 (2021). https://doi.org/10.1039/d1qm01011e
29. H.X. Li, W. Zhang, K.N. Sun, J. Guo, K. Yuan et al., Manganese-based materials for rechargeable batteries beyond lithium-ion. Adv. Energy Mater. **11**(25), 2100867 (2021). https://doi.org/10.1002/aenm.202100867
30. Y.G. Cao, M.J. Xiao, X.Z. Sun, W.J. Dong, F.Q. Huang, Recent advances on high-capacity sodium manganese-based

oxide cathodes for sodium-ion batteries. Chem. Eur. J. **29**, e202202997 (2023). https://doi.org/10.1002/chem.202202997

31. A. Zhou, R. Chi, Y. Shi, X. Zhao, X. Li et al., Manganese-based cathode materials for aqueous rechargeable zinc-ion batteries: recent advance and future prospects. Mater. Today Chem. **27**, 101294 (2023). https://doi.org/10.1016/j.mtchem.2022.101294
32. Y.X. Chang, L.Z. Yu, X.X. Xing, Y.J. Guo, Z.Y. Xie et al., Ion substitution strategy of manganese-based layered oxide cathodes for advanced and low-cost sodium ion batteries. Chem. Rec. **22**(10), e202200122 (2022). https://doi.org/10.1002/tcr.202200122
33. J. Chen, W.L. Xu, H.Y. Wang, X.H. Ren, F.Y. Zhan et al., Emerging two-dimensional nanostructured manganese-based materials for electrochemical energy storage: recent advances, mechanisms, challenges, and prospects. J. Mater. Chem. A **10**(40), 21197–21250 (2022). https://doi.org/10.1039/d2ta05309h
34. L.Y. Liu, Y.C. Wu, L. Huang, K.S. Liu, B. Duployer et al., Alkali ions pre-intercalated layered MnO_2 nanosheet for zinc-ions storage. Adv. Energy Mater. **11**(31), 2101287 (2021). https://doi.org/10.1002/aenm.202101287
35. G.G. Yadav, J.W. Gallaway, D.E. Turney, M. Nyce, J.C. Huang et al., Regenerable Cu-intercalated MnO_2 layered cathode for highly cyclable energy dense batteries. Nat. Commun. **8**, 14424 (2017). https://doi.org/10.1038/ncomms14424
36. D.G.G.J.M. Tarascon, B. Wilkens, W.R. Mc Kinnon, P. Barboux, Chemical and electrochemical insertion of na into the spinel λ-MnO_2 phase. Solid State Ionics **57**, 113–120 (1992). https://doi.org/10.1016/0167-2738(92)90072-W
37. J.F. Whitacre, T. Wiley, S. Shanbhag, Y. Wenzhuo, A. Mohamed et al., An aqueous electrolyte, sodium ion functional, large format energy storage device for stationary applications. J. Power Sources **213**, 255–264 (2012). https://doi.org/10.1016/j.jpowsour.2012.04.018
38. M. Minakshi, Looking beyond lithium-ion technology - aqueous NaOH battery. Mater. Sci. Eng. B-Adv. **177**(20), 1788–1792 (2012). https://doi.org/10.1016/j.mseb.2012.09.003
39. X.Q. Zhang, J.W. Chen, J.J. Ye, T.W. Zhang, Z.G. Hou, Revealing the competitive intercalation between Na^+ and H^+ into $Na_{0.44}MnO_2$ in aqueous sodium ion batteries. Adv. Energy Mater. **13**(17), 2204413 (2023). https://doi.org/10.1002/aenm.202204413
40. D.J. Kim, R. Ponraj, A.G. Kannan, H.W. Lee, R. Fathi et al., Diffusion behavior of sodium ions in $Na_{0.44}MnO_2$ in aqueous and non-aqueous electrolytes. J. Power Sources **244**, 758–763 (2013). https://doi.org/10.1016/j.jpowsour.2013.02.090
41. H. Lim, J.H. Jung, Y.M. Park, H.N. Lee, H.J. Kim, High-performance aqueous rechargeable sulfate- and sodium-ion battery based on polypyrrole-mwcnt core-shell nanowires and $Na_{0.44}MnO_2$ nanorods. Appl. Surf. Sci. **446**, 131–138 (2018). https://doi.org/10.1016/j.apsusc.2018.02.021
42. J.Z. Sun, Y. Dong, C.Y. Kong, Synthesis of $Na_2MnFe(CN)_6$ and its application as cathode material for aqueous rechargeable sodium-ion battery. J. New Mater. Electrochem. Syst. **19**(3), 117–119 (2016). https://doi.org/10.14447/jnmes.v19i3.306
43. H.C. Gao, J.B. Goodenough, An aqueous symmetric sodium-ion battery with NASICON-structured $Na_3MnTi(PO_4)_3$. Angew. Chem. Int. Ed. **55**(41), 12768–12772 (2016). https://doi.org/10.1002/anie.201606508
44. Z.X. Liu, G. Pang, S.Y. Dong, Y.D. Zhang, C.H. Mi et al., An aqueous rechargeable sodium-magnesium mixed ion battery based on $NaTi_2(PO_4)_3$-MnO_2 system. Electrochim. Acta **311**, 1–7 (2019). https://doi.org/10.1016/j.electacta.2019.04.130
45. M.S. Chae, A. Chakraborty, S. Kunnikuruvan, R. Attias, S. Maddukuri et al., Vacancy-driven high rate capabilities in calcium-doped $Na_{0.4}MnO_2$ cathodes for aqueous sodium-ion batteries. Adv. Energy Mater. **10**(37), 2002077 (2020). https://doi.org/10.1002/aenm.202002077
46. M.Q. Zhang, T.B. Dong, D.G. Li, K. Wang, X.Z. Wei et al., High-performance aqueous sodium-ion battery based on graphene-doped $Na_2MnFe(CN)_6$-zinc with a highly stable discharge platform and wide electrochemical stability. Energy Fuels **35**(13), 10860–10868 (2021). https://doi.org/10.1021/acs.energyfuels.1c01095
47. H. Kanoh, W.P. Tang, Y. Makita, K. Ooi, Electrochemical intercalation of alkali-metal ions into birnessite-type manganese oxide in aqueous solution. Langmuir **13**(25), 6845–6849 (1997). https://doi.org/10.1021/la970767d
48. S. Devaraj, N. Munichandraiah, Effect of crystallographic structure of MnO_2 on its electrochemical capacitance properties. J. Phys. Chem. C **112**(11), 4406–4417 (2008). https://doi.org/10.1021/jp7108785
49. Y. Zhang, C.L. Yuan, K. Ye, X. Jiang, J.L. Yin et al., An aqueous capacitor battery hybrid device based on Na-ion insertion-deinsertion in lambda-MnO_2 positive electrode. Electrochim. Acta **148**, 237–243 (2014). https://doi.org/10.1016/j.electacta.2014.10.052
50. M. Minakshi, D. Meyrick, Electrochemical energy storage device for securing future renewable energy. Electrochim. Acta **101**, 66–70 (2013). https://doi.org/10.1016/j.electacta.2013.02.075
51. P.Y. Wang, X.B. Yan, Recent advances in Mg-Li and Mg-Na hybrid batteries. Energy Storage Mater. **45**, 142–181 (2022). https://doi.org/10.1016/j.ensm.2021.11.027
52. Y. Liu, Y. Qiao, W.X. Zhang, H. Wang, K.Y. Chen et al., Nanostructured alkali cation incorporated delta-MnO_2 cathode materials for aqueous sodium-ion batteries. J. Mater. Chem. A **3**(15), 7780–7785 (2015). https://doi.org/10.1039/c5ta00396b
53. Y. Liu, Y. Qiao, W.X. Zhang, H.H. Xu, Z. Li et al., High-performance aqueous sodium-ion batteries with $K_{0.27}MnO_2$ cathode and their sodium storage mechanism. Nano Energy **5**, 97–104 (2014). https://doi.org/10.1016/j.nanoen.2014.02.010
54. Y. Liu, Y. Qiao, X.D. Lou, X.H. Zhang, W.X. Zhang et al., Hollow $K_{0.27}MnO_2$ nanospheres as cathode for high-performance aqueous sodium ion batteries. ACS Appl. Mater.

© The authors https://doi.org/10.1007/s40820-023-01162-x

Interfaces **8**(23), 14564–14571 (2016). https://doi.org/10.1021/acsami.6b03089

55. X.Q. Shan, F.H. Guo, K. Page, J.C. Neuefeind, B. Ravel et al., Framework doping of ni enhances pseudocapacitive Na-ion storage of (Ni)MnO_2 layered birnessite. Chem. Mater. **31**(21), 8774–8786 (2019). https://doi.org/10.1021/acs.chemmater.9b02568
56. Q.L. Wei, X.Q. Chang, D. Butts, R. DeBlock, K. Lan et al., Surface-redox sodium-ion storage in anatase titanium oxide. Nat. Commun. **14**(1), 7 (2023). https://doi.org/10.1038/s41467-022-35617-3
57. J. Yu, X. Huang, Y. He, D. Tang, T. Huang, L. Liu, H. Wu, D.L. Peng, D. Zhao, K. Lan, Q. Wei, Compacted mesoporous titania nanosheets anode for pseudocapacitance-dominated, high-rate, and high-volumetric sodium-ion storage. SmartMat (2023). https://doi.org/10.1002/smm2.1192
58. Q. Wei, T. Huang, X. Huang, B. Wang, Y. Jiang et al., High-rate sodium-ion storage of vanadium nitride via surface-redox pseudocapacitance. Interdiscip. Mater. **2**(3), 434–442 (2023). https://doi.org/10.1002/idm2.12080
59. X.Q. Shan, D.S. Charles, W.Q. Xu, M. Feygenson, D. Su et al., Biphase cobalt-manganese oxide with high capacity and rate performance for aqueous sodium-ion electrochemical energy storage. Adv. Funct. Mater. **28**(3), 1703266 (2018). https://doi.org/10.1002/adfm.201703266
60. H. Usui, S. Suzuki, Y. Domi, H. Sakaguchi, Impacts of MnO_2 crystal structures and Fe doping in those on photoelectrochemical charge-discharge properties of TiO_2/MnO_2 composite electrodes. ACS Sustain. Chem. Eng. **8**(24), 9165–9173 (2020). https://doi.org/10.1021/acssuschemeng.0c02964
61. M. Ren, H.Y. Fang, C.C. Wang, H.X. Li, F.J. Li, Advances on manganese-oxide-based cathodes for Na-ion batteries. Energy Fuels **34**(11), 13412–13426 (2020). https://doi.org/10.1021/acs.energyfuels.0c02897
62. N. Jabeen, A. Hussain, Q.Y. Xia, S. Sun, J.W. Zhu et al., High-performance 2.6 V aqueous asymmetric supercapacitors based on in situ formed $Na_{0.5}MnO_2$ nanosheet assembled nanowall arrays. Adv. Mater. **29**(32), 1700804 (2017). https://doi.org/10.1002/adma.201700804
63. W.H. Zuo, Y. Yang, Synthesis, structure, electrochemical mechanisms, and atmospheric stability of Mn-based layered oxide cathodes for sodium ion batteries. Acc. Mater. Res. **3**(7), 709–720 (2022). https://doi.org/10.1021/accountsmr.2c00058
64. X.Q. Shan, F.H. Guo, D.S. Charles, Z. Lebens-Higgins, S.A. Razek et al., Structural water and disordered structure promote aqueous sodium-ion energy storage in sodium-birnessite. Nat. Commun. **10**, 4975 (2019). https://doi.org/10.1038/s41467-019-12939-3
65. B.H. Zhang, Y. Liu, Z. Chang, Y.Q. Yang, Z.B. Wen et al., Nanowire $Na_{0.35}MnO_2$ from a hydrothermal method as a cathode material for aqueous asymmetric supercapacitors. J. Power Sources **253**, 98–103 (2014). https://doi.org/10.1016/j.jpowsour.2013.12.011
66. Y. Liu, B.H. Zhang, S.Y. Xiao, L.L. Liu, Z.B. Wen et al., A nanocomposite of MoO_3 coated with PPy as an anode material for aqueous sodium rechargeable batteries with excellent electrochemical performance. Electrochim. Acta **116**, 512–517 (2014). https://doi.org/10.1016/j.electacta.2013.11.077
67. X. Zhou, A.L. Zhao, Z.X. Chen, Y.L. Cao, Research progress of tunnel-structural $Na_{0.44}MnO_2$ cathode for sodium-ion batteries: a mini review. Electrochem. Commun. **122**, 106897 (2021). https://doi.org/10.1016/j.elecom.2020.106897
68. M.S. Chae, Y. Elias, D. Aurbach, Tunnel-type sodium manganese oxide cathodes for sodium-ion batteries. ChemElectroChem **8**(5), 798–811 (2021). https://doi.org/10.1002/celc.202001323
69. B. Tekin, S. Sevinc, M. Morcrette, R. Demir-Cakan, A new sodium-based aqueous rechargeable battery system: the special case of $Na_{0.44}MnO_2$/dissolved sodium polysulfide. Energy Technol. **5**(12), 2182–2188 (2017). https://doi.org/10.1002/ente.201700245
70. H. Li, S.Y. Liu, T.C. Yuan, B. Wang, P. Sheng et al., Electrochemical mechanism of $Na_{0.44}MnO_2$ in alkaline aqueous solution. Acta Phys. Chim. Sin. **36**(5), 1905027 (2020). https://doi.org/10.3866/PKU.WHXB201905027
71. T.J. Sun, C. Liu, J.Y. Wang, Q.S. Nian, Y.Z. Feng et al., A phenazine anode for high-performance aqueous rechargeable batteries in a wide temperature range. Nano Res. **13**(3), 676–683 (2020). https://doi.org/10.1007/s12274-020-2674-3
72. Z.W. Guo, Y. Zhao, Y.X. Ding, X.L. Dong, L. Chen et al., Multi-functional flexible aqueous sodium-ion batteries with high safety. Chem **3**(2), 348–362 (2017). https://doi.org/10.1016/j.chempr.2017.05.004
73. Z. Li, D. Young, K. Xiang, W.C. Carter, Y.M. Chiang, Towards high power high energy aqueous sodium-ion batteries: The $NaTi_2(PO_4)_3$/$Na_{0.44}MnO_2$ system. Adv. Energy Mater. **3**(3), 290–294 (2013). https://doi.org/10.1002/aenm.201200598
74. W. Wu, A. Mohamed, J.F. Whitacre, Microwave synthesized $NaTi_2(PO_4)_3$ as an aqueous sodium-ion negative electrode. J. Electrochem. Soc. **160**(3), A497–A504 (2013). https://doi.org/10.1149/2.054303jes
75. B.D. Zhao, Q.Y. Wang, S. Zhang, C. Deng, Self-assembled wafer-like porous $NaTi_2(PO_4)_3$ decorated with hierarchical carbon as a high-rate anode for aqueous rechargeable sodium batteries. J. Mater. Chem. A **3**(22), 12089–12096 (2015). https://doi.org/10.1039/c5ta02568k
76. B.D. Zhao, B. Lin, S. Zhang, C. Deng, A frogspawn-inspired hierarchical porous $NaTi_2(PO_4)_3$-C array for high-rate and long-life aqueous rechargeable sodium batteries. Nanoscale **7**(44), 18552–18560 (2015). https://doi.org/10.1039/c5nr06505d
77. G. Pang, P. Nie, C.Z. Yuan, L.F. Shen, X.G. Zhang et al., Enhanced performance of aqueous sodium-ion batteries using electrodes based on the $NaTi_2(PO_4)_3$/MWNTs–$Na_{0.44}MnO_2$ system. Energy Technol. **2**(8), 705–712 (2014). https://doi.org/10.1002/ente.201402045
78. L.L. Ke, J. Dong, B. Lin, T.T. Yu, H.F. Wang et al., A $NaV_3(PO_4)_3$@C hierarchical nanofiber in high alignment:

exploring a novel high-performance anode for aqueous rechargeable sodium batteries. Nanoscale **9**(12), 4183–4190 (2017). https://doi.org/10.1039/c7nr00793k

79. C. Deng, S. Zhang, Z. Dong, Y. Shang, 1D nanostructured sodium vanadium oxide as a novel anode material for aqueous sodium ion batteries. Nano Energy **4**, 49–55 (2014). https://doi.org/10.1016/j.nanoen.2013.12.014
80. T.T. Gu, M. Zhou, M.Y. Liu, K.L. Wang, S.J. Cheng et al., A polyimide-MWCNTs composite as high performance anode for aqueous Na-ion batteries. RSC Adv. **6**(58), 53319–53323 (2016). https://doi.org/10.1039/c6ra09075c
81. Y. Wang, Z. Feng, D. Laul, W. Zhu, M. Provencher et al., Ultra-low cost and highly stable hydrated $FePO_4$ anodes for aqueous sodium-ion battery. J. Power Sources **374**, 211–216 (2018). https://doi.org/10.1016/j.jpowsour.2017.10.088
82. G. Yee, S. Shanbhag, W. Wu, K. Carlisle, J. Chang et al., TiP_2O_7 exhibiting reversible interaction with sodium ions in aqueous electrolytes. Electrochem. commun. **86**, 104–107 (2018). https://doi.org/10.1016/j.elecom.2017.11.013
83. X.Q. Zhang, Z.G. Hou, X.N. Li, J.W. Liang, Y.C. Zhu et al., Na-birnessite with high capacity and long cycle life for rechargeable aqueous sodium-ion battery cathode electrodes. J. Mater. Chem. A **4**(3), 856–860 (2016). https://doi.org/10.1039/c5ta08857g
84. L. Rakocevic, S. Strbac, J. Potocnik, M. Popovic, D. Jugovic et al., The Na_xMnO_2 materials prepared by a glycine-nitrate method as advanced cathode materials for aqueous sodium-ion rechargeable batteries. Ceram Int. **47**(4), 4595–4603 (2021). https://doi.org/10.1016/j.ceramint.2020.10.025
85. F.P. Gu, X.L. Yao, T.J. Sun, M.H. Fang, M. Shui et al., Studies on micron-sized $Na_{0.7}MnO_{2.05}$ with excellent cycling performance as a cathode material for aqueous rechargeable sodium-ion batteries. Appl. Phys. A Mater. **126**(8), 658 (2020). https://doi.org/10.1007/s00339-020-03799-6
86. B.H. Zhang, Y. Liu, X.W. Wu, Y.Q. Yang, Z. Chang et al., An aqueous rechargeable battery based on zinc anode and $Na_{0.95}MnO_2$. Chem. Commun. **50**(10), 1209–1211 (2014). https://doi.org/10.1039/c3cc48382g
87. S. Liu, T. Lei, Q.Q. Song, J. Zhu, C.B. Zhu, High energy, long cycle, and superior low temperature performance aqueous Na-Zn hybrid batteries enabled by a low-cost and protective interphase film-forming electrolyte. ACS Appl. Mater. Interfaces **14**(9), 11425–11434 (2022). https://doi.org/10.1021/acsami.1c23806
88. Z.G. Hou, X.N. Li, J.W. Liang, Y.C. Zhu, Y.T. Qian, An aqueous rechargeable sodium ion battery based on a $NaMnO_2$-$NaTi_2(PO_4)_3$ hybrid system for stationary energy storage. J. Mater. Chem. A **3**(4), 1400–1404 (2015). https://doi.org/10.1039/c4ta06018k
89. W. Wu, S. Shabhag, J. Chang, A. Rutt, J.F. Whitacre, Relating electrolyte concentration to performance and stability for NaTi2(PO4)3/$Na_{0.44}MnO_2$ aqueous sodium-ion batteries. J. Electrochem. Soc. **162**(6), A803–A808 (2015). https://doi.org/10.1149/2.0121506jes
90. S. Maddukuri, A. Nimkar, M.S. Chae, T.R. Penki, S. Luski et al., $Na_{0.44}MnO_2$/polyimide aqueous Na-ion batteries for large energy storage applications. Front. Energy Res. **8**, 615677 (2021). https://doi.org/10.3389/fenrg.2020.615677
91. H. Li, S.Y. Liu, T.C. Yuan, B. Wang, P. Sheng et al., Influence of NaOH concentration on sodium storage performance of $Na_{0.44}MnO_2$. Acta Phys. Chim. Sin. **37**(3), 1907049 (2021). https://doi.org/10.3866/PKU.WHXB201907049
92. L.M. Suo, O. Borodin, Y.S. Wang, X.H. Rong, W. Sun et al., Water-in-salt electrolyte makes aqueous sodium-ion battery safe, green, and long-lasting. Adv. Energy Mater. **7**(21), 1701189 (2017). https://doi.org/10.1002/aenm.201701189
93. S.L. Bai, J.L. Song, Y.H. Wen, J. Cheng, G.P. Cao et al., Effects of zinc and manganese ions in aqueous electrolytes on structure and electrochemical performance of $Na_{0.44}MnO_2$ cathode material. RSC Adv. **6**(47), 40793–40798 (2016). https://doi.org/10.1039/c6ra01768a
94. M.S. Chae, H.J. Kim, J. Lyoo, R. Attias, Y. Elias et al., Boosting tunnel-type manganese oxide cathodes by lithium nitrate for practical aqueous Na-ion batteries. ACS Appl. Energy Mater. **3**(11), 10744–10751 (2020). https://doi.org/10.1021/acsaem.0c01781
95. H.Z. Guo, Z.P. Shao, Y.X. Zhang, X.S. Cui, L.H. Mao et al., Electrolyte additives inhibit the surface reaction of aqueous sodium/zinc battery. J. Colloid Interface Sci. **608**, 1481–1488 (2022). https://doi.org/10.1016/j.jcis.2021.10.085
96. R. Chua, Y. Cai, P.Q. Lim, S. Kumar, R. Satish et al., Hydrogen-bonding interactions in hybrid aqueous/nonaqueous electrolytes enable low-cost and long-lifespan sodium-ion storage. ACS Appl. Mater. Interfaces **12**(20), 22862–22872 (2020). https://doi.org/10.1021/acsami.0c03423
97. Z.G. Hou, X.Q. Zhang, J.W. Chen, Y.T. Qian, L.F. Chen et al., Towards high-performance aqueous sodium ion batteries: Constructing hollow $NaTi_2(PO_4)_3$@C nanocube anode with Zn metal-induced pre-sodiation and deep eutectic electrolyte. Adv. Energy Mater. **12**(14), 2104053 (2022). https://doi.org/10.1002/aenm.202104053
98. R. Chua, Y. Cai, Z.K. Kou, R. Satish, H. Ren et al., 13 V superwide potential window sponsored by Na-Mn-O plates as cathodes towards aqueous rechargeable sodium-ion batteries. Chem. Eng. J. **370**, 742–748 (2019). https://doi.org/10.1016/j.cej.2019.03.251
99. Y.S. Wang, L.Q. Mu, J. Liu, Z.Z. Yang, X.Q. Yu et al., A novel high capacity positive electrode material with tunnel-type structure for aqueous sodium-ion batteries. Adv. Energy Mater. **5**(22), 1501005 (2015). https://doi.org/10.1002/aenm.201501005
100. F. Zhang, W.F. Li, X.D. Xiang, M.L. Sun, Highly stable Na-storage performance of $Na_{0.5}Mn_{0.5}Ti05O_2$ microrods as cathode for aqueous sodium-ion batteries. J. Electroanal. Chem. **802**, 22–26 (2017). https://doi.org/10.1016/j.jelechem.2017.08.042
101. M. Jayakumar, K. Hemalatha, K. Ramesha, A.S. Prakash, Framework structured $Na_4Mn_4Ti_5O_{18}$ as an electrode for Na-ion storage hybrid devices. Phys. Chem. Chem. Phys. **17**(32), 20733–20740 (2015). https://doi.org/10.1039/c5cp02866c
102. S. Boyd, R. Dhall, J.M. LeBeau, V. Augustyn, Charge storage mechanism and degradation of P2-type sodium

© The authors https://doi.org/10.1007/s40820-023-01162-x

transition metal oxides in aqueous electrolytes. J. Mater. Chem. A **6**(44), 22266–22276 (2018). https://doi.org/10.1039/c8ta08367c

103. A.C. Nwanya, M.M. Ndipingwi, O. Anthony, F.I. Ezema, M. Maaza et al., Impedance studies of biosynthesized $Na_{0.8}Ni_{0.33}Co_{0.33}Mn_{0.33}O_2$ applied in an aqueous sodium-ion battery. Int. J. Energy Res. **45**(7), 11123–11134 (2021). https://doi.org/10.1002/er.6594
104. F.P. Gu, T.J. Sun, X.L. Yao, M. Shui, J. Shu, Studies on the improved electro-chemical performance and the sodium ion migration mechanism of $Na_{0.44}MnO_2$-CNT electrodes for aqueous sodium batteries. J. Phys. Chem. Solid **149**, 109771 (2021). https://doi.org/10.1016/j.jpcs.2020.109771
105. F.X. Yin, Z.J. Liu, Y. Zhao, Y.T. Feng, Y.G. Zhang, Electrochemical properties of an na4mn9o18-reduced graphene oxide composite synthesized via spray drying for an aqueous sodium-ion battery. Nanomaterials **7**(9), 253 (2017). https://doi.org/10.3390/nano7090253
106. A.D. Tevar, J.F. Whitacre, Relating synthesis conditions and electrochemical performance for the sodium intercalation compound $Na_4Mn_9O_{18}$ in aqueous electrolyte. J. Electrochem. Soc. **157**(7), A870–A875 (2010). https://doi.org/10.1149/1.3428667
107. J.F. Whitacre, A. Tevar, S. Sharma, $Na_4Mn_9O_{18}$ as a positive electrode material for an aqueous electrolyte sodium-ion energy storage device. Electrochem. Commun. **12**(3), 463–466 (2010). https://doi.org/10.1016/j.elecom.2010.01.020
108. Y.G. Zhang, Z. Bakenov, T.Z. Tan, J. Huang, Polyacrylonitrile-nanofiber-based gel polymer electrolyte for novel aqueous sodium-ion battery based on a $Na_4Mn_9O_{18}$ cathode and Zn metal anode. Polymers **10**(8), 853 (2018). https://doi.org/10.3390/polym10080853
109. G.H. Yuan, J.M. Xiang, H.F. Jin, Y.Z. Jin, L.Z. Wu et al., Flexible free-standing $Na_4Mn_9O_{18}$/reduced graphene oxide composite film as a cathode for sodium rechargeable hybrid aqueous battery. Electrochim. Acta **259**, 647–654 (2018). https://doi.org/10.1016/j.electacta.2017.11.015
110. F.X. Yin, Z.J. Liu, S. Yang, Z.Z. Shan, Y. Zhao et al., $Na_4Mn_9O_{18}$/carbon nanotube composite as a high electrochemical performance material for aqueous sodium-ion batteries. Nanoscale Res. Lett. **12**, 569 (2017). https://doi.org/10.1186/s11671-017-2340-1
111. Z.Z. Shan, Y.S. He, T.Z. Tan, Y.G. Zhang, X. Wang, Preparation of $Na_4Mn_9O_{18}$/carbon nanotube/reduced graphene oxide by spray drying as cathode materials for sodium ion batteries. Solid State Sci. **94**, 77–84 (2019). https://doi.org/10.1016/j.solidstatesciences.2019.05.019
112. X.Q. Shan, D.S. Charles, Y.K. Lei, R.M. Qiao, G.F. Wang et al., Bivalence Mn_5O_8 with hydroxylated interphase for high-voltage aqueous sodium-ion storage. Nat. Commun. **7**, 13370 (2016). https://doi.org/10.1038/ncomms13370
113. X.Q. Shan, F.H. Guo, W.Q. Xu, X.W. Teng, High purity Mn_5O_8 nanoparticles with a high overpotential to gas evolution reactions for high voltage aqueous sodium-ion electrochemical storage. Front. Energy **11**(3), 383–400 (2017). https://doi.org/10.1007/s11708-017-0485-3
114. S. Qiu, Y.K. Xu, X.Y. Wu, X.L. Ji, Prussian blue analogues as electrodes for aqueous monovalent ion batteries. Electrochem. Energy Rev. **5**(2), 242–262 (2022). https://doi.org/10.1007/s41918-020-00088-x
115. B.X. Xie, B.Y. Sun, T.Y. Gao, Y.L. Ma, G.P. Yin et al., Recent progress of prussian blue analogues as cathode materials for nonaqueous sodium-ion batteries. Coord. Chem. Rev. **460**, 214478 (2022). https://doi.org/10.1016/j.ccr.2022.214478
116. J. Han, H. Zhang, A. Varzi, S. Passerini, Fluorine-free water-in-salt electrolyte for green and low-cost aqueous sodium-ion batteries. Chemsuschem **11**(21), 3704–3707 (2018). https://doi.org/10.1002/cssc.201801930
117. K. Shin, Y.P. Zheng, F. Zhang, S. Wu, Y.B. Tang, Facile ion-exchange strategy for Na^+/K^+ hybrid-ion batteries with superior rate capability and cycling performance. ACS Appl. Energy Mater. **3**(7), 7030–7038 (2020). https://doi.org/10.1021/acsaem.0c01060
118. S. Qiu, X.Y. Wu, M.Y. Wang, M. Lucero, Y. Wang et al., NASICON-type $Na_3Fe_2(PO_4)_3$ as a low-cost and high-rate anode material for aqueous sodium-ion batteries. Nano Energy **64**, 103941 (2019). https://doi.org/10.1016/j.nanoen.2019.103941
119. J.S. Chen, C. Liu, Z.X. Yu, J.T. Qu, C. Wang et al., High-energy-density aqueous sodium-ion batteries enabled by chromium hexacycnochromate anodes. Chem. Eng. J. **415**, 129003 (2021). https://doi.org/10.1016/j.cej.2021.129003
120. Z.G. Hou, W.T. Mao, Z.X. Zhang, J.W. Chen, H.S. Ao et al., Bipolar electrode architecture enables high-energy aqueous rechargeable sodium ion battery. Nano Res. **15**(6), 5072–5080 (2022). https://doi.org/10.1007/s12274-022-4113-0
121. M. Pasta, R.Y. Wang, R. Ruffo, R.M. Qiao, H.W. Lee et al., Manganese-cobalt hexacyanoferrate cathodes for sodium-ion batteries. J. Mater. Chem. A **4**(11), 4211–4223 (2016). https://doi.org/10.1039/c5ta10571d
122. K. Nakamoto, R. Sakamoto, M. Ito, A. Kitajou, S. Okada, Effect of concentrated electrolyte on aqueous sodium-ion battery with sodium manganese hexacyanoferrate cathode. Electrochemistry **85**(4), 179–185 (2017). https://doi.org/10.5796/electrochemistry.85.179
123. L.W. Jiang, L.L. Liu, J.M. Yue, Q.Q. Zhang, A.X. Zhou et al., High-voltage aqueous Na-ion battery enabled by inert-cation-assisted water-in-salt electrolyte. Adv. Mater. **32**(2), 1904427 (2020). https://doi.org/10.1002/adma.201904427
124. D. Reber, R. Grissa, M. Becker, R.S. Kuhnel, C. Battaglia, Anion selection criteria for water-in-salt electrolytes. Adv. Energy Mater. **11**(5), 2002913 (2021). https://doi.org/10.1002/aenm.202002913
125. M.A. Oliver-Tolentino, J. Vazquez-Samperio, S.N. Arellano-Ahumada, A. Guzman-Vargas, D. Ramirez-Rosales et al., Enhancement of stability by positive disruptive effect on Mn-Fe charge transfer in vacancy-free Mn-Co hexacyanoferrate through a charge/discharge process in aqueous Na-ion batteries. J. Phys. Chem. C **122**(36), 20602–20610 (2018). https://doi.org/10.1021/acs.jpcc.8b05506

126. Y. Liu, C. Sun, Y. Li, H.B. Jin, Y.J. Zhao, Recent progress of Mn-based nasicon-type sodium ion cathodes. Energy Storage Mater. **57**, 69–80 (2023). https://doi.org/10.1016/j.ensm.2023.02.005
127. Y. Yuan, Q.Y. Wei, S.K. Yang, X.Y. Zhang, M. Jia et al., Towards high-performance phosphate-based polyanion-type materials for sodium-ion batteries. Energy Storage Mater. **50**, 760–782 (2022). https://doi.org/10.1016/j.ensm.2022.06.008
128. H. Zhang, X.P. Tan, H.H. Li, S. Passerini, W. Huang, Assessment and progress of polyanionic cathodes in aqueous sodium batteries. Energy Environ. Sci. **14**(11), 5788–5800 (2021). https://doi.org/10.1039/d1ee01392k
129. L. Sharma, A. Manthiram, Polyanionic insertion hosts for aqueous rechargeable batteries. J. Mater. Chem. A **10**(12), 6376–6396 (2022). https://doi.org/10.1039/d1ta11080b
130. M. Minakshi, D. Meyrick, Reversible sodiation in maricite $NaMn_{1/3}Co_{1/3}Ni_{1/3}PO_4$ for renewable energy storage. J. Alloys Compd. **555**, 10–15 (2013). https://doi.org/10.1016/j.jallcom.2012.11.203
131. Y. Zhou, Z.S. Zhang, Y. Zhao, J.F. Liu, K.H. Lam et al., Cost-effective, long-term aqueous rechargeable hybrid sodium/zinc batteries based on Zn anode and $Na_3MnTi(PO_4)_3$ cathode. Chem. Eng. J. **425**, 130459 (2021). https://doi.org/10.1016/j.cej.2021.130459
132. J.T. Wu, H.J. Liu, H.P. Bu, X. Zhang, H.L. Zhang et al., Manganese-based NASICON structured $Na_{1+2x}Mn_xTi_{2-x}(PO_4)_3$ as promising cathode in aqueous sodium ion battery. J. Alloys Compd. **934**, 167872 (2023). https://doi.org/10.1016/j.jallcom.2022.167872
133. P.R. Kumar, A. Kheireddine, U. Nisar, R.A. Shakoor, R. Essehli et al., $Na_4MnV(PO_4)_3$-rGO as advanced cathode for aqueous and non-aqueous sodium ion batteries. J. Power Sources **429**, 149–155 (2019). https://doi.org/10.1016/j.jpowsour.2019.04.080
134. B.W. Xie, R. Sakamoto, A. Kitajou, K. Nakamoto, L.W. Zhao et al., Cathode properties of $Na_3MnPO_4CO_3$ prepared by the mechanical ball milling method for Na-ion batteries. Energies **12**(23), 4534 (2019). https://doi.org/10.3390/en12234534
135. X.Y. Guo, Z.B. Wang, Z. Deng, B. Wang, X. Chen et al., Design principles for aqueous Na-ion battery cathodes. Chem. Mater. **32**(16), 6875–6885 (2020). https://doi.org/10.1021/acs.chemmater.0c01582
136. K. Shiprath, H. Manjunatha, K.C.B. Naidu, A. Khan, A.M. Asiri et al., $Na_3MnPO_4CO_3$ as cathode for aqueous sodium ion batteries: Synthesis and electrochemical characterization. Mater. Chem. Phys. **248**, 122952 (2020). https://doi.org/10.1016/j.matchemphys.2020.122952
137. N. Nzimande, A. Haruna, P. Mwonga, B. Rasche, F. Cummings et al., Ceria-spiderweb nanosheets unlock the energy-storage properties in the "sleeping" triplite ($Mn_2(PO_4)F$). ACS Appl. Energy Mater. **4**(11), 13085–13097 (2021). https://doi.org/10.1021/acsaem.1c02734
138. Y.S. Wang, J. Liu, B.J. Lee, R.M. Qiao, Z.Z. Yang et al., Ti-substituted tunnel-type $Na_{0.44}MnO_2$ oxide as a negative electrode for aqueous sodium-ion batteries. Nat. Commun. **6**, 6401 (2015). https://doi.org/10.1038/ncomms7401
139. Y. Wang, F.Y. Zhou, Y.H. Li, P. Shi, S.Y. Xu et al., $Na_2[Mn_3Vac_{0.1}Ti_{0.4}]O_7$: A new layered negative electrode material for aqueous Na-ion batteries. J. Alloys Compd. **918**, 165765 (2022). https://doi.org/10.1016/j.jallcom.2022.165765
140. M. Pasta, C.D. Wessells, N. Liu, J. Nelson, M.T. McDowell et al., Full open-framework batteries for stationary energy storage. Nat. Commun. **5**, 3007 (2014). https://doi.org/10.1038/ncomms4007
141. A. Firouzi, R.M. Qiao, S. Motallebi, C.W. Valencia, H.S. Israel et al., Monovalent manganese based anodes and co-solvent electrolyte for stable low-cost high-rate sodium-ion batteries. Nat. Commun. **9**, 861 (2018). https://doi.org/10.1038/s41467-018-03257-1
142. J. Yun, F.A. Schiegg, Y.C. Liang, D. Scieszka, B. Garlyyev et al., Electrochemically formed $Na_xMn[Mn(CN)_6]$ thin film anodes demonstrate sodium intercalation and deintercalation at extremely negative electrode potentials in aqueous media. ACS Appl. Energy Mater. **1**(1), 123–128 (2018). https://doi.org/10.1021/acsaem.7b00022
143. K. Nakamoto, R. Sakamoto, Y. Sawada, M. Ito, S. Okada, Over 2 V aqueous sodium-ion battery with prussian blue-type electrodes. Small Methods **3**(4), 1800220 (2019). https://doi.org/10.1002/smtd.201800220
144. S. Wheeler, I. Capone, S. Day, C. Tang, M. Pasta, Low-potential prussian blue analogues for sodium-ion batteries: Manganese hexacyanochromate. Chem. Mater. **31**(7), 2619–2626 (2019). https://doi.org/10.1021/acs.chemmater.9b00471
145. M.G. Wu, W. Ni, J. Hu, J.M. Ma, NASICON-structured $NaTi_2(PO_4)_3$ for sustainable energy storage. Nano-Micro Lett. **11**(1), 44 (2019). https://doi.org/10.1007/s40820-019-0273-1
146. P. Lei, K. Liu, X. Wan, D.X. Luo, X.D. Xiang, Ultrafast Na intercalation chemistry of $Na_2Ti_{3/2}Mn_{1/2}(PO_4)_3$ nanodots planted in a carbon matrix as a low cost anode for aqueous sodium-ion batteries. Chem. Commun. **55**(4), 509–512 (2019). https://doi.org/10.1039/c8cc07668e
147. Y. Shang, X.X. Li, J.J. Song, S.Z. Huang, Z. Yang et al., Unconventional Mn vacancies in Mn-Fe prussian blue analogs: Suppressing jahn-teller distortion for ultrastable sodium storage. Chem **6**(7), 1804–1818 (2020). https://doi.org/10.1016/j.chempr.2020.05.004

© The authors https://doi.org/10.1007/s40820-023-01162-x